ELECTRON PARAMAGNETIC RESONANCE IN SOME TRANSITION METAL IONS IN SINGLE CRYSTALS

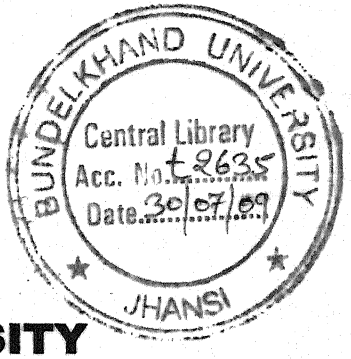

THESIS

SUBMITTED TO

BUNDELKHAND UNIVERSITY

JHANSI, U.P, INDIA

FOR
THE DEGREE OF DOCTOR OF PHILOSOPHY
IN
PHYSICS

BY

BHARAT MORBHATT

UNDER THE SUPERVISION OF

DR. N.L. SHUKLA
EX. READER AND HEAD,
DEPARTMENT OF PHYSICS,
ATARRA P.G. COLLEGE,
ATARRA (BANDA), U.P.

2003

I

dedicated this piece of research work

to my Dearest Mummy, Papa

and Sister Guziya

CERTIFICATE

This is to certify that the present thesis entitled **"Electron Paramagnetic Resonance in Some Transition Metal Ions in Single Crystals"** embodies the unaided research work of Mr. Bharat Morbhatt. This work was carried out under my supervision and has not been submitted elsewhere for a degree.

Mr. Bharat Morbhatt has attended the research center, Post Graduate Department of Physics, Atarra P.G. College, Atarra (Banda), U.P., more than three hundred days.

It is worth mentioning here that necessary and desired corrections have been incorporated in this thesis as per the Examiner's report.

Dated: 18 / 7 / 2003
Resubmission on : 20 / 8 / 2005

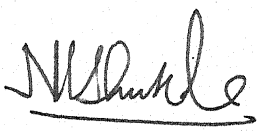

(Dr. N.L. Shukla)
Principal,
Pt. J. N. P. G. College,
Banda, UP.
Ex. Reader and Head
Department of Physics
Atarra P.G. College,
Atarra (Banda) U.P.
(Supervisor)

DECLARATION

I hereby declare that the thesis entitled **"Electron Paramagnetic Resonance in Some Transition Metal Ions in Single Crystals"** being submitted for the degree of Doctor Philosophy in Physics, Bundelkhand University, Jhansi, U.P,. is an original piece of research work done by me under the supervision of **Dr. N.L. Shukla**, Reader and Head, Department of Physics, Atarra P.G. College, Atarra (Banda), U.P., and to the best of my knowledge, any part or whole of this thesis has not been submitted for a degree or any other qualification of any university or examining body in India/elsewhere

The following corrections have been made and incorporated at proper places in the text of the thesis as per the examiner's report.

1. A proper acknowledgment and vote of thanks have been given in the pages of acknowledgements for IIT, Kanpur.
2. Special importance has been given to put the reference literature from 1991 to 2003 to make the study up to date and comparative observation have been also appended to make the thesis self sufficient and elaborative.
3. Various research findings have been presented in conferences / seminars of different scientific academies and certain research papers have been communicated in reputed journals which are still in the process of publication.

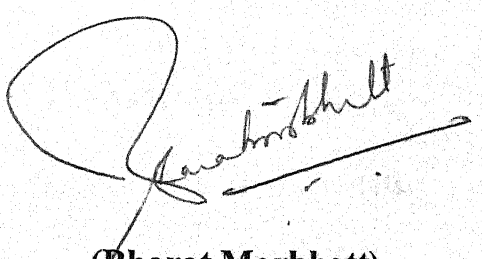

Dated: 18 / 7 /2003
Resubmission on : 20 / 8 / 2005

(Bharat Morbhatt)

ACKNOWLEDGEMENTS

In the first place and above all I thank my GOD, Lord JESUS CHRIST for making it possible that this work has reached the present state. It is only HIS mercy and grace that this work exists in my name.

I take this opportunity to express my gratitude and regards to **Dr. N.L. Shukla** for his kind and able guidance and the special interest that he took in my work, without which the present work would not have been possible. I am highly thankful to him for accepting me as his student, helping and supervising me through the subject to reach to the present stage. I cannot thank him enough for being so considerate and caring towards me.

The help rendered by the **Head of the Department of Physics and Dr. Prem Chand, Indian Institute of Technology, Kanpur** for providing Central EPR facility for recording the spectra is also thankfully acknowledged.

I am equally grateful to **Prof (Dr.) R.B. Lal**, Honorable Vice Chancellor, Allahabad Agriculture Institute-Deemed University, Allahabad for helping me tremendously in his own special way, during the various stages of the work. It is an undeniable fact that the remains a never-ending source of inspiration and motivation to me. I am also thankful to **Mrs. Sudha Lal**, wife of Dr. R.B. Lal and Jonathan Akshay Lal, son of Dr.R.B. Lal, for taking me no less than a family member.

I am thankful to **Prof. K.N. Pathak**, Honorable Vice Chancellor, Punjanb University, Chandigarh, **Prof. K.N. Srivastava**, School of Physics, Central Univesity, Hyderabad, **Dr. B.N. Mishra**, Retired Professor of Physics, Allahabad university, Allahabad and **Dr. S. R. Shukla**, Senior Scientist, SSPL, Delhi, who have helped me directly or indirectly in various ways during the progress of this research work from time to time.

I am thankful to **Dr. Ramesh Chandra**, Co-ordinator, IDD programme, AAI-DU for his interest and encouragement during the progress of the work. I extend my thanks to **Dr. D.N. Pandey**, Ex-Principal, Atarra P.G. College, Atarra, (Banda), for his kind help time to time. I have been benefited greatly by the discussion we had during the progress of the work.

I take the opportunity to express my respect and regards to **Mr. Ajit Paul** and **Mrs. V.Paul** (Bhaiya and Bhabhiji) who have shown boundless affection, patience and moral support that has contributed a lot in my progress.

I wish to express my deep sense of indebt ness to my respected Mother, **Mrs. P. Morbhatt** and Father, **Mr. A.K. Morbhatt,** since the work is present shape is due to their lively interest, constructive suggestions and all round persuasion, encouragement and moral upliftment whenever I was feeling down. They are a perennial source of inspiration and blessings to me. All the credit of my success goes to my Papa-Mummy. I can never thank them enough for always being there for me. I owe a special thanks to my sweet little sister **Guriya (Surabhi), Bari Didi (Ms. S. Morbhatt)** and all the family members who have

always supported and backed me up in the times of distress and difficulties during the research work.

I am highly thankful to **Mrs. Kusum Lata Shukla (Respected Aunty ji),** wife of Dr. N.L. Shukla, for being so affectionate and caring. She has been very patient, warm, welcoming and understanding even when the work demanded the odd hours of the day.

In the end, I can not forget to thank my dear friends **Dr. Dinesh Kumar, Er. Sandeep G.M. Prasad, Dr. George Prince, Mr. Ajay P. Srivastava** and **Mr. Rajneesh Khare** for their support and valuable advice time to time.

August, 2005

(Bharat Morbhatt).

LIST OF PUBLICATION

1. EPR Study of Manganese doped Ammonium Bromide single crystal, N.L. Shukla, Bharat Morbhatt, A.P. Srivastava, S.K. Mishra, R.K. Shukla and Vikas Mishra, Proceeding of the Third Conference of International Academy of Physical Sciences, 139(1999)
2. EPR Study of some Vanadyl doped single crystals, N.L. Shukla, Bharat Morbhatt and Ajay Pratap Srivastava, Journal of Internatinal Academy of Physical Sciences (2000). [In press].
3. Effect of exposure to Lithium and Iodine Vapours of transitions ions doped cermics. Presented at the fourth conference of International Academy of Physical Science, Feb. 25-27 (2001) at Chitrakoot. N.L. Shukla, R.K. Shukla, Bharat Morbhatt, S.K. Mishra, Vikas Mishra and A.P. Srivastava.
4. Experimental investigation of $(ZrO_2)_{0.8}$ $(Y_2O_3)_{0.2}$. ceramic compound Presented at the Fourth Conference of International Academy of Physical Science. Feb. 25-27 (2001) at Chitrakoot. N.L. Shukla, R.K. Shukla, Bharat Morbhatt, S.K. Mishra, Vikas Mishra and A.P. Srivastava.
5. EPR Study of Mn^{2+}: Cd $(im)_6$ $(NO_3)_2$. Presented at the 2^{nd} National Seminar on New Dimensions of Higher Physics and Information Technology, Dec. 16-17 (2001) at Kanpur. N.L. Shukla, A.P. Srivastava, Rajneesh Khare and Bharat Morbhatt.

6. Single crystal EPR study of Cu^{2+}: Cd1mS. Presented at the 2nd National Seminar on New Dimension of Higher Physics and Information Technology, Dec 16-17 (2001) at Kanpur. N.L. Shukla and Bharat Morbhatt.

7. Analysis of EPR spectra in MN^{2+}:$NaNO_2$. Presented at the Fifth Conference of International Academy of Physical Science, April 07-09 (2002) at Bundelkhand University, Jhansi. N.L. Shukla and Bharat Morbhatt.

8. Spectrum-II in Mn^{2+}:$NaNO_2$ Presented at the Fifth Conference of International Academy of Physical Science, April 07-09 (2002) at Bundelkhand University, Jhansi. N.L. Shukla, R.K. Shukla, S.K. Mishra and Bharat Morbhatt.

CONTENTS

CHAPTER-6

****

CHAPTER – 1

INTRODUCTION

INTRODUCTION

The Electron Paramagnetic Resonance (EPR) has become one of the most powerful tools for studying the wide varieties of physical, chemical and biological effects and also for the study of magnetic behaviour of paramagnetic substances. It was first observed by E.J. Zavoisky [1] in 1945 at USSR. Later on Cummerow and Halliday [2], Bleaney and Penrose [3] obtained well resolved resonance spectra of paramagnetic ions of the first transition series. A. Abragam, B. Bleaney, J.H.E. Griffiths, K.W.H. Stevens and their co-workers did the major developmental work in the techniques of EPR at the Clarendon laboratory, Oxford.

If a static magnetic field is applied to a system of free electrons (L=0, S= ½), the electrons align themselves either parallel or antiparallel to the applied magnetic field. On applying electromagnetic field of frequency ν in a direction perpendicular to a DC magnetic field, the transitions of the electrons from lower level to upper level according to the selection rule $\triangle M_S = \pm 1$ take place and sharp absorption of power occurs provided the relation.

$$h\nu = g\beta H \qquad (1.1.1)$$

is satisfied. Mostly the population ratio of the two energy states is given by the Maxwell-Boltzmann distribution relation:

$$n_1 / n_2 = e^{-\Delta E / kT}$$

where n_1 and n_2 are the number of free electrons in the upper and lowers state respectively and E is the energy separation between the two states. In case of single spin system the population of the ground state is slightly in excess of the population of the upper state. Factually for a temperature of about 300^0K and magnetic field 3000 gauss, the excess population in the ground state is only about 0.07 percent; yet the whole phenomenon of EPR depends upon this difference. If this resonance absorption of the radiation is to continue, there must be some other mechanism, apart from the stimulated emission which allows the electrons of the upper state to lose energy and drop to lower state, otherwise after sometime the population of the lower state will be zero and absorption will cease. Spin - lattice interaction, spin-spin interaction and exchange interaction are the important processes by which electrons lose energy and come to ground state and the absorption becomes a steady process [4].

Th Hyperfine splitting of an Electron Paramagnetic Resonance line is obtained when the interaction between the unpaired electron and the magnetic nucleus takes place within the molecule. It is of extreme importance in determining the distribution of unpaired electron density and leads us to reach the valuable information regarding the intra and inter molecular

interactions. The total Hamiltonian of the system inclusive of EPR and Hyperfine processes is given by:-

$$\mathcal{H} = g\,\beta\ \vec{H}\ .\ \vec{S}\ .\ + A\ \vec{S}\ .\ \vec{I} \qquad (1.1.3)$$

assuming the ion to be free. But the unpaired electron is not always free and is bound in the molecule by a number of forces. The above Hamiltonian will be modified for a macroscopic body containing a paramagnetic as well as a large number of diamagnetic components. A brief discussion is given in chapter two of the thesis.

The substances possessing a resultant electronic magnetic moment exhibit the phenomenon of EPR. The materials processing this property are transition elements, electrons trapped in radiation damages, impurities in semiconductors, free radicals and many other biological materials. The EPR study gives the various significant information about the system which are mentioned below:

(i) The phenomenon of Electron Paramagnetic Resonance under certain conditions is found useful in providing the information about the bulk properties like susceptibility and specific heat of the system.

(ii) The resonance spectrum is extremely sensitive to the surrounding of the paramagnetic ion in the system. Thus

it also provides information about the symmetry of the surroundings, the nature and the strength of the bonding between the ion and its immediate diamagnetic neighbour.

(iii) The width of the resonance lines in a fully resolved spectrum depends on a number of factors such as (a) spin – lattice interaction (b) spin-spin interaction and (c) exchange interaction etc. The study of the width of the EPR lines provides complete information about the strength and nature of the these magnetic as well as non magnetic interactions present in the system.

(iv) Electronic transitions provide resonance spectra which help to obtain reliable interpretation about the nuclear spin of the paramagnetic ion. The values of nuclear dipole and nuclear quadrupole moments may also be found approximately.

(v) From the analysis of the observed hyperfine structure we can draw conclusions concerning the nature of the sample and the character of the delocalization of the molecular orbital of the unpaired electron.

Thus there are various parameters of EPR spectrum e.g. lineshape, line width, g-value, intensity of the signal and hyperfine splitting constant etc., from which a variety of information about the paramagnetic molecule can be obtained.

Apart from these points, the information derived from the EPR spectrum also depends upon the nature and form of the specimen used.

Concentrated specimens used for EPR study usually provide single line spectrum [5-8]. In the case of polycrystalline samples, on gets linewidth and g-value averaged out over all possible orientations of the crystallites present in the samples. The Hyperfine structure [9-15] is studied in the diluted solutions of the complexes. When magnetically diluted single crystals are used for EPR study [16-20] we obtain most significant information. Results of directional anisotropies in line width and g-value which are obtained only from single crystal study, gives information about the configurations of the ions present in the complexes. A.Abragam et al have developed most of the theory on crystal fields and electron paramagnetic resonance [21,22,23]. It is no always possible to grow a magnetically dilute single crystal. However, it has been shown possible to obtain the similar type of information from powder and glass state EPR spectra [8,22].

Among the transition group elements, Copper is of great importance because of the reason that most of the discoveries associated with microwave spectra of solid state have been first observed in Cu^{2+} salts [28-30]. McGarvey [9], Cohn [10], Kozyrev [11], Kivelson and Wilson [15], Chary and Sastry [24],

Misra and Sharma [25-27], have investigated the paramagnetic resonance spectra of the transition metal ions.

The present research work reported in this thesis is being distributed and presented in six chapter including the first chapter of Introduction which basically deals with a brief explanation of the phenomenon of EPR and the experimental techniques used.

The second chapter of the thesis explains in detail, the theory of the EPR investigations of the systems for the present thesis. A brief discussion on the crystal field effects, covering the weak intermediate crystal field and strong crystal field is given. The spin Hamiltonain and various type of interactions have also been discussed. The theory related to the EPR spectra of liquid, powder and their expected line shapes are described. Besides, the above discussion, method of the computation of resonance field has also been mentioned in short.

The third chapter carries the description of the experimental techniques used in the characterization work/analysis of the present investigation. The techniques employed are:

a) Electron Paramagnetic Resonance (EPR), [X-band, Varian E-109].

b) X-ray diffraction (XRD) [Rich and Seifert, Model-2002].

c) Scanning Electron Microscopy (SEM) [JEOL, JSM-840-A].

Fourth chapter of the thesis carries the experimental investigations and studies carried out on Zirconium Yitrium Oxide $(ZrO_2)_{0.8}$ $(Y_2O_3)_{0.2}$ ceramic compound employing the techniques of X-ray diffraction (XRD), Scanning electron microscopy (SEM) and Electron Paramagnetic Resonance (EPR). The effect of doing of transition metal ions (Mn, Cu & V) with a fixed concentration on the host ceramic samples have been investigated. The results obtained are presented and discussed in details.

The fifth chapter deals in the study of Mn^{2+}. A thorough EPR investigation and analysis has been carried out on the sample of diammonium oxalate monohydrate $[(NH_4)_2\ C_2O_4.H_2O]$ single crystal doped with Manganese (Mn^{2+}) ion for the first time. The study leads us to an understanding that Mn^{2+} ions substitutes for NH_4^+ ion in the crystal lattice and associated with the first neighbour NH_4^+ vacancy in such a way that the z axis of the complex lies in ab plane. The spectrum has been fitted to a spin Hamiltonian appropriate for orthorhombic symmetry.

Finally, in the sixth chapter, a detailed EPR study of Cu^{2+} ion doped is the single crystal of Cis-Catena-μ-Sulphato-Aquotris Imidozol Cadamium (II) is given. EPR spectra of the powder sample was also recorded and is accounted for in the chapter. A thorough analysis of both the spectra with the determination of bonding parameter and various EPR parameters has been done. The

spectrum has been fitted to a spin Hamiltonian appropriate for Cu^{2+} in rhombic symmetry. The results obtained are presented and discussed in details.

REFERENCES

1. E.J. Zavoisky, J. Phys. (USSR) **9**(1945) 211; ibid **10**(1946) 197.
2. R.L. Cummerow and D. Halliday, Phys. Rev. **70** (1946), 433.
3. B. Bleaney and R.P. Penrose, Nature 157, (1946) 339.
4. G.E. Pake, Paramagnetic Resonance, W.A. Benjamin Inc., New York (1962).
5. H. Kumagai, K. Ono, I. Hayashi, H. Abe, I. Shimada, H. Shono, H. Ibamato and S. Tachimori, J. Phys. Soc. Japan, **9** 369 (1954).
6. C. Maclean and G.J.W. Kor; Appl. Sci. Res., **48**, 425 (1955).
7. B.N. Misra and S.K. Gupta, J. Mag. Resonance, **12** 126 (1973).
8. F.K. Neubuhl, J. Chem. Phys., **33** 1074(1960).
9. B.R. McGarvey, J. Chem. Phys., **60**, 71 (1956(.
10. M. Cohn and J. Townsend, Nature, **173**, 1090 (1954).
11. B.M. Kozyrev, Disc. Faraday Soc; **19**, 135 (1955).
12. B. B. Garrett and L.O. Morgan, J. Chem. Phys., **44**, 890 (1966).

13. B.N. Misra, S.D. Sharma and S.K. Gupta, IL Nuovo Cimento **19**, 129 (1974).

14. M.P. Eastman, G.R. Kooser, M.R. Das and J.H. Freed, J. Chem. Phys., **51**, 2690 (1969).

15. D. Kivelson and R. Wilson, J. Chem. Phys., **44**, 154, 4440, 4445 (1966).

16. B. Bleaney and D.J.E. Ingram, Proc. Roy. Soc., **A205**, 336 (1951).

17. M. Weger and W. Low; Phys Rev., **111**, 1526 (1958).

18. H.C. Box and H.G. Freund, J. Chem. Phys., **40**, 817 (1968).

19. B. Bleaney, K.D. Bowers and D.J.E. Ingram, Proc. Roy. Soc., **A228**, 147 (1955).

20. R. Janakiraman and G.C. Upreti, J. Chem. Phys., **54**, 2336 (1971).

21. A. Abragam and B. Bleaney, Electron Paramagnetic Resonance of Transition Ions, Clarendon Press, Oxford (1970).

22. D. Kivelson and R. Neiman, J. Chem. Phys., **35**, 156 (1961).

23. K.D. Bowers and J. Owen, Reports on Progress in Physics, **18**, 304 (1955).

24. M.N. Chary and B.A. Sastry, Indian J. Pure and Appl. Phys., **15**, 172 (1977).

25. B.N. Misra and S.D. Sharma, J. Chem. Phys., **63**, 5322 (1975).

26. B.N.Misra and S.D. Sharma, J. Mag. Reso., **24**, 1 (1976).

27. B.N. Misra and S.D. Sharma, Indian J. Pure and Appl. Phys., **15**, 719 (1977).

28. D.J.E. Ingram, Proc. Phys. Soc., **A62**, 664 (1949).

29. B. Bleaney and D.J.E. Ingram, Proc. Roy. Soc., **A63**, 408. (1950).

30. B. Bleaney, K.D. Bowers and D.J.E. Ingram, Proc. Phys. Soc., **A 64**, 758 (1951).

CHAPTER – 2

THEORETICAL CONSIDERATION OF ELECTRON PARAMAGNETIC RESONANCE

2.1 INTRODUCTION

When a free ion with a resultant angular momentum $\vec{J}$ is subjected to a static magnetic field $\bar{B}$ then it has 2J +1 energy levels and the energies of the various states are given as:

$$E_{M_J} = g\beta BM_J \qquad (2.1.1)$$

where M_J= J -1 -----, - J+1-J, B is the static magnetic field. g is the spectroscopic splitting factor and β is the Bohr magneton. The electrons in the unfilled 3d, 4d, 4f, 5d and (5f, 6d) shells are responsible for paramagnetism in iron, palladium, rare earth, platinum and actinide group complexes. A resonance absorption line corresponding to the energy difference. E between the E_{M_J} levels differing in M_J value by ± 1 should be observed. Therefore, the resonance condition becomes:

$$\Delta E = h\nu = g\ \beta\ B \qquad (2.1.2)$$

The resonance condition for free electron is shown in Fig. 2.1. The intensities of these transitions are given by the square of the matrix element connecting M_J^{th} and $(M_J+1)^{th}$ levels. The intensities are governed by the following relation.

$$[Intensity]_{M_J \leftrightarrow M_J \pm 1} \propto [J(J+1) - M_J(M_J \pm 1)] \qquad (2.1.3)$$

Thus transitions with different $M_J \leftrightarrow M_J \pm 1$ values will have different intensities. For the case of J = 5/2 the five transitions

corresponding to $\Delta M_J = \pm 1$ would have intensities in 5:8:9:8:5 ratio.

2.2 CRYSTAL FIELD EFFECTS

The energy levels of ions in a crystalline environment differ from the free ion energy levels. When a metal ion is placed in a crystalline field, the degeneracy of the d-orbitals will be removed by the electrostatic interactions. The spin degeneracy will remain until a magnetic field is applied. When the species contains more than one unpaired electron, the spin degeneracy can also be resolved by crystal field. Thus the spin levels may be split even in the absence of a magnetic field; this phenomenon is called zero field splitting. The theoretical explanation of zero -filed splitting in S-state ions was given by van Vleck and Penny [1], Sharma et. al. [2], Narayana [3], Chatterjee et al.[4] and Watanabe [5].

The EPR splitting of energy levels occurs under the effect of two types of fields; crystal field around the ion and the applied magnetic field. The crystal field is also called the internal splitting field and the energy splitting caused by this field are called 'Crystal field splitting' or 'Internal field splitting' or 'Zero field splitting' (ZFS) since it happens in the absence of external magnetic field. For the paramagnetic ion in a crystal, there are two

types of interactions; interactions between the paramagnetic ions (dipolar) and interactions between the paramagnetic ion and the nearest neighbours (ligand field). Former interaction is large in concentrated paramagnetic complexes but can be reduced effectively to a negligibly small value by dilution i.e. by doping small amounts of paramagnetic complex in an isomorphous diamagnetic host. Thus each ion may be considered isolated from other paramagnetic ions and to be independent. The latter interactions of paramagnetic ion with diamagnetic ligands modify the magnetic properties of the paramagnetic ions. The crystal field (CF) theory assumes that the ligands influence the magnetic ion through the electric field which they produce at its site and their orbital motions get modified. The crystal field interaction is affected by the electrostatic screening by the outer electronic shells. Depending upon its magnitude relative to other interactions, the crystalline field interaction is generally classified into three categories.

2.2 (i) Weak Crystal Field

When the crystal field interaction is weaker than the spin-orbit coupling (this is the case with the rare-earth and certain actinide compounds). It is due to the fact that the unfilled shell, 4f or 5f lies fairly deep within the ion and is shielded by the closed 5s and 5p or 6s and 6p shells respectively.

2.2 (ii) Intermediate Crystal Field

When the crystal field interaction is greater than spin-orbit coupling but is less than the Coulombic interaction between electrons. The best example of these are hydrated salts of the iron group. This situation is described by regarding the orbital motion as clamped due to crystal field and making it unable to respond to an applied magnetic field. This is know as "quenching of orbital angular momentum" and the magnetic properties are all due to spin which is affected only weakly by crystal field through spin-orbit coupling.

2.2 (iii) Strong Crystal Field

The crystal field is said to be strong when the crystal field interaction is of the order of Coulombic interaction between electrons. For the 4d and 5d transition group ions there is a tendency of covalent bonding due to which the orbitals of the metal ion and neighbouring ligands overlap appreciably. In this case due to strong covalent bonding the crystal field assumption remains no longer valid.

2.3 HYPERFINE INTERACTION

Hyperfine interaction are mainly magnetic dipole interactions between the electronic magnetic moment and the

nuclear magnetic moment of the paramagnetic ion. The origin of this can be understood simply by assuming that the nuclear moment produces a magnetic field B_N at the magnetic electrons and the modified resonance condition is:

$$\Delta E = h\nu = g\beta|B+B_N| \qquad (2.3.1)$$

The hyperfine interaction is highly characteristic one. Identification of paramagnetic and its isotopics in characteristic by the hyperfine structure (HFS) in the EPR spectra is the simplest method. The interaction of the magnetic electron with nuclei of the ligands gives rise to super hyperfine structure (SHFS) on the HFS in the EPR spectra.

2.4 THE SPIN HAMILTONIAN

The EPR, the unpaired electron is not isolated or free, but frequently interacts with a variety of nuclei and electrons. Therefore the right handside in eqn. (2.1.2) becomes the sum of various terms. The state of affairs may be expressed from the quantum mechanical view point in terms of a Hamiltonian. The electronic interactions which contribute to the total energy of the ion may be described by the following Hamilton [6-10].

$$\mathcal{H} = \mathcal{H}_o + \mathcal{H}_{cr} + \mathcal{H}_{s-o} + \mathcal{H}_{s-s} + \mathcal{H}_z + \mathcal{H}_{hf} + \mathcal{H}_q + \mathcal{H}_n + \mathcal{H}_e$$

(2.4.1)

Where

$\mathcal{H}_0$ = Free ion energy [~ 10^5 cm^{-1}]

$\mathcal{H}_{cr}$ = Electrostatic energy [~$10^4 cm^{-1}$]

$\mathcal{H}_{S\text{-}0}$ = Spin orbit interaction energy [~10^2 -10^3 cm^{-1}]

$\mathcal{H}_{S\text{-}S}$ = Spin-spin interaction energy [~1cm^{-1}]

$\mathcal{H}_Z$ = Interaction of electron with the external field or Zeeman energy=$\beta B(L+2S)$[~1cm^{-1}]

$\mathcal{H}_{hf}$ = Dipole-dipole interaction between the electron and nuclear-magnetic moments [~10^{-1} cm^{-1} -10^{-3} cm^{-1}]

$\mathcal{H}_q$ = Quadrupole interaction between electron and nucleus [~10^3 cm^{-1}]

$\mathcal{H}_n$ = Nuclear Zeeman energy = $g_N\beta_N B.I$ [~$10^4 cm^{-1}$]

$\mathcal{H}_e$ = Energy of exchange effects between electrons.

Practical EPR spectroscopy concerns itself mainly with the $\mathcal{H}_{S\text{-}S}$, $\mathcal{H}_Z$ and $\mathcal{H}_{h\text{-}f}$ i.e. the fine structure, Zeeman splitting and hyperfine interactions as the nuclear Zeeman and quadrupole interactions are usually small. The best way to consider all the

energy contributions is to express them in the following form including the nuclear Zeeman and quadrupole terms [10].

$$\mathcal{H} = \beta\vec{B}.\tilde{g}.\vec{S} + \vec{S}.\tilde{D}.\vec{S}. + \vec{S}.\tilde{A}.\vec{I} - \beta_N\vec{B}.\tilde{g}_N\vec{I} + \vec{I}.\tilde{Q}.\vec{I}. \qquad (2.4.2)$$

where $\vec{S}$ and $\vec{I}$ are the electronic spin and nuclear spin operators respectively and are equivalent to $\vec{J}$ operators from mathematical point of view and $\tilde{g}$, $\tilde{D}$, $\tilde{A}$, $\tilde{Q}$ and $\tilde{g}_N$ are all second rank tensor quantities. The first term represents Zeeman interaction with the applied field B, the presence of orbital momentum is taken into account by allowing the splitting factor $\tilde{g}$ to differ from the spin-only value (2.0023). $\tilde{D}$ in the second term represents the crystal field splitting. The third term expresses the hyperfine interaction between S and I. The fourth term expresses the nuclear Zeeman interaction and the last term expresses the quadrupole coupling between nuclear spin I and the electric field gradient. In principal axes system (Tensors in diagonalised eqn. Form) eqn. (2.4.2) can be written as (neglecting the nuclear Zeeman interaction).

$$\mathcal{H} = \beta\left(g_x B_x S_x + g_y B_y S_y + g_z B_z S_z\right) + D\left[S_z^2 - 1/3S(S+1)\right] +$$

$$E\left(S_x^2 - S_y^2\right) + A_x S_x I_x + A_y S_y I_y + A_z S_z I_z + Q'\left[I_z^2 - 1/3(I+1)\right] + Q''\left(I_x^2 - I_y^2\right) \qquad (2.4.3)$$

where $D = D_z - 1/2[D_x + D_y]$, $E = 1/2[D_x - D_y]$

$$Q' = Q_z - 1/2[Q_x + Q_y],\ Q'' = 1/2[Q_x - Q_y]$$

and g_x,g_y, g_z and A_x, A_y, A_z are the components of g and A tensors respectively along principal axes. In Eqn. (2.4.3) the Parameters "D" and "E" are generally known as fine structure parameters and are the measure of the ZFS of energy states described by the spin-Hamiltonian. "D" and "E" represent the axial and rhombic parts of the crystal field splitting respectively. For the so called axial symmetry $E = Q_{||} = O$ and $g_z = g_{||}$; $g_x = g_y = g_{\perp}$, $A_z = A_{||}$ and $A_x = A_y = A_{\perp}$.

2.5 COVALENCY EFFECTS AND SUPER-HYPERFINE STRUCTURE

A detailed examination reveals that the approximation of ligand ion in CF theory is not strictly valid, and the overlap of the wave functions of the ligand ions with that of the metal ion must be taken into account. Stevens[11] considered this problem for the first time for the complexes of the ions from 4d and 5d groups which are bonded in a strongly covalent manner. Owen [12,13] studied the same for some ions from 3d group. The main effects of the covalency on EPR can be listed as follows:

(i). The covalent bond reduces the orbital contributions to the g-factor. The evidence for reduction of the orbital contribution has been obtained from the spectra Ti^{3+} in

alum [14], Fe^{2+} in MgO [15, 16]and ZnF_2 [17] and Co^{2+} in MgO [18, 19] and ZnF_2 [17].

(ii). The hyperfine interaction parameter 'A' is reduced. The experimental evidence comes from the work of Title [20] who studied the paramagnetic resonance of Mn^{2+} in a variety of host lattices and proved that the hyperfine constant. "A", decrease linearly with the increase of covalency.

(iii). There may be an additional SHFS structure on the HF lines due to the interaction between the magnetic electrons and the surrounding nuclei. The effect was first found by Owen and Stevens in ammonium chlororidate [21], and subsequently for a number of transition metal ions in ZnF_2 by Tinkham [17] and by several other workers [22-25] in various host lattices.

2.6 KRAMERS' THEOREM AND THE JAHN-TELLER [J-T] EFFECT

The Kramer's theorem [26] states that in a crystalline field of any symmetry, a system having an odd number of electrons will always possess at least a two-fold spin degeneracy which can be lifted by the application of a magnetic field. These states were

referred to as Kramer's doublet and assures the observation of EPR in the so called Kramer's (odd number of electrons).

According to J-T effect [27-28], a symmetrical non-linear molecule having a degenerate electronic energy level can not have stable configuration and will therefore distort to a configuration of lower symmetry and thus the degeneracy of the electronic state is lifted, or in other words the disposition of the nuclei adjusts in such a way that the symmetry of a complex gets lowered.

Van Vleck [29] estimated that for iron group, a splitting of few hundred cm^{-1} and for rare earth group about 10^{-2} cm^{-1} may be caused by J-T effect. In the case of paramagnetic ions embedded in diamagnetic hosts, the symmetry of the ligand field is also reduced due to Jahn-Teller effect. This effect is prominently noticeable in the case of Cu^{2+} in trigonal field [30-32] and Fe^{2+} in octahedral field [15-16].

2.7 SPIN LATTICE AND SPIN-SPIN RELAXATIONS

In EPR three processes are commonly described for transferring energy from the excited spin system to the lattice [spin lattice relaxation (SLR)] direct, Raman and Orbach process. In the direct process for the two-level system, relaxation occurs through transfer of energy from a single spin to a single

vibrational mode of the crystalline lattice which has essentially the same frequency [33]. When relaxation is by the direct process, $T_1 \propto 1/B^2T$ [34] (where T_1 is the SLR time) and is independent of the spin concentration. Therefore, the temperature and magnetic field can serve as variables either for the study or for the control of T_1. Actually, the "direct" process is important only at low temperatures.

At high temperatures, the indirect or Raman process predominates. Here a phonon is inelastically scattered in the process of flipping a spin. Energy is conserved and this process was strongly temperature dependent with $T_1 \propto 1/T^7$ for $T < \theta_D$, $T_1 \propto 1/T^2$ for $T > \theta_D$ where θ_D is the Debye temperature [35]. Experimental results are in fair agreement with theory at high temperature but not at low temperature where the direct process is important.

In the orbach process, there are two transitions one after the other which occur via an intermediate state. When electron is transferred from a level m to level n in the ground manifold of states by absorbing energy equal to $h\nu$, then by stimulated transition, it goes to a level q which is higher in energy than n by an amount Δ. Spontaneous transition then takes place from level p to m which release a phonon of energy equal to $(h\nu + \Delta)$. The relaxation rate is given by

$$\frac{1}{T_1} \propto e^{-\Delta/kT} \qquad (2.7.1)$$

where k is the Boltzmann factor. This relaxation process is active in the case of rare-earth ions.

The theory of spin-spin relaxation (S-SR) has been developed by Van Vleck [36], Pryce and Stevens [37] where two main types of interactions between the ions have been recognized; the dipole-dipole and the exchange interaction. The dipoles are close enough so that they experience various local fields resulting from the dipolar fields of their neighbours. In the case of exchange interaction, the energy transfer takes place by means of mutual spin flips between neighbouring spins. As the spins are in thermal equilibrium among themselves and if the equilibrium is disturbed, it is re-established exponentially with a time constant T_2 called the SSR time. The resonance line width is proportional to $1/T_2$.

2.8 EPR OF LIQUIDS

The paramagnetic complexes in liquid solutions can be considered as micro-crystals tumbling in a random way as they jostled by the molecular motions of the solvent [38]. Considering the effect of only motional modulation of anisotropic g and A tensors on the line-width Kivelson [39] developed the theory of

ESR line width in dilute solutions. Because of the tumbling motion, the orientation of micro-crystals varies with respect to the external magnetic field. The spin Hamiltonian under this condition can be written as:

$$\mathcal{H}_{spin} = \mathcal{H}^{(0)} + \mathcal{H}^{(1)} + F(t) \qquad (2.8.1)$$

where

$$\mathcal{H}^{(0)} = g_0 \beta_0 S_Z H_Z$$

$$\mathcal{H}^{(1)} = hA_0 S_Z + \frac{1}{2} A_0 [I^+ S^- + I^- S^+],$$

$$g_0 = 1/3 (g_x + g_y + g_Z)$$

$$A_0 = 1/3 (A_x + A_y + A_Z)$$

F (t) is the time dependent part of the Hamilton and depends upon the anisotropy of g and A. Assuming that the spectral lines are well resolved, that the Zeeman term is the largest term in energy and the lines-shapes are Lorentzian, Wilson and Kivelson [40] gave the expression of line-width ΔH as

$$\Delta H = a_1 + a' + a_2 + a_3 + a_4 \qquad (2.8.2)$$

$$a_1 = a_0 + a = \frac{1}{43}\left[(\Delta\gamma \ H_0)^2\right](4 + 3u) + \frac{1}{40} b^2 [I + 1]$$

$$= (3 + 7u)\frac{1}{8} b^2 (I + 1)(A_0 / \omega_0) \text{if} - \frac{1}{30}$$

$$= \Delta\gamma \ H_0 b_1 (I + 1)(A_0 / \omega_0)(1 + u),$$

$$a_2 = \frac{1}{13}(b\Delta\gamma\gamma H_0)(4 + 3u) - \frac{2}{43}(\Delta\gamma H_0)^2 (4 + 3u + 3uf)(A_0 / \omega_0)$$

$$= \frac{1}{20} b^2 I(I + 1)(A_0 / \omega_0)(4 + 3u + 7uf) + \frac{1}{40} b^2 (A_0 / \omega_0) \times (3+2y)\,[2I(I+1)-1]$$

$$a_3 = A_0 = \frac{b^2}{40}(5 - u) + \frac{1}{8} b^2 (A_0 / \omega_0) uf = \frac{1}{30}(\Delta\gamma / H_0 b)$$

$$= (A_0 / \omega_0)(7 + 5u + 12uf)$$

$$a_4 = \frac{1}{10} b^2 (A_0 / \omega_0)(1 + u + uf)$$

in these expressions

$u = (1 + \omega_0^2 \tau_c^2)^{-1}$, $f = \omega_0^2 \tau_c^2 u$,

$b = \frac{2}{3}(A_{||} - A_{\perp})$ rad / sec, $\Delta\gamma = \beta_0 \Delta g / h$, $\Delta g = g_{||} - g_{\perp}$

Where ω_0 is the microwave frequency in rad/sec and τ_c is the orientational correlation time expressed as:

$$\tau_c = \frac{4}{3} \frac{\pi r^3 \eta}{kT} \qquad (2.8.3)$$

and η is the viscosity of the solution. a_0 is called the residual line-width due to some unspecified mechanisms. The most important of these mechanisms is the spin rotational relaxation mechanism, a relaxation mechanism because of the interaction of the rotational magnetic moment of paramagnetic molecule with its spin or nuclear magnetic moment. Atkins and Kivelson [41],

following Hubbard theory [42], gave the following expression for the line-width due to this mechanism:

$$a_0 \sim \alpha_{RS} = \frac{2}{\sqrt{3}} \frac{h}{\beta_0 g} \frac{1}{12\pi r^3} \left[\Delta g_{\parallel}^2 + 2\Delta g_{\perp}^2\right] \frac{kT}{\eta}, \qquad (2.8.4)$$

Where $\Delta g_{\parallel} = g_{\parallel} - 2.0023$, $\Delta g_{\perp} = g_{\perp} - 2.0023$, r the molecular radius of the equivalent rotating sphere in the solution and the remaining symbols have their usual meaning.

Among many suggestions to explain the observed line-width an idea analogous to electric field fluctuation mechanism in solids [43, 44] was applied in the case of liquids. In this process the electric fields constituting the crystal or molecular binding fields are modulated by the molecular vibrations and by collisions with surrounding diamagnetic molecules, and these fluctuations of electric field affect the spin by means of spin-orbit interactions. The lattice vibrations in crystals replace the Brownian motion in solutions as the source of modulation. Kivelson developed [43] the contributions of three most significant electric field fluctuation mechanisms in solutions as:

$$W(1) = 64(\lambda/\Delta)^2 = \left(\frac{\phi' q_0}{\Delta r_0}\right)^2 \frac{(\omega_0 \tau_c)^2 \tau_c^{-1}}{1 + \omega_0^2 \tau_c^2} \text{ (Van Vleck direct)} \quad (2.8.5)$$

$$W(2) = 32(\lambda/\Delta)^2 = \left(\frac{\phi' q_0}{\Delta r_0}\right)^2 \tau_0^{-1} \text{ (Van Vleck Raman)}, \omega_0^2 \tau_c^2 \le 1,$$

(2.8.6)

$$W(3) = 16(\lambda / \Delta)^2 = \left(\frac{(\phi' q_0)^2}{\Delta r_0}\right)^2 \left(\frac{\Delta}{\delta}\right)^2 \frac{\tau_0^{-1}}{[\exp(h\delta / kT - 1)]}$$

(Orbach),

$$\delta^2 \tau_c^2 \geq 1, \qquad (2.8.7)$$

Where λ = spin orbit coupling constant for a given ion, Δ=crystal field splitting parameter, r_0 = characteristic intermolecular distance, τ_c = mean correlation time for intermolecular fluctuations, q_0 = typical root-mean-square value of q_i; q_i's are the amplitudes of intermolecular oscillations, $h\delta$=exciting energy of the first excited state.

$$\phi' = \Sigma \left| (hV_{CF} / \delta q_1) r_0 \right|$$

is a potential indicating the approximate magnitude of the crystal or molecular binding field. However, out of these three electric field fluctuation mechanisms only Orbach process was found to be useful.

2.9 POWDER EPR SPECTRA

In the polycrystalline samples the polycrystals (crystallites) randomly oriented with respect to the static magnetic field (46-48). Consequently, EPR corresponding to all possible orientations of these small crystallites is obtained. The individual EPR signals

usually overlap because of finite individual line widths to form what we normally call a "powder EPR pattern". For discussing the powder line-shapes, we consider a spherical coordinate system shown in Fig. 2.1 in which the orientation of the paramagnetic species defined by the orthogonal axes, x, y and z; θ and ϕ are the angles specifying the orientation of B in this coordinate system. Now, the number of crystallites with a magnetic field orientation between θ and $\theta + d\theta$ and between ϕ and $\phi + d\phi$ proportional to the solid angle $d\theta$ [49] where

$$d\Omega \propto \text{Sin}\ \theta\ d\theta\ d\phi = d \cos \theta\ d\phi \qquad (2.9.1)$$

The powder EPR pattern then the ensemble average of the resonance condition over all equally probable elements of solid angle ($d\Omega$) summed over all allowed transitions. The EPR absorption at field H in the magnetic field interval dH may be expressed in terms of a normalized "shape function" [50] S(H) given by

$$S(H)\, dH \propto (4\pi)^{-1} \sum_r \int_H^{H+dH} P_r(\Omega)\, d\Omega(H_r) \qquad (2.9.2)$$

Eqn. (2.9.2) integrated over those elements of solid angle $d\Omega$ (H_r) such that $H < H_r < H + dH$, where H_r is the appropriate resonance condition corresponding to rth transition. In general, $d\Omega$ is a multi-valued function of H_r, there being more than one value of cos θ and ϕ for some resonance fields H_r. $P_r(\Omega)$ is the

transition probability for the rth component and is normally independent of Ω except in the case where we have strong g-anisotrpy (51-54). Thus, $P_r(\Omega)$ may be taken outside the integral sign of Eqn. (2.9.2) in most situations, and the EPR powder patterns for each resonance transition to be multiplied by one of these factors before adding all pattern together to get the total absorption line-shapes.

However, in situations where all elements of solid angle not equally probable, [55], an additional factor such as p(Ω) must be included in Eqn. (2.9.2), where P (Ω) dΩ gives the probability of a site being oriented in an element of solid angle dΩ at Ω.

The resonance conditions described above represented idealized δ-function line-shapes, which are seldom observed in the actual spectra. Several line broadening mechanisms operative in actual situations Line-broadening from dipole-dipole interactions can be expressed empirically by a normalized "Gaussian Function" of the following form [56].

$$Y_{Gi}(H-H_r)=\left(\frac{1n2}{\pi}\right)^{1/2}\frac{y_0}{\Delta H}\exp.\left[\frac{(-1n2)(H-H_r)^2}{\Delta H^2}\right] \qquad (2.9.3)$$

Where $Y_G=\left(\frac{ln\,2}{\pi}\right)^{1/2}\frac{1}{\Delta H}$ *and* H_r represents the resonant field corresponding to an appropriate resonance condition. The quantity ΔH referred to as the half-width at half-maximum

(HWHM) of a pure absorption line in the absence of microwave power saturation. The equation for the corresponding first derivative of the Gaussian Function is:

$$Y'_G(H - H_r) = -\frac{2}{\pi}\frac{(ln\,2)^{3/2}}{\Delta H^3}.(H - H_r).\ Exp.\left[-\frac{ln\,2}{\Delta H}.(H - H_r)^2\right] \quad (2.9.4)$$

The peak-to-peak width of the derivate line-shape (ΔH_{PP}) is related to ΔH by the following relation

$$\Delta H = (ln2/2)^{1/2}\ \Delta H_{pp} \quad (2.9.5)$$

Line broadening from "Exchange Interaction" can often be approximated theoretically by a normalized Lorentzian function, characterized by the following expression [57]:

$$Y_L(H - H_r) = 1/\pi.\frac{\Delta H}{\Delta H^2 + (H - H_r)^2} \quad (2.9.6)$$

The corresponding first derivative line-shape is:

$$Y'_L(H - H_r) = -\left(\frac{2}{\pi}\right)\frac{\Delta H\,(H - H_r)}{[\,\Delta H^2 + (H - H_r)^2\,]^2} \quad (2.9.7)$$

For Lorentzian line ΔH and (ΔH_{PP}) are related by the following relation:

$$\Delta H = \frac{\left(\sqrt{3}\,\Delta H_{pp}\right)}{2} \quad (2.9.8)$$

Dilute paramagnetic systems (such as radical species diluted in a liquid) often exhibit spectral line-shapes which can normally be approximated by a Lorentzian function. Moreover, in some

systems, the presence of more than one independent line-broadening mechanism complicates the spectral shape, and then each component line-width should be given by Eqns. (2.9.3-2.9.5) and (2.9.6.–2.9.8), respectively. Although not common, a combination of Lorentzian and Gaussian lines was some times observed due to the presence of several types of interaction in the spin system. Such combinations are often represented by a "Voigt" shape function [57].

To account for the above broadening mechanism, an additional term representing the appropriate line line-shape, e.g. Eqn. (2.9.2-2.9.4) and (2.9.5-2.9.7), should be added to in Eqn. (2.9.2), which then involves a double integral. If we neglect the dependence of the lines-shapes functions on orientations [58], which normally is unimportant in the powder lines-shape calculations [59], we can take the line-broadening terms outside of the integral sign in Eqn. (2.9.2), thus giving a convolution of the ideal delta function line-shape.

Since analytical solutions to most powder EPR pattern problems generally impossible to carry out in practice , Eqn. (2.9.2) quite often solved numerically by using a computer. It might be said that without high-speed digital computers that are available these days, this task would be nearly impossible. As a consequence powder EPR spectrometry would have been more

limited in its applications than it is today. The normal procedure for obtaining solutions to Eqn. (2.9.2) comprises summation of all contributions to the shape function, S(H), over a grid in (cos θ, ϕ) space by various numerical integration algorithm [60].

The next section illustrates the powder patterns expected for several systems under different symmetry conditions.

2.10 THE EXPECTED POWDER LINE-SHAPES

2.10.1 Pattern without Hyperfine Splitting:

For paramagnetic systems with axial symmetry, we find from Eqn. (2.18) that the shape function S (H) can be expressed as:

$$S(H)\, dH \propto \mathrm{Sin}\theta\, d\theta \qquad (2.10.1)$$

Or

$$S(H) \propto \mathrm{Sin}\,\theta / (dH/d\theta) \qquad (2.10.2)$$

Eqns. (2.10.1) and (2.10.2) reflect the fact that very large number of radicals with axes nearly perpendicular to the field direction will be present in the system and only a few radicals will have their axis aligned close to the field direction. This means that we expect to see two "extrema' in the powder spectra.

The resonance field (H_r) is given by:

$$H_r = \frac{h\nu}{\beta} \quad \frac{1}{\left(g_{\parallel} \cos^2\theta + g_{\perp} \sin^2\theta\right)} \qquad (2.10.3)$$

Eqn. (2.10.3) shows the expected angular variation of Hr (Fig. 2.2). Differentiating Eqn. (2.10.3), in order to evaluate $dH/d\theta$, we write Eqn. (2.10.2) into the form

$$S(H) \propto \left(\frac{h\nu}{\beta}\right)^2 \quad \frac{1}{H_r^3 \left(g_{\parallel}^2 - g_{\perp}^2\right) \cos\theta} \qquad (2.10.4)$$

We see, therefore, that due to the presence of "cos θ" term in the denominator of Eqn. (2.10.4), S (H) rises monotonically from a finite value determined by $g_{\parallel}$ to infinity, i.e., at a field determined by $g_{\parallel}$, as $\theta \rightarrow 90^0$. This behaviour is shown by the s-function line-shape in Fig. 2.2(a) where the powder patterns obtained for various amounts of line-broadening are also depicted. The two extrema, therefore, correspond to $g_{\parallel}$ and $g_{\perp}$, respectively, so that the resonance field lies between $h\nu/g_{\parallel}\beta$ and $h\nu/g_{\perp}\beta$. The corresponding first derivative spectra would be of the type shown in Fig. 2.2. (c). Levedev [61] gives a more complete description of such theoretical line-shapes for systems with axial symmetry.

For powder specimens with an orthorhombic g-tensor, there are three turning points in the EPR spectrum corresponding to the three principal g-tensor components, g_{xx}, g_{yy} and g_{zz}; g_{yy} being the intermediate in the spectrum [49]. The diagnostic features of the

absorption line-shapes and its first-derivative for such a situation are shown in Fig. 2.3.

2.10.(ii) Patterns with Hyperfine Splitting:

The simple line-shapes patterns in Figs. 2.2 and Fig. 2.3 are modified in the presence of electron-nuclear hyperfine interaction. Assuming the unpaired electron to be interacting with a set of magnetically equivalent I = 2 nuclei, the line-shape pattern of Fig. 2.2(c) becomes modified to that shown in Fig. 2.4.(a). The powder pattern becomes more complicated when interacting magnetic nuclei have spin I > 1/2 , for example, for I= 3/2, and an isotropic hyperfine interaction, the pattern would be according to Fig. 2.4.(c).

In several simple situations it may be possible to determine some or all of the components of g and A simply from the experimentally observed spectra. Otherwise, the extraction of rather precise Hamiltonian parameters usually rests on the "Computer Simulation" until the best fit is achieved between experimental and calculated line-shapes.

2.11.(i) COMPUTATION OF RESONANCE FIELDS

The EPR transitions result from a matching of energy levels of a spin in a magnetic field by the microwave quantum used. Thus the validity of the phenomenological SH used may be testified by comparing the observed and computed values of resonance fields with the help of solution of SH matrix (with the known values of parameters) as and subsequently matching the possible energy level differences to the microwave quantum. The SH matrix can be solved either by perturbation method or by exact numerical diagnolization on digital computers. The perturbation methods are applicable to the cases where the Zeeman term is dominant and are thus of limited applicability only to cases with small ZFS and small hyperfine interaction. The energy levels given in the fine structure in the EPR are labeled by quantum numbers M_s and those giving the hyperfine structure by m_I. Though the labelling is done as if these are pure quantum numbers, they have no other meaning except their use for labelling. In the perturbation expressions which involve these numbers and treat them as pure quantum numbers an error is introduced due to their real value being defined for $\Delta M_S = \pm 1$ and $\Delta m_I = 0$. The transitions possible in violation of the above rules are termed as forbidden transitions and may involve $\Delta M_S = \pm 2, \pm 3$ etc. and $m_I = \pm 1, \pm 2$ etc.

The resonance fields are calculated from the exact solution of SH matrix and by finding an interval (H, H +δH) by interactive

procedure such that for a value H_j of the magnetic field $F_j\left(=|E_{jj} - E_{j+\Delta M}| - \frac{h\nu}{\beta}\right) \leq 0$ and for $(H_j - \delta H)$, $F_j \geq 0$ where E_j are the levels involved in the transition, ΔM is a positive or negative integer including zero depending on the transition under consideration being "allowed" or "forbidden", $h\nu$ is the microwave quantum and δH is a small number pre-selected based on the experimental accuracy of the resonance fields ($\delta H \sim 10^{-1} - 10^{-3}$ Gauss). The value H_j thus computed corresponds to the resonance field position for the transition under consideration. The process is repeated until the total number of observed transitions have been considered and their position computed (in Gauss).

2.11.(ii) Method For S = ½ Ions

For S = ½ and I = 3/2 or 7/2 for example Cu^{2+}, Co^{2+} and $V0^{2+}$ the fine structure terms are dropped from the SH and it assumes the simpler form:

$$\mathcal{H} = \beta.\bar{S}.\tilde{g}.\bar{H} + \bar{I}.\tilde{A}.\bar{S}. + \bar{I}..\tilde{P}.\bar{I}. - \beta_N \bar{H}.\tilde{g}_N.\bar{I} \qquad [2.11.(ii).1]$$

In most of the cases the last two terms are found to be very small and may generally be dropped from the spin Hamiltonian. For axial symmetry the SH (II-2.7) is sometimes written in terms of more customary symbols in the following form [49):

$$\mathcal{H} = g_{\parallel} \beta S_Z H_Z + \beta g_{\perp} (S_x H_x + S_y H_y) + A S_Z I_Z + B (S_x I_x + S_y I_y) +$$

$$+ O\left[3I_z^2 - I(I+1)\right] + \gamma\,\beta_N\,\bar{H}.\bar{I} - R\;I_z H_z - R_\perp\left(H_x I_x + H_y I_y\right)$$

[2.11.(ii).2]

Bleaney [50] in his classic paper has obtained the expressions for the resonance fields applying perturbation method and Low [9] has given the expressions for resonance fields for both the allowed and the forbidden transitions. Extensive discussion of the perturbation method and the above SH may be found in literature [12,48]. For the analysis of Cu^{2+} (S=1/2, I=3/2) and $V0^{2+}$ (S=1/2, I=7/2) EPR spectra spin Hamiltonian paramagnetics are obtained. The parameters thus obtained were next refined by obtaining minimizing F. Here F $\left(=\sum_i\left(H_0^i - H_T^i\right)^2\right)$, where H_0^i and H_T^i are the experimentally observed and calculated resonance field values respectively and H_T^i are computed by the method described earlier through the exact numerical diagonalization of a SH matrix (8 x 8 for Cu^{2+}) and 16 x 16 for $V0^{2+}$.

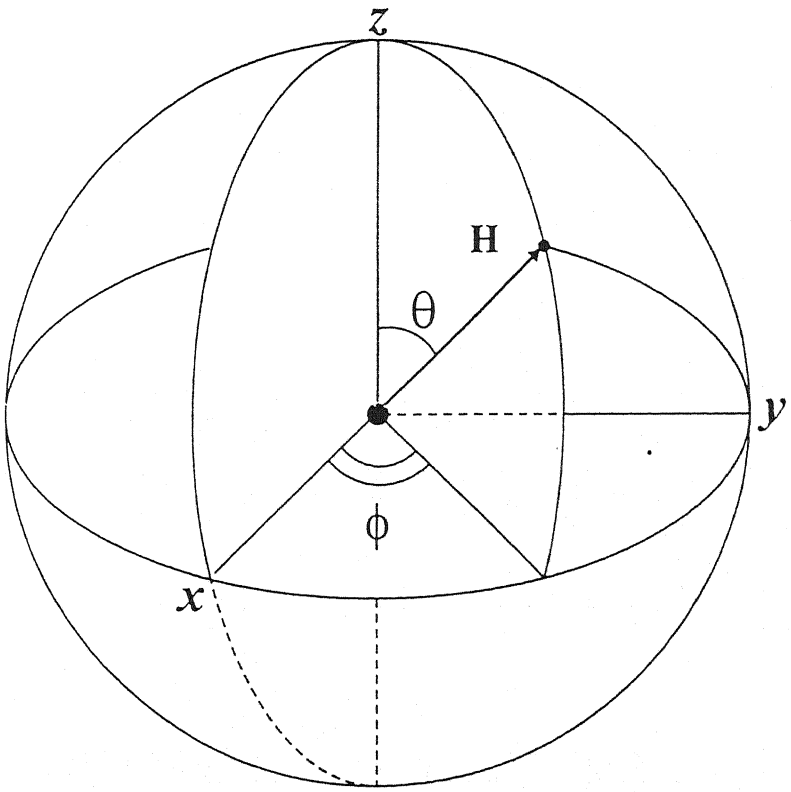

Fig2.1.

Axis system and polar coordinates showing the orientation of H

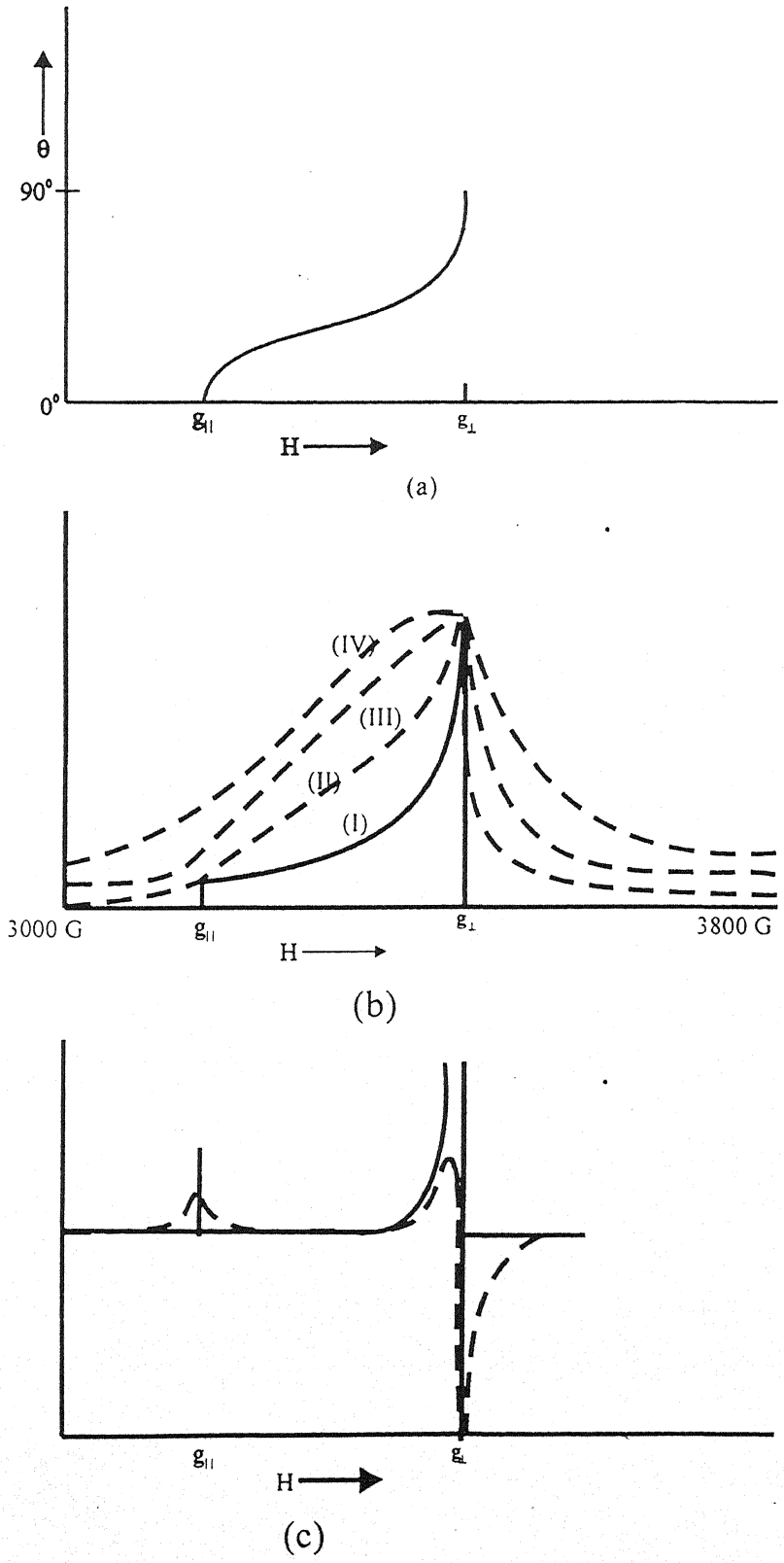

Fig. 2.2: Powder EPR Pattern for a system (S= 1/2, I=0) with axial symmetry ($g_{||}>g_{\perp}$)

(a) Angular dependence of the resonance filed position.

(b) Absorption line shapes: The δ-function line shape (I) is broadened by Lorentazian shape functions of width 10G (II), 50G (III) and 100G(IV) respectively.

(c) Derivative line shape: Solid is the δ-function line shape.

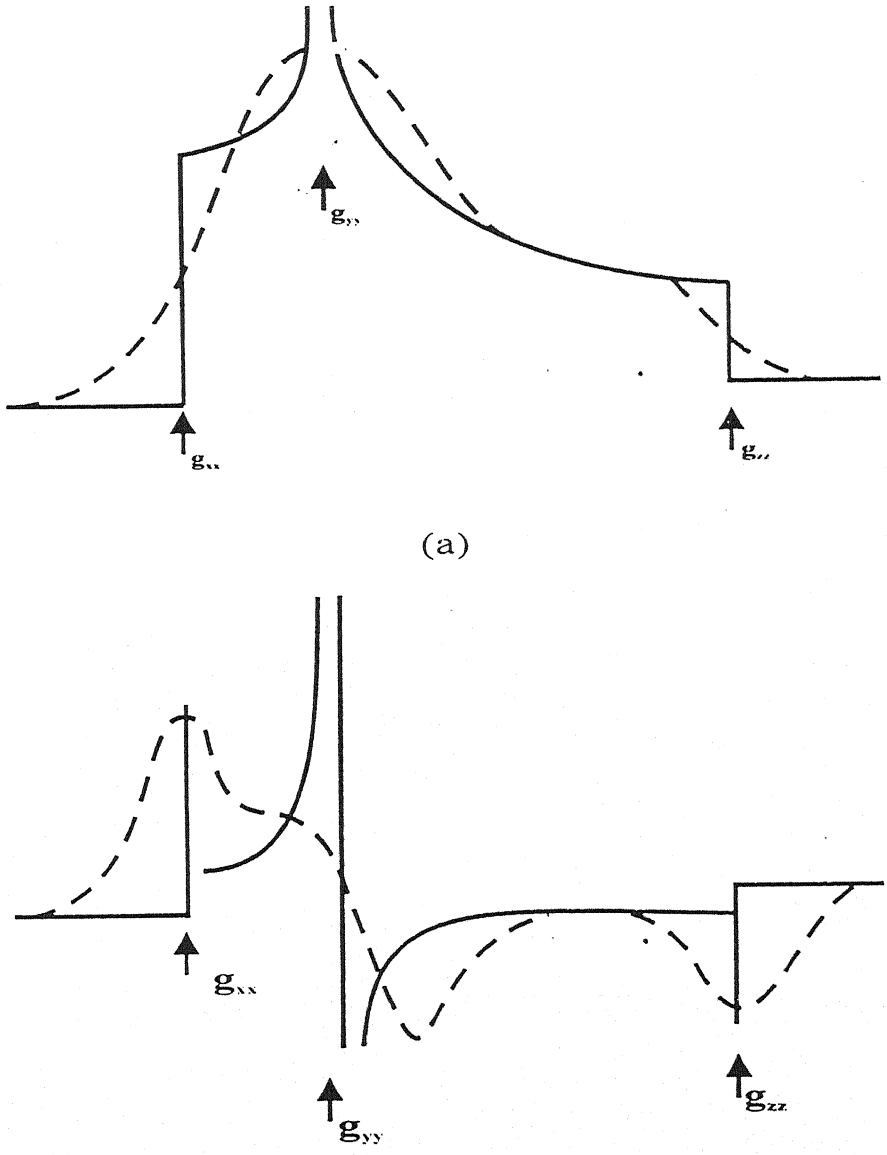

Fig. 2.3: Powder EPR Pattern for an orthorhombic g-tensor with I=0
(a) Absorption Curves
(b) Derivative Curves
The solid and broken lines are respectively δ-function line and broadened line.

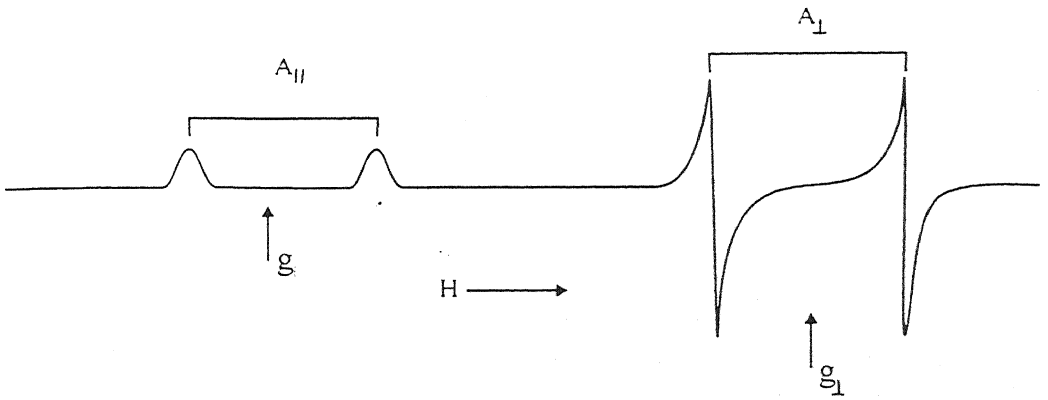

(a)

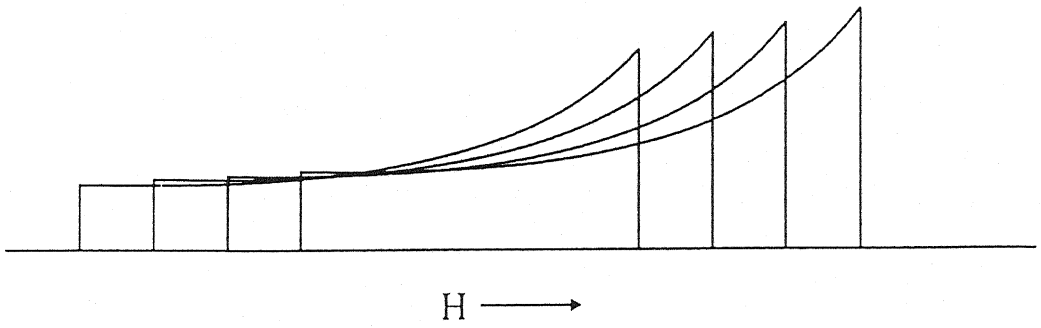

(b)

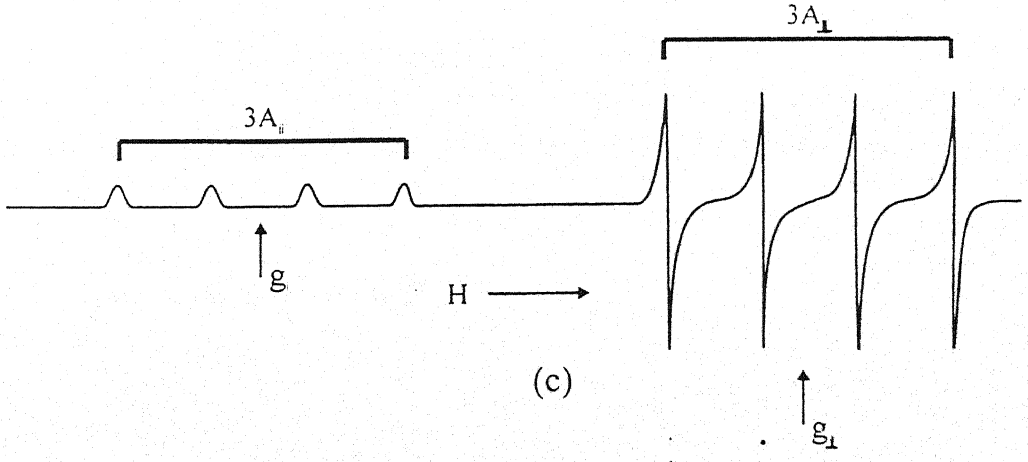

(c)

Fig. 2.4: Powder patterns for an S = 1/2 axial symmetry system ($g_{II} > g_{\perp}$) with isotropic A- tensor:
(a) Derivative line showing hyperfine interaction with I = 1/2.
(b) Idealised absorption positions for hyperfine interaction with I = 3/2
(c) Derivative line corresponding to (b) including some line broadening.

REFERENCES

1. J.H. Van Vlack and W.Q. Penny, Phil. Mag., **17**, 961 (1934).
2. R.R. Sharma, T.P. Das and R. Orbach, Phys. Rev., **149**, 257 (1966); 388 (1967) and **171**, 378 (1968).
3. P.A. Narayana, Phys. Rev. Lett., **B10**, 2676 (1974).
4. R. Chatterjee, M.R. Smith and H.A. Buckmaster, Canad. J. Phys., **54**, 1224 (1976).
5. H. Watanabe, Progr. Theor, Phys., **18**, 405 (1957).
6. A Abragam and M.H.L. Pryce, Proc. Roy. Soc., **A205**, 135 (1951).
7. S.A. Al'tshuler, B.M. Kozyrev. "Electron Paramagnetic Resonance", Academic Press, New York (1964).
8. R.S. Anderson, "Electron Spin Resonance", Methods of Experimental Physics, **3**, 441 (1962).
9. R.S. Alger, Electron Paramagnetic Resonance, Techniques and Applications, Inter-science Publications, John Wiley and Sons, New York, London, Sydney (1968).
10. A. Abragam and B. Bleaney, "Electron paramagnetic Resonance of Transition Ions", Oxford University Press (Clarendon), Oxford (1970).
11. K.W.H. Stevens, Proc. Roy. Soc, **A219**, 542 (1953).
12. J. Owen., Discus. Faraday. Soc., **19**., 127 (1955).

13. J. Owen, Proc. Roy. Soc., **A227**, 183 (1955).

14. B. Bleaney, G.S. Bogle., A.H. Cooke, H.J. Duffus, M.C.M. O'Brien and K.W.H. Stevens, Proc., **A 68**, 57 (1955).

15. W. Low, Ann. New York Acad. Sci., **72**, 69 (1958).

16. W. Low, Phys. Rev., **101**, 1827 (1956).

17. M. Tinkham, Proc. Roy. Soc., **A 236**, 535 and 549 (1956).

18. W. Low, Phys. Rev. **109**, 865 (1958).

19. W. Low and D. Shaltiel, J. Phys. Chem. Solids, **6**, 315 (1958).

20. R.S. Title, Phys. Rev., **131**, 623 (1963).

21. J. Owen and K.W.H. Stevens, Nature, **171**, 836 (1953).

22. S. Ogawa, J. Phys. Soc. Japan, **15**, 1475 (1960).

23. J.E. Drumheller, J. Chem. Phys., **38**, 970 (1963).

24. W.J., Weighle and W.H. Tanttila, J. Chem. Phys., **41**, 274 (1964).

25. T.L. Estle and W.C. Holton, Phys. Rev., **150**, 159 (1968).

26. H.A. Kramers, Proc. Amsterdam Acad. Sci., **33**, 959 (1930).

27. H.A. Jahn and E. Teller, Proc. Roy. Soc., **A161**, 220 (1937).

28. H.A. Jahn, Proc. Roy. Soc., **A 164**, 117 (1938).

29. J.H. Van Vleck, J. Chem. Phys., **7**, 72 (1939).

30. B. Bleaney and K.D. Bowers, Proc. Phys. Soc., **A65**, 667 (1952).

31. D. Biji and A.C. Ross-Innes, Proc. Phys. Soc., **A66**, 954 (1953).

32. B. Bleaney, K.D. Bowers, and R.S. Trenam, Proc. Roy. Soc., **A 228**, 157 (1955).

33. J.A. Giordmaine, L.E. Alsop, F.R. Nash and C.H. Townes, Phys. Rev., **109**, 302 (1958).

34. G.E. Pake, "Paramagnetic Resonance", Benjamin, New York (1962).

35. W. Low, "Paramagnetic Resonance in Solids", Solid State Physics Suppl., **2**, 150 (1960).

36. J.H. Van Vlack, Phys. Rev., **74**, 1168 (1948).

37. M.H.L., Pryce and K.W.H. Stevens, Proc. Phys Soc., **A63**, 36 (1950).

38. H.M. McConnell, J. Chem. Phys., **25**, 709 (1956).

39. D. Kivelson, J. Chem. Phys., **27**, 1087 (1957): **33**, 1094 (1960).

40. R. Wilson, D. Kivelson, J. Chem. Phys., **44, 154, 4440, 4445** (1966).

41. P.S. Hubbard, Phys. Rev., **131**, 1155 (1962).

42. J.H. Van Vleck, Phys. Rev., **57**, 426 (1940).

43. R.Orbach, Proc. Phys. Soc., **A77**, 821 (1961).

44. D. Kivelson, J. Chem. Phys., **45**, 1324 (1966).

45. F.J. Adrian, J. Colloid Interface Sci., **26**, 317 (1968).

46. P.H. Kasai and R.J. Bishop, Jr. in Zeolite Chemistry and Washington, E.C.(1976), p. 350.

47. W.N. Delgass, G.L. Haller, R. Kellerman and J.H. Lunsford, "Spectroscopy in Heterogeneous Catalysis", Academic Press, New York (1979), p. 183.

48. F.K. Kneubuhl, J. Chem. Phys., **33**, 1074 (1960).

49. C.P. Slichter, "Principles of Magnetic Resonance" (second revised and expanded edition), Springer-Verlag, Berlin (1980), p. 259.

50. C.A. McDowell, P. Raghunathan and J.C. Tait, J. Chem. Phys., **59**, 5858 (1973).

51. B. Blaney, Proc. Phys. Soc., London **75**, 621 (1960).

52. T. Vangard and R. Assa, "Paramagnetic Resonance", Vol., 2, Ed. W. Low, Academic Press, New York (1963), p. 509.

53. A Isomoto, H. Watari and M. Kotani, J. Phys. Soc. Japan, **29**, 1571 (1970).

54. H.M. McConnell and B.G. McFarland, Quart. Rev. Biophys., **3**, 91 (1970).

55. C.P. Poole, Jr., "Electron Spin Resonance", Interscience, New York (1967), p. 778.

56. Reference 21, p. 783.

57. J. Maruani, Chem. Phys. Lett., PS7PS, 29 (1970).

58. A. Abragam, "The Principles of Nuclear Magnetism", Clarendon Press, Oxford (1961), p. 220.

59. See, for example, (a) R. Lefebvre and J. Maruani, J. Chem. Phys., **42**, 1480 and 1496; (b) R. Breslow and F.J. Owens, Chem. Phys. Lett., **16**, 20 (1972) and references therein (c).

CHAPTER – 3

EXPERIMENTAL TECHNIQUES

3.1 ELECTRON PARAMAGNETIC RESONANCE (EPR)

EPR spectra were recorded on a Varian E-line century series spectrometer model E- 109 at Indian Institute of Technology, Kanpur. The spectrometer operates at X-band frequency (9.4 GHz). All the EPR spectra have been recorded with 100 kHz field modulation. The maximum power available with this spectrometer is 200 mW. The recording of EPR spectra only in absorption mode is possible and the first as well as the second derivative of absorption signal can be recorded. The schematic diagram of the EPR spectrometer is shown in Fig. 3.1. Rectangular cavity E-231 which operates in TE_{102} mode with unloaded Q > 7000 is used throughout the experiments. The field stability of the spectrometer after stabilization of the order of 10 ppm with temperature coefficient of 2 ppm/^{0}C is between 300 mT and 1T. The signal to noise ratio with E-231 cavity at 100 kHz field modulation is approximately equal to 180.

For EPR studies with single crystals it is required to know the crystal field (X, Y, Z) axis. For this purpose a two axes goniometer (Fig. 3.2) is used which provides a possibility of rotation of the magnetic field in any desired plane of the crystal. The X, Y, Z were determined employing the following method. The crystal was rotated first independently about a horizontal and

a vertical axis and a particular orientation was searched where the spread of the fine structure was maximum. Thus knowing one direction of maximal spread in fine structure spread were searched in a plane normal to the first direction of maximal spread. The directions are referred to Z, Y and X according to the spread of spectrum.

Once the axes is known the crystal is cut to facilitate the angular rotation of the crystal about a desired direction. The Varian model E- 229 goniometer permits an accurate rotation of samples in steps of 1^0. Powder samples were filled in quartz sample tube with typical outer diameter (OD) 4mm. For liquid samples either such sample tubes or a flat quartz liquid sample cell was used as per need. Spectra of liquid nitrogen temperature (LNT) were recorded with the Varian model E257/WL-257 variable temperature accessory automatically controls the sample temperatures within the range of 573 ^{0}K to 88 ^{0}K. It provides means to maintain the desired temperature with an accuracy better than 1 ^{0}K. For attaining the temperature of boiling liquid nitrogen (LNT) a liquid nitrogen quartz Dewar compatible with-231 cavity, provided with a cold finger, was used. Typical designs of sample tube and dewar are shown in Fig. 3.3. The actual temperature at the sample was measured with the help of an indicator using a copper constantan thermocouple in contact with the sample. The

overall accuracy of the measured temperature is 1K. The temperature stability at the sample was found to be within ± 1^0K, after stabilization.

3.2 X-RAY DIFFRACTION (XRD)

The samples were examined by XRD, using ISO Debye Flex Powder Diffractometer Model 2002 from Rich and Seifert Company FRG. The diffractometer uses CuK α radiation (λ = 1.5418 $\overset{0}{A}$) obtained from a copper target using an inbuilt Ni-monochomating filter (density 0.019 g/cm^3, thickness 0.021 mm). The diffractograms were taken in the range 2θ = 20^0 to 90^0 for all the samples, with the following conditions.

1. Scan speed= 3 degree per min. (in 2 θ)
2. Chart speed = 15 mm per minutes
3. Counts per min (CPM) = 10 K
4. Time constant = 10 sec.
5. Accelerating voltage /current = 30 KV/20mA.

The existence of various peaks in the XRD patterns was used to identify the phases present in the samples. The details of identification of phases are based on intensity variation semi empirical method which will be discussed in the relevant chapters.

The schematic diagram of the XRD is shown in Fig. 3.4. Diffractometer designed somewhat like a Debye-Scherrer camera, except that a movable counter replaces the strip of film. In both instruments, essentially monochromatic radiation is used and the X-ray detector (film or counter) placed on the circumference of a circle centered on the powder specimen. A powder specimen C. in the form of a flat plate, supported on a table H, which can be rotated about an axis O perpendicular to the plane of the drawing. The X-ray source S, the line focal spot on the target T of the X-ray tube S is also normal to the plane of the drawing and therefore parallel to the diffractometer axis O. X-ray diverge from this source and diffracted by the specimen to form a convergent diffracted beam which comes to a focus at the slit F and then enter the counter G. A and B are special slits which define and collimate the incident and diffracted beams. The filter is usually placed in a special holder (not shown) in the diffracted, rather than the incident, beam; a filter in the diffracted beam not only serves its primary function (suppression of K radiation) but also decrease background radiation originating in the specimen.

The receiving slits and counter are supported on the carriage E, which may be rotated about the axis 0 and whose angular position 2 may be read on the graduated scale K. The supports E and H are mechanically coupled so that a rotation of the counter

through 2x degrees automatically accompanied by rotation of the specimen through X degrees. This coupling ensures that the angles of incidence on, and reflection from, the flat specimen will always be equal to one another and equal to half the total angle of diffraction, an arrangement necessary to preserve focusing conditions. The counter may be power-driven at a constant angular velocity about the diffractometer axis or moved by hand to any desired angular position.

3.3 SCANNING ELECTRON MICROSCOPE (SEM)

The scanning electron micrographs of the samples coated with gold were taken by the JEOL scanning electron microscope JSM-840, equipped with a detector connected to a PC on which the KEVEX Quantex Software is installed. By operating the JEOL JSM-840A in analytical mode and detecting the emitted X-Ray by Kevex detector, the quantitative analysis of the samples is made possible. The morphological studies are carried out using SEM studies for all the samples of pure, VO^{2+}, Mn^{2+} and Cu^{2+} doped ceramics.

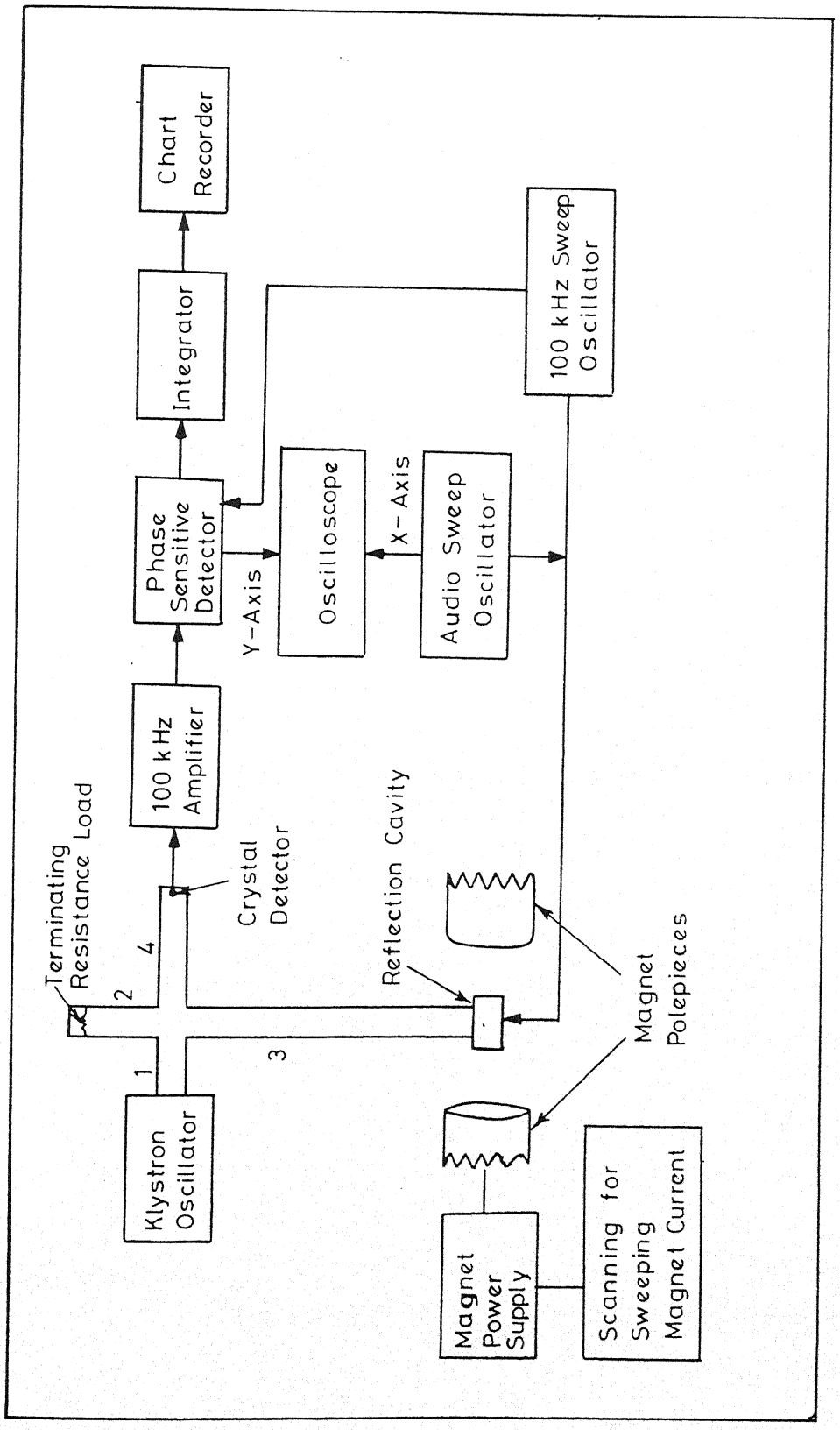

Fig. 3.1: Block diagram of the EPR spectrometer.

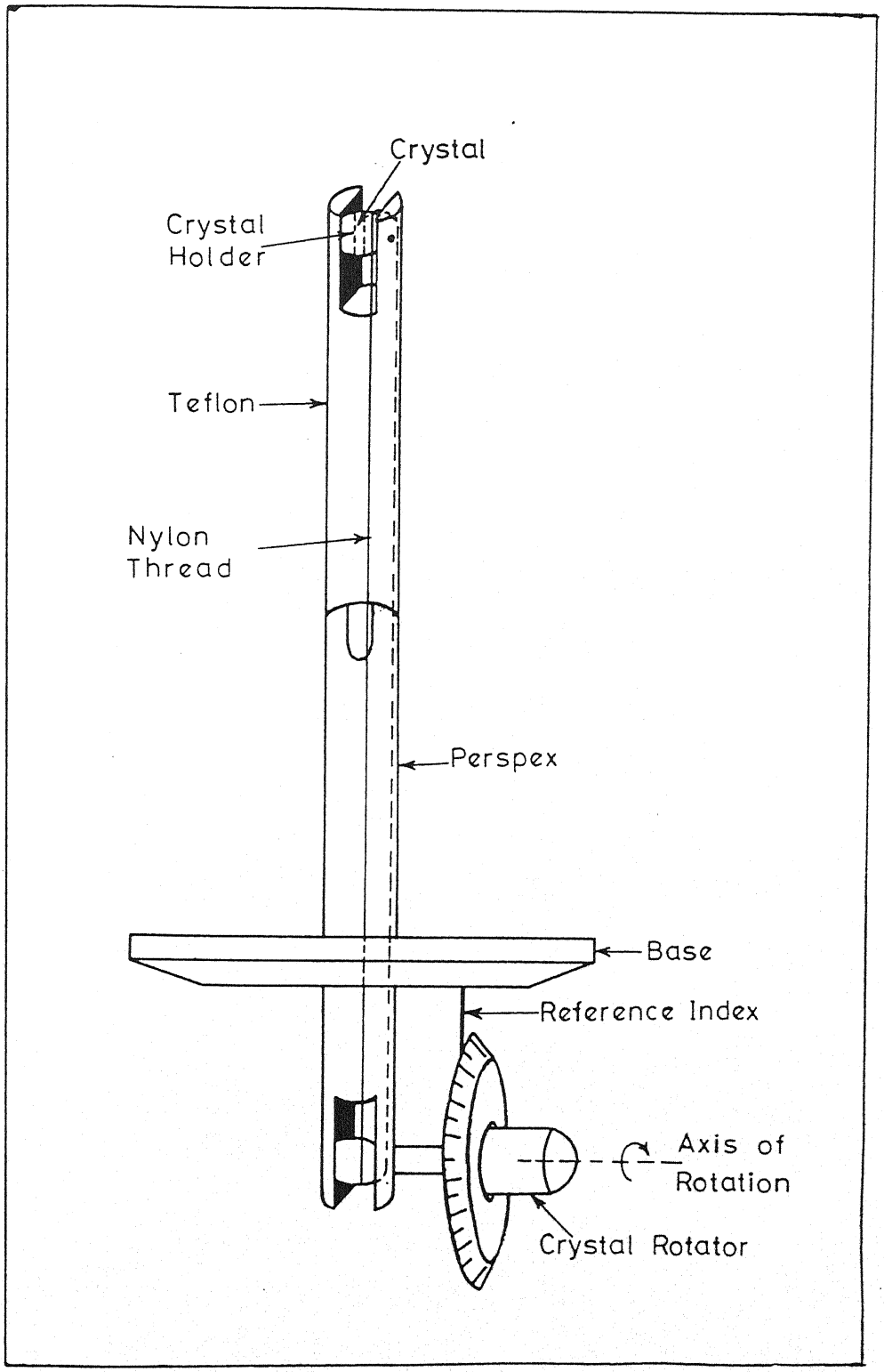

Fig. 3.2: Device to rotate the single crystal inside the cavity about a horizontal axis.

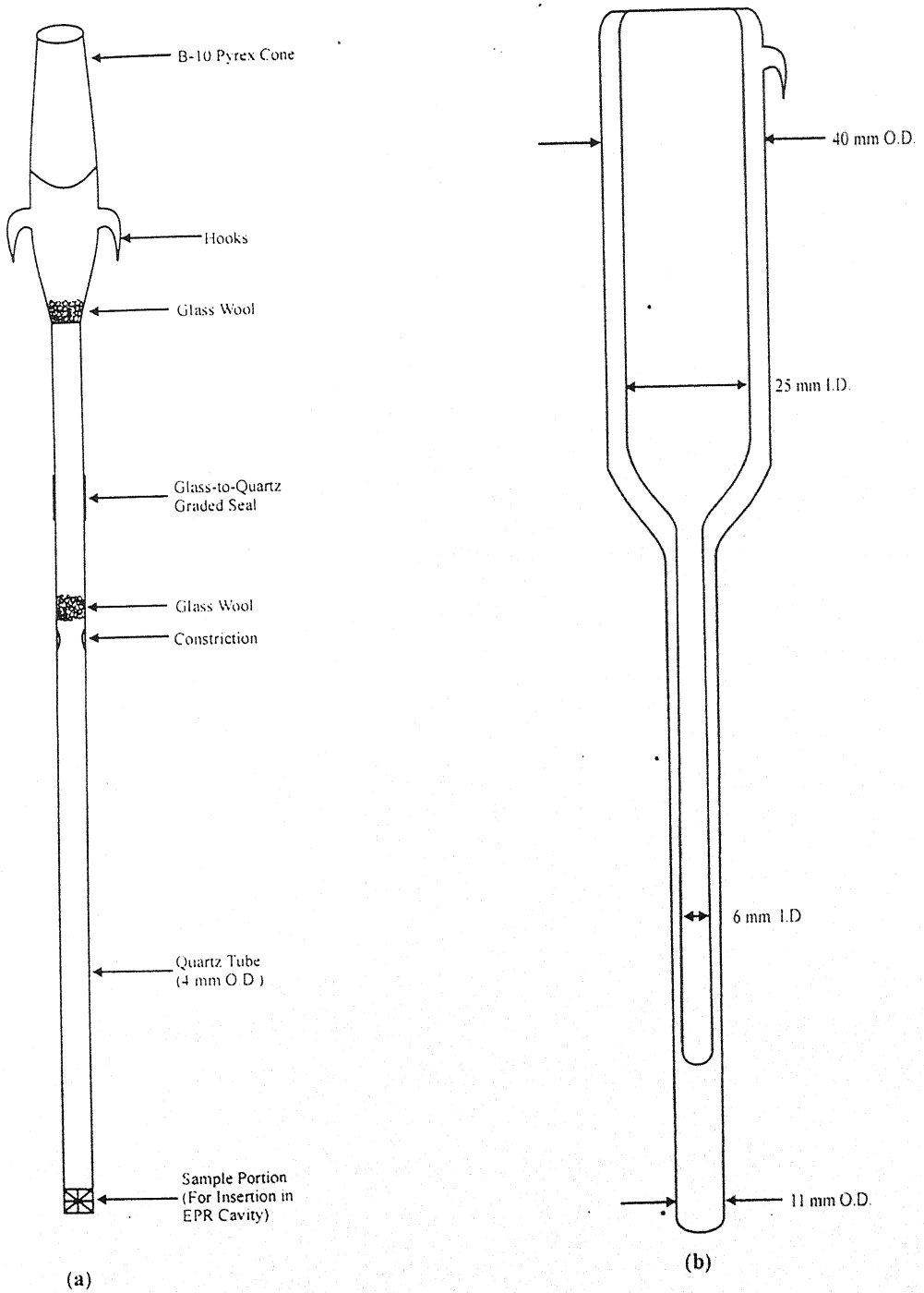

Fig. 3.3 (a) A typical sample tube used in the EPR experiments
(b) Quartz liquid nitrogen dewar used for the EPR measurements.

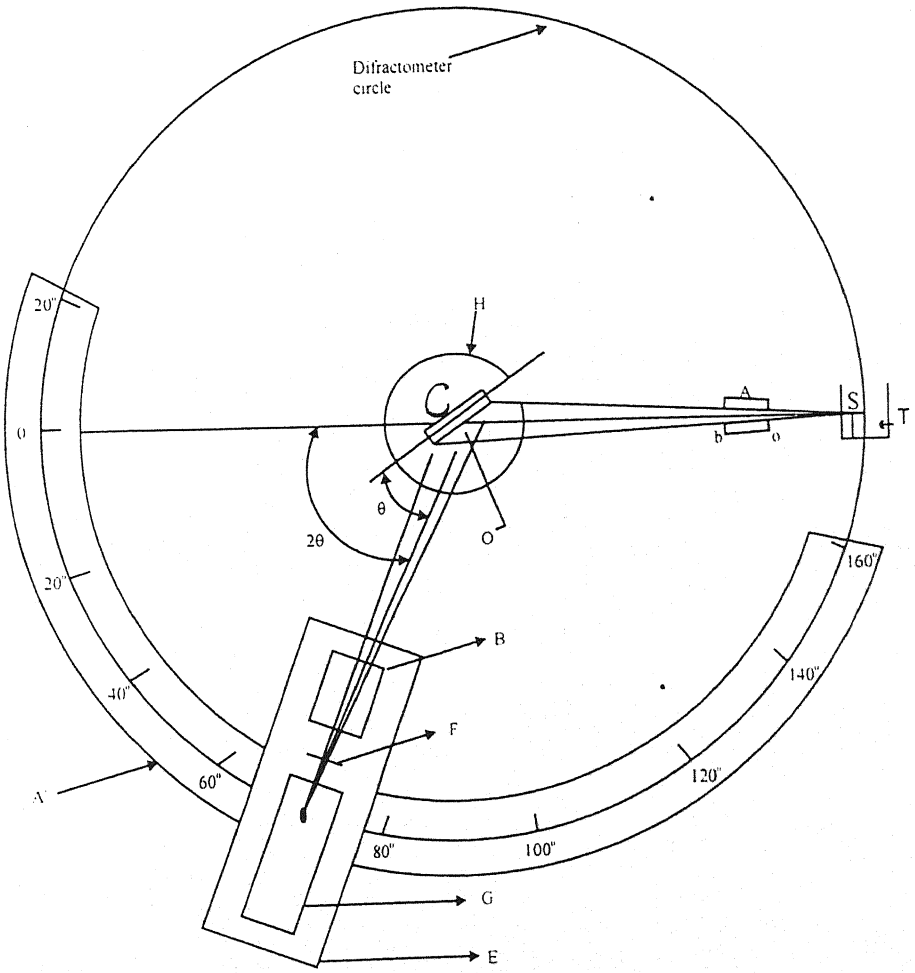

Fig 3.4: X-ray diffractometer (Schematic)

CHAPTER – 4

EXPERIMENTAL INVESTIGATIONS ON $(ZrO_2)_{0.8}(Y_2O_3)_{0.2}$

4.1 INTRODUCTION

Stabilized zirconia (ZrO_2) has been widely used for many years. The ever increasing applications of the oxide in high technology ceramics, particularly in wear parts and as solid electrolytes, has attracted a great deal of attention [1]. Owing to their important applications as high temperature materials, zirconia ceramics have received considerable attention from the view point of their sintering behaviour and control of the microstructures which develop during the sintering process, so that the resulting materials meet the requirements needed for these applications. In order to produce high performance zirconia cermics, solid state sintering has traditionally been adopted as the favoured fabrication route. This route has often required the use for high firing temperature for the achievement of high density in zirconia materials. Several approaches have proved to be effective in reducing these temperatures. Amongst these approaches, the use of reactive powders such as CaO, Y_2O_3 or rare earth oxides has received particular attention [5]. It has been reported that yitria (Y_2O_3) stabilized zirconia compact sintered at 1200°C are found to have the highest density [3]. Zirconia-based coatings are commonly used as thermal barrier coatings (TBCs), are increasingly being employed to provide thermal insulation to

critical air-cooled mechanical components of gas turbine engines, thereby improving their efficiency [4]. There are three well defined polymorphs in ZrO_2 based ceramic materials namely, monoclinic, tetragonal and cubic phases [5]. It has been stabilized in cubic phase by the addition of variable amounts of R_2O_3 (R= rare earth or yitrium) or CaO. One of the best stabilizers is Y_2O_3.

The phase diagram of the $ZrO_2 - Y_2O_3$ system indicates that the cubic phase exists in the range of composition from 6 to 40 mole % of Y_2O_3 [6]. In the case of $ZrO_2 - Y_2O_3$ solid solution the stabilization of cubic phase takes place when the concentration of Y_2O_3 is not more than 10 mole %.

In the present chapter, the polycrystalline ceramic samples of $(ZrO_2)_{0.8} - (Y_2O_3)_{0.2}$ pure as well as doped with a 1 wt% concentration of trasition (V, Mn and Cu), elements were synthesized in order to investigate their structural and magnetic features using x-ray diffraction (XRD), scanning electron microscopy (SEM) and electron paramagnetic resonance (EPR). EPR is hoped to provide information about the valence state of the transition metal ions doped in the ceramic and about the local environment of the doped transtion metal ions. The structural information obtained from XRD and electron microsocpoy can be correlated with the EPR results together more understanding regarding the microstructural and other properties of the ceramics.

4.2 EXPERIMENTAL

The synthesis of polycrystalline ceramic samples of required stoichiometry in pure as well as doped form has been done using standard high temperature solid state reaction technique. This technique involves grinding of the constituents together followed by pelletization and sintering at high temperature. High purity (99.99%) Zr and Y from Aldrich (USA) in the desired stoichiometry for $(ZrO_2)_{0.8}(Y_2O_3)_{0.2}$ were taken. The transition metal impurities were taken in the following form for the purpose of doping. $Cu(NO_3)3H_2O$, $MnCl_24H_2O$, V_2O_5. A fixed concnetratoin (1 wt%) of the impurity complex was added to the base ceramic. All the constitutents were well mixed together in an agate mortar and pestle and then pelletized in the form of thin cylindrical pellets under the applicaton of a pressure of 6 ton/cm^2. The pelletized materials were kept for sintering at a temperature of 1550^{0}C in a glower furnace for 24 hours. Thus formed materials were then characterized through x-ray diffraction (XRD), scanning electron microscopy (SEM) and electron paramagnetic resonance (EPR) techniques in order to investigate their structural and magnetic properties. The sample code and the composition are given in Table 4.I.

The XRD patterns of all the samples were recorded using a Rich Seifert Isodebyflex 2002 diffactometer and Cu-Kα radiation with monochromator. The recording conditions were scan speed (ss) 3^0/min, Time constant Tc = 10 Sec., count per minute (CPM) 10K, current/voltage = 20 MA/30KV. The SEM micrographs were taken using JEOL 840 SEM. All the micrographs were taken at a fixed magnification of x 4000 at 15 KV. EPR measurements were done with the help of an X-band EPR spectrometer (Varian E-109) using 100 Khz phase sensitive detection. The phase composition of the samples has been evaluated using the XRD studies .The size of grains and morphological features have been studied with the help of SEM. EPR measurements were carried out to examine the magnetic state of the impurity ion and various changes during and after the synthesis of the samples. The results obtained through the above techniques are presented and discussed here.

4.3 RESULTS AND DISCUSSION

(i) X-ray Diffraction:

Figure 4.1 (a) shows the x-ray diffraction (XRD) pattern for sample SZYP. It is evident that the XRD pattern consists of three phases namely, monoclinic, tetragonal and cubic. After indexing the observed XRD pattern d values are calculated. The observed

values of d (d_{obs}), calculated values (d_{cal}), the miller indices and relative intensities of the peaks are collated in Table 4.II. The values of the d_{obs} are calculated using Bragg's Formula:

$$d_{obs} = \frac{\lambda}{2 \sin\theta} \qquad (4.3.1)$$

where λ is the wavelength of Cu-Kα, θ is the diffraction angle and d_{obs} is the interplaner distance.

The values of d_{cal} have been calculated using the following expressions and lattice parameters from literature [7,8]:

$$for\ cubic\ \frac{1}{d^2_{cal}} = \frac{h^2 + k^2 + l^2}{a^2} \qquad (4.3.2.)$$

$$for\ tetragonal\ \frac{1}{d^2_{cal}} = \frac{h^2 + k^2}{a^2} + \frac{l^2}{c^2} \qquad (4.3.3.)$$

$$for\ monoclinic\ \frac{1}{d^2_{cal}} = \frac{1}{\sin^2\beta}\left[\frac{h^2}{a^2} + \frac{k^2 \sin^2(\beta)}{b^2} + \frac{l^2}{c^2} - \frac{2hl}{ac}\cos(\beta)\right] \qquad (4.3.4.)$$

The phase composition for the samples has been evaluated using intensity variation semiempirical method [7,8].

In order to make quantitative analysis of the monoclinic, tetragonal and cubic phases existing in the samples, we have used the following expressions:-

$$I_M = \left[\frac{I_m(1\,\bar{1}\,\bar{1}) + I_m(111)}{I_m(1\,\bar{1}\,\bar{1}) + I_m(111) + I_{t,c}(111)}\right] \times 100 \qquad (4.3.5.)$$

$$I_T = (I - I_M)\left[\frac{I_t(400) + I_t(004)}{I_t(400) + I_t(004) + I_c(400)}\right] \times 100 \quad (4.3.6)$$

and $I_c+I_m+I_T = 100$

were I_M, I_T and I_C are the percentages of monoclinic, tetragonal and cubic phases respectively. We have assumed that the intensity of various peaks of respective phases represent the amount of the particular phases, for example intensity of reflexion (111) represents the amount of monoclinic phase.[24]

Fig .4.1 (b to d) depict the XRD patterns for samples SZYV, SZYMn and SZYCu. Two samples exhibit essentially the same kind of patterns except SZYV sample. The percentage of phase composition of the samples has been estimated using earlier expressions and the values obtained are given in Table – 4.III.

From the above crystallographic data, we can say that all the samples exhibit monolicnic phase as the dominant phase. It is also worthmentioning that in earlier studies ZrO_2 doped with 12 mol % of Y_2O_3 were found to contain almost monoclinic phase [5].

(ii) Scanning Electron Microscopy Studies:

The SEM micrographs for all the samples are shown in Fig.4.2(a-d). It is evident from the micrographs that all the samples comprise two major kinds of phases. One of them being brighter (white), while the other is darker (black). At the time of preparation of these samples for SEM studies, we have observed

an interesting fact that during the sputtering of Ag metal upon the samples, there was illumination of light. We can attribute this phoneomenon to luminescences of materials. All the samples seem to have the nearly uniform microstructure. The average grain size varies from sample to sample. Generally, sintering temperature, duration preparation methods, particle size of unsintered mixture etc. are the parameters which affect the microstructure of the final product. It should be stressed here that we have subjected a fixed heat treatment for sintering to all the samples. Therefore, the variation in average grain size may be attributed to the effect of various dopants.[22]

It may also be noted from these micrographs that all samples display an overall increase in grain size as compared to the pure sample SZYP. This increase probably results due to the presence of impurity ions which favours the particles assemblage of doped samples. The grain size estimate obtained from the SEM pictures indicate two ranges of particle-size; large grain (>5 μm) and smaller grains (<1 μm).

(iii) Electron paramagnetic resonance studies:

(a) Pure Sample SZYP:

The EPR spectrum of the powdered (finely crushed) undoped sample SZYP comprise a narrow resonance line near $g \cong 2$

superimposed on a broad EPR signal spectrum for pure sample (SZYP). Fig. 4.3 shows EPR spectrum of SZYP at RT. As mentioned earlier we have used 99.99% pure ZrO_2 for synthesizing the SZYP samples, therefore the presence of any extrinsic paramagnetic impurity is not expected. However the sample indicates the presence of some paramagnetic centers in the synthesized material SZYP. It is not possible to identify the exact nature and cause of these centers. The narrow signal is situated at g_{eff} = 1.975± 0.005 and the width of this signal ΔH is ≅ 25±3G. The width of the broad signal is ≅290G and is situated around g_{eff} ≅2.05. These paramagnetic centers may be artefact of synthesis process since these signals are present in all the samples prepared for the present study. The interesting aspect of these signals is that their widths and positions remain essentially temperature independent between RT and LNT. The narrow signal is marked by p and its position is denoted by g_p(Table 4.IV) where the parameters obtained from EPR study are collated. As revealed by X-ray the SZYP samples comprises mainly of monoclinic and tetragonal phases. The two signals may result from these phases present in the synthesized sample.

(b) Vanadium doped sample SZYV:

Vanadium has three oxidation states which are of interest from the EPR point of view. V^{4+} is isoelectronic with Ti^{3+} and

favours an octahedral coordination with oxygen. However, and V-O bond is usually much shorter than the rest in the VO_6 octahedron. Thus V^{4+} is subjected to a crystal field of compressed tetragonal character. The representative of factors are : $g_{||} = 1.914$ $g_{|} = 1.957$ [20]. Tetravalent vanadium is found to form VO^{2+} (Vanadyl) ion (i.e. V^{4+} in close association with O^-). Favourably Vanadyl ion and its complexes contain one unpaired electron to give EPR spectrum. The g factor lies between 1.9 and 2. In magnetically dilute system V^{4+} and VQ^{2+} show a fairly large hyperfine splitting due to isotope ^{51}V which has nuclear spin I = 7/2 and is 99.8% abundant. The EPR results can be explained in terms of the spin Hamiltanian of the following type with S = 1/2 and I = 7/2.

$$\mathcal{H} = \beta \vec{S}.\tilde{g}.\vec{H} + \vec{I}.\tilde{A}.\vec{S}. \qquad (4.3.7)$$

The g and A parameters are anistropic, the later being more anistropic in nature. Typical values of $A_{||} = A\dot{z} \cong 150 \times 10^{-4}$ Cm^{-1} and $A_{\perp}$ $(= A_x + A_y) \cong 50 \times 10^{-4}$ cm^{-1}. Trivalent vandadium V^{3+} has an electronic structure $3d^2$. The ^3F free ion ground state is split by an octahedral coordination leaving an orbital triplet lowest. The trigonal component of crystal field further splits this to give an orbital singlet ground state. The three fold spin degencracy is lifted by the combined effect of trigonal field and spin orbit coupling. EPR signal may be observed form $m_s = \pm 1$ states with

$g_{||}$~1.9 and the resonance field (neglecting hyperfine structure) is given approximately by

$$B_0 = \frac{h\nu}{2g_{||}\beta \cos\theta} \qquad (4.3.8)$$

where θ is the angle between magnetic field and the trigonal axis [11].

The EPR spectrum of Vanadium doped samle SZYV is shown in Fig. 4.4. In the light of the above discussion the observed spectrum is attributed to the vanadyl form of the ion. The observed spectrum represents the typical powder spectra of vanadyl complexes with axial symmetry [9]. For the axial symmetry the resonance field for hyperfine structure is give by [14-16].

$$B_m = B_0 - \frac{km}{g\beta} - \left[I(I+1) - m^2\right]\frac{A_\perp^2 (A_{||}^2 + K^2)}{4B_0K^2 (g\beta)^2}$$

$$- \left(\frac{A_{||}^2 - A_\perp^2}{K}\right)^2 \left(\frac{g_{||}g_\perp}{g}\right)^2 \frac{m^2 \sin^2 2\theta}{8g^2 \beta^2 B_o} \qquad (4.3.9)$$

where $B_o = \frac{h\nu}{g\beta}$, $g^2 = g_{||}^2 \cos^2\theta + g_\perp^2 \sin^2\theta$

$$K^2g^2 = A_{||}^2 g_{||}^2 \cos^2\theta + A_\perp^2 g_\perp^2 \sin^2\theta.$$

m varies from 7/2 to – 7/2 and θ is the angle between V=0 bond of the vanadyl ion and the applied magnetic field B. Identifying the lines corresponding to $\theta = 0^0$ (II-spectrum) and

$\theta=90^0$ ($\perp$-spectrum) in the powder EPR spectrum shown in Fig.4.4. Spin Hamiltonian parameters viz g_{II}, $g_\perp$, A_{II} and $A_\perp$ have been calculated and are given in Table 4.IV along with other data. These parameters obtained for vanadyl complex in SZYV are in good agreement with those of vanadyl ions in axially compressed C_{4v} vanadyl complexes [16]. Therefore the vanadium impurity seems to enter the host lattice in the form of a vanadyl complex. The possible site may be Zr^{4+} having an octahedral environment of oxygen.

(c) Manganese doped sample SZYMn :

The EPR spectrum of manganese doped sample is shown in Fig. 4.5. In addition to the two signals observed for the undoped sample SZYP two more signals (marked as a and c in the Fig. 4.5) are observed. The positions are described by the effective g-values ($g_a \cong 2.1$ and $g_b \cong 2.0$) and the line widths are $\Delta H_a \cong 16G$ and $\Delta H_c \cong 25G$. Divalent manganese Mn^{2+} had d^5 electronic state and the free ion ground state is $^6S_{5/2}$. The 6 fold spin degeneracy is lifted by spin orbit coupling giving rise to there Kramers' doublets. In general three are (2S +1) = 5 allowed EPR transitions corresponding to M = ±1. Due to the nuclear spin I = 5/2 each fine structure transition shows a characteristic hyperfine splitting into six components corresponding to m = o. Therefore, a thirty line

spectrum is expected for Mn^{2+} in a crystal [9-15]. The observed structure less narrow line at g ≅ 2.2 could be attributed to an exchange narrowed EPR signal of Mn^{2+} impurities. Such single line EPR signal of Mn^{2+} provides indication that manganese forms a concentrated phase in the host matrix. This may result due to aggregates of manganese (II) complex formed in the host matrix similar to Suzuki phase in alkali halides [17]. The EPR parameters of the observed EPR signals corresponding to Fig. 4.5 for SZYMn are collated in Table 4.IV. The origin of the second signal at g≅2.1 is not known. It is interesting to compare these results with those reported by Stempi et al [18,24] for manganese doped single crystals of $(ZrO_2)_{0.8}(Y_2O_3)_{0.2}$. They have observed a six line spectrum at g≅2 with hyperfine parameter A ≅ 83G and attributed it to Mn^{2+} ion substituting either Zr^{4+} or Y^{3+} ions at lattice sites. Our results indicate that in SZYMn sample a phase separation of manganese complex occurs. However, this could be confirmed using X-ray and SEM studies because of inadequate resolution and low impurities concentration.

(d) Copper doped Sample SZYCu :

Powder EPR spectrum of copper doped sample is shown in Fig 4.6. As explained in earlier chapter Cu^{2+} with $3d^9$ configuration may be regarded as a single hole in the filled $3d^{10}$ configuration. Its EPR spectrum would be similar to d^1

configuration. Since the two naturally occurring isotopes of copper (^{63}Cu and ^{65}Cu) have nuclear spins I = 3/2, the EPR spectra are explained by the following spin Hamiltonian with S= 1/2 and I=3/2 [9,12].

$$\mathcal{H} = \beta.\vec{S}.\tilde{g}.\vec{H} + \vec{I}.\tilde{A}.\vec{S} \qquad (4.3.10)$$

In an axial crystalline field the position of resonance lines are expressed by eq. (4.3.8) given for the case of VO^{2+} ions with the difference that here m_I takes on values from 3/2 to –3/2. In the powdered sample one observes characteristic peaks corresponding to parallel (||, i.e. $\theta = 0^0$) and perpendicular (⊥, i.e. $\theta = 90^0$) orientations similar to the case of VO^{2+} ions in axial symmetry [15,16]. The || and ⊥ components are identified in the EPR spectrum of copper doped sample SZYCu shown in Fig. 4.6. The values of $g_{||}$, $g_{\perp}$, $A_{||}$ and $A_{\perp}$ are given in Table 4.IV. Since $g_{||} > g_{\perp} > 2$ hence the unpaired electron resides in dx^2-y^2 ground state orbital and the Cu^{2+} ion experiences a tetragonally distorted octahedral crystal field around it [15] in the host under study.

4.4 CONCLUSION

The results of EPR, SEM and XRD studies of $(ZrO_2)_{0.8}$ $(Y_2O_3)_{0.2}$ samples synthesized by solid state reaction route show

that the favorable phases are monoclinic and tetragonal. Small amounts of doped impurities of transition metal ions are not found to change the composition of the system noticeably. However, EPR studies reveal that vanadium and copper enter the host lattice in paramagnetic valence states. The vanadium impurity seems to form vanadyl complex and is believed to replace Zr^{4+} ions at octahedral sites. The copper ion is in Cu^{2+} state and its ground state is $d_{x^2-y^2}$.

The Cu^{2+} ion is subjected to an axially distorted octahedral crystalline field at the site of incorporation in the host lattice [20,21]. Mn^{2+} ion creates occurrence of trigonal distortion which is probably due to charge compensation requirements. The origin of broadening has been traced out to be due to the dipolar effect of impurity ions.

Table: 4.I: Sample codes and doped impurity:

S.N.	Sample	Doped impurity*	Stoichiometry of samples
1.	SZYP	P	$(ZrO_2)_{0.8}$ $(Y_2O_3)_{0.2}$
2.	SZYV	V_2O_5	"
3.	SZYMn	$MnCl_2$	"
4.	SZYCu	$Cu(NO_3)_2$	"

* The concentration of each dopant is 1 wt % of $(ZrO_2)_{0.8}$ $(Y_2O_3)_{0.2}$ and P stands for pure.

Table: 4.II :Crystallographic data estimated from XRD studies for SZYP samples (M= Monoclinic, T= Tetragonal and C= Cubic).

hkl	Phases	d_{obs} A^0	d_{cal} A^0	$(d_{obs}- d_{cal})$ A^0	$(I/I_o)_{obs}$ %
[110], [011] [111]	M	3.60	3.64	0.05	24
[11$\bar{1}$]	M	3.12	3.16	0.04	77
[111]	T, C	3.02	2.97	0.05	100
[111]	M	2.80	2.84	0.04	76
[200], [002]	M,C	2.59	2.56	0.03	30
[210]	M	2.30	2.28	0.02	8
[102]	M	2.17	2.18	0.01	21
[112]	T	2.06	2.10	0.04	10
[112]	M	1.98	2.01	0.03	20
[022]	M	1.86	1.85	0.01	70
[002], [220], [220]	T,C,M	1.80	1.81	0.01	72
[002], [300]	M	1.68	1.69	0.01	16
[013], [221]	M	1.64	1.64	0.00	38
[113], [311], [311], [131]	T,C,M	1.56	1.55	0.01	49
[222], [222], [311]	C, M	1.47	1.47	0.00	16
[132]	T	1.34	1.37	0.03	6
[104]	M	1.31	1.32	0.01	26
[400], [004]	C, T	1.29	1.28	0.01	16
[400]	C	1.26	1.26	0.00	16
---	-	1.22	1.23	0.01	10
[114]	T	1.21	1.21	0.00	20
[400]	T	1.10	1.10	0.00	11
[004]	T	1.09	1.09	0.00	9

Table 4.III: Shows the relative phase composition:

S.No.	Sample code	Relative concentration of phase (%)		
		M	T	C
1.	SZYP	61	33	6
2.	SZYV	65	30	5
3.	SZYMn	63	32	5
4.	SZYCu	62	32	6

M = Monoclinic, T= Tetragonal and C=Cubic

TABLE 4.IV

PARAMETERS DERIVED FROM EPR STUDIES

Sample Code	g values	Hyper fine parameters A (Gauss)	Line width ΔH (Gauss)
SZYP	$g_P = 1.975 \pm 0.005$		$\Delta H_P = 23\pm3$
	ga = 2.05±0.05		ΔHa = 2.90±20
SZYV	$g_P = 1.975\pm0.005$		
	$g_{\parallel} = 1.980\pm0.005$	$A_{\parallel} = 166$	Δ HP = 25±3
	$g_{\perp}=1.935\pm0.005$	$A_{\perp}= 66$	
SZYMn	$G_P = 1.975\pm0.005$		$\Delta H_P = 25\pm3$
	$g_a = 2.10\pm0.05$		ΔH = 16±4
	$g_C = 2.00\pm0.05$		$\Delta H_C= 25\pm2$
SZYCu	g_P 1.975±0.005	$A_{\parallel} = 56$, $A_{\perp} = 24$	Δ H = 22±3

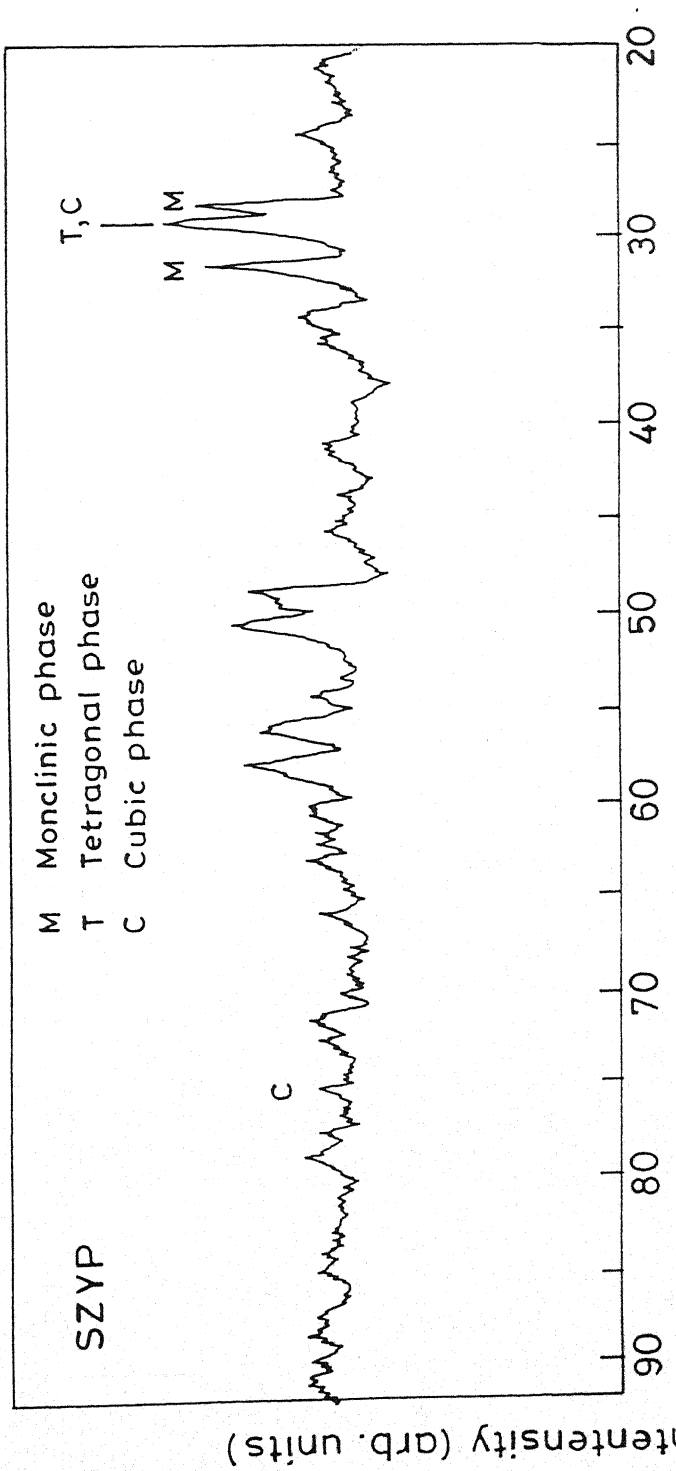

Fig. 4.1 (a): X-ray diffraction pattern of sample SZYP.

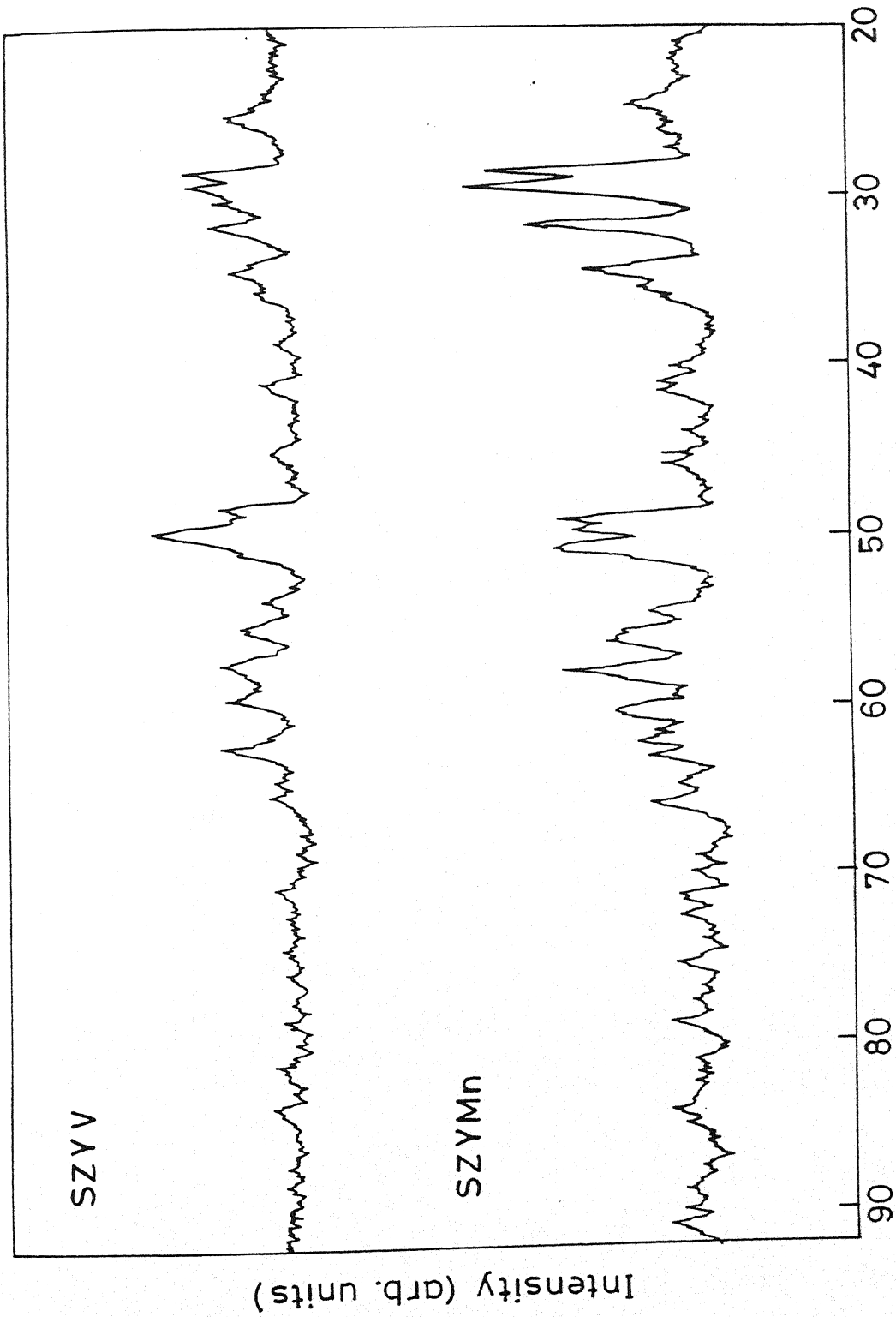

Fig. 4.1 (b & c) X-ray diffraction patterns of samples SZYV and SZYMn

Fig. 4.1 (d): X-ray diffraction pattern of sample SZCu.

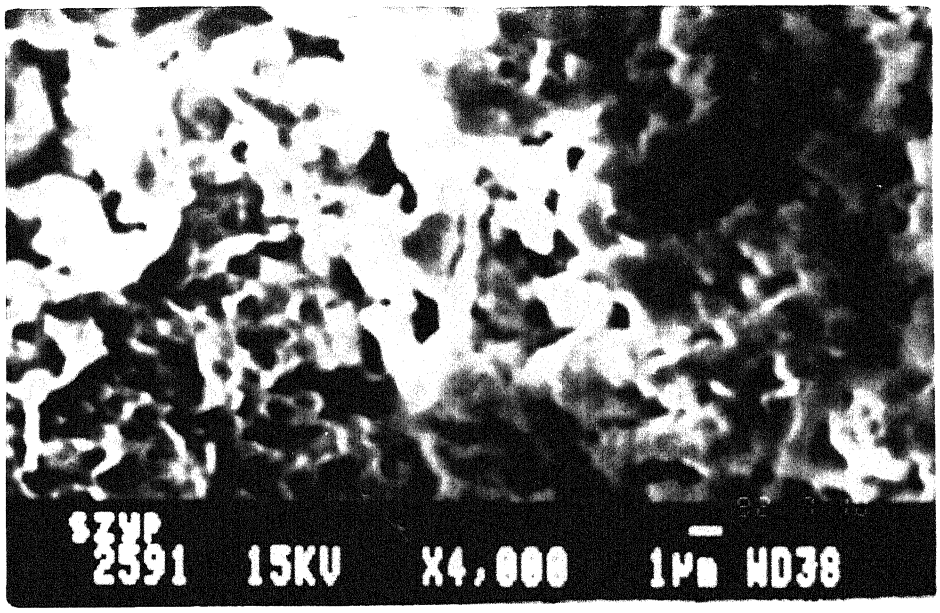

2591 15KV x4,000 1μm WD38

Fig. 4.2(a). SEM Micrograph of sample SZYP.

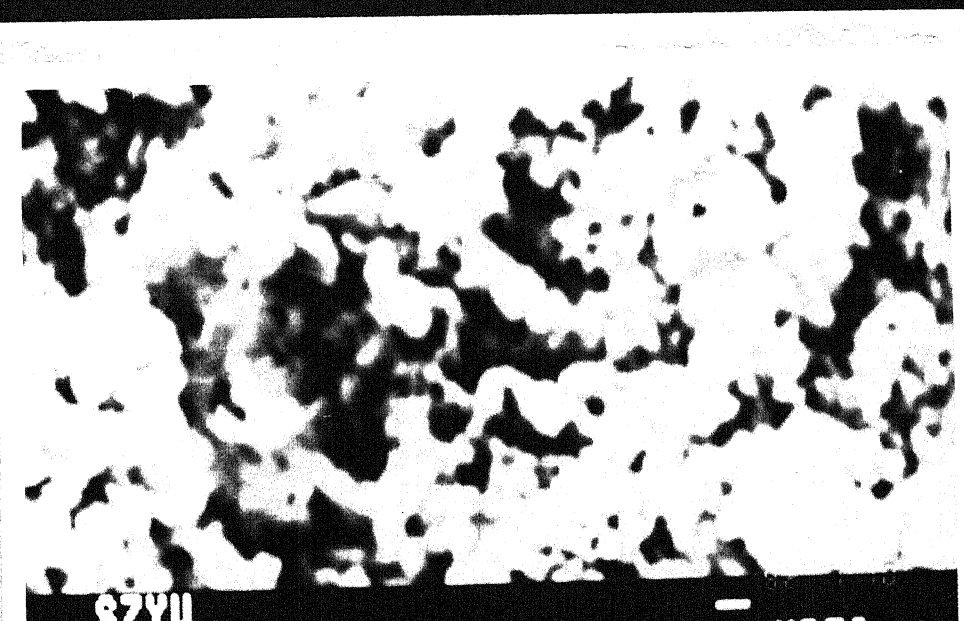

2600 15KV x4,000 1μm WD38

Fig. 4.2(b). SEM Micrograph of sample SZYV.

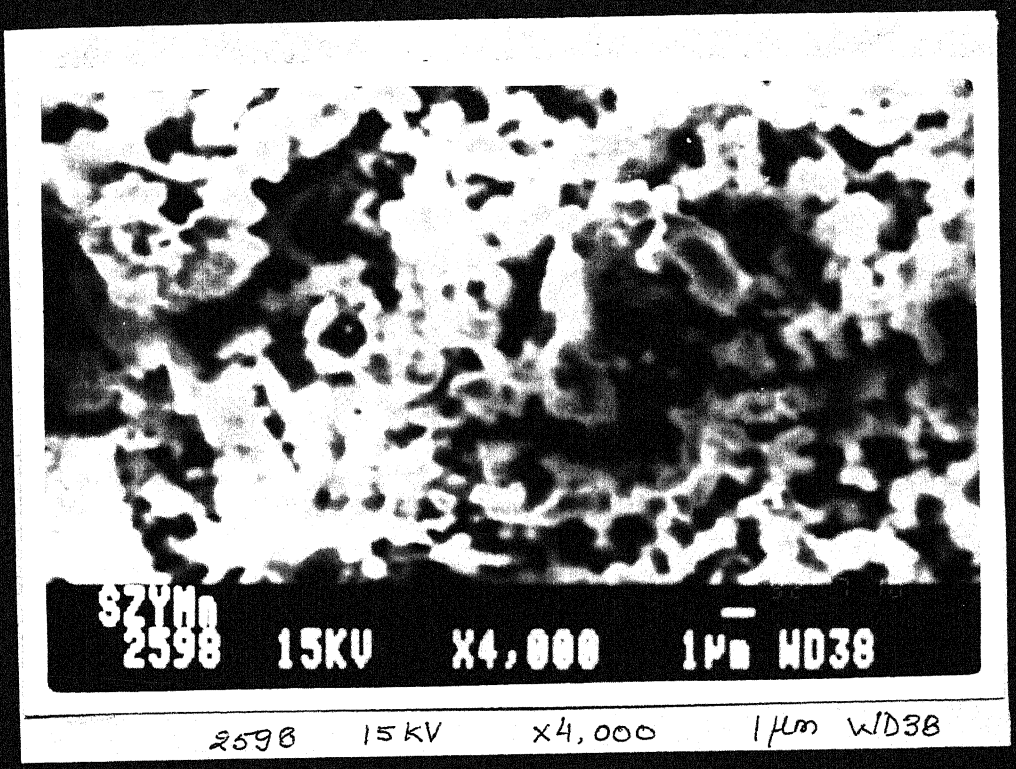

Fig. 4.2(c). SEM Micrograph of sample SZYMn.

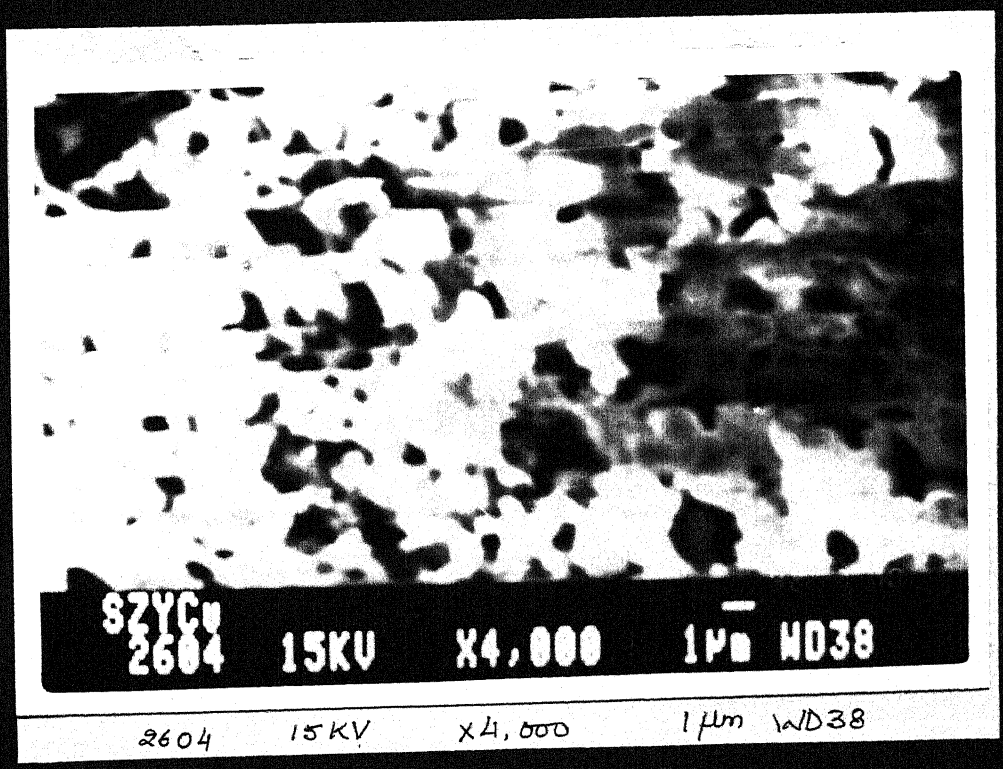

Fig. 4.2(d). SEM Micrograph of sample SZYCu.

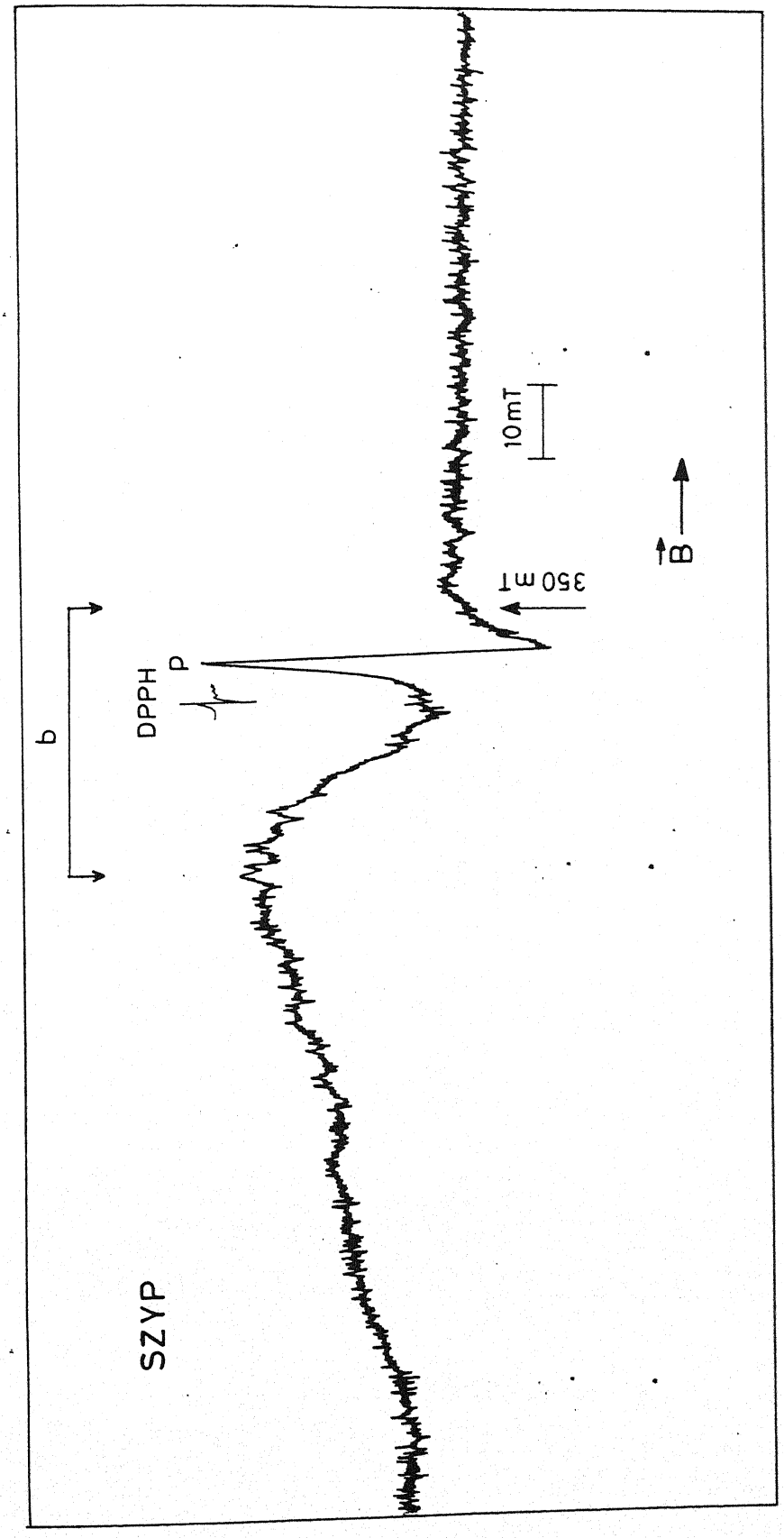

Fig. 4.3: EPR spectrum of sample SZYP at room temperature.

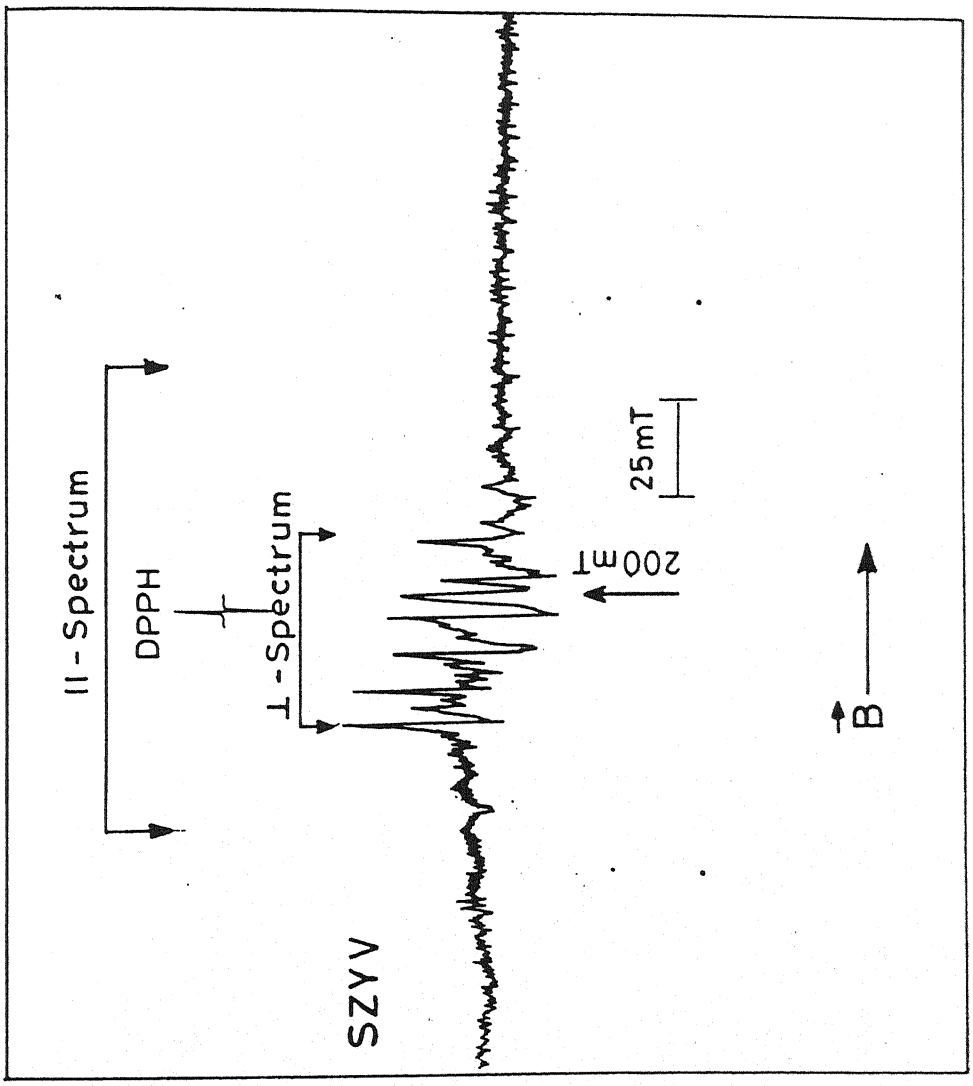

Fig. 4.4: EPR spectrum of sample SZYV.

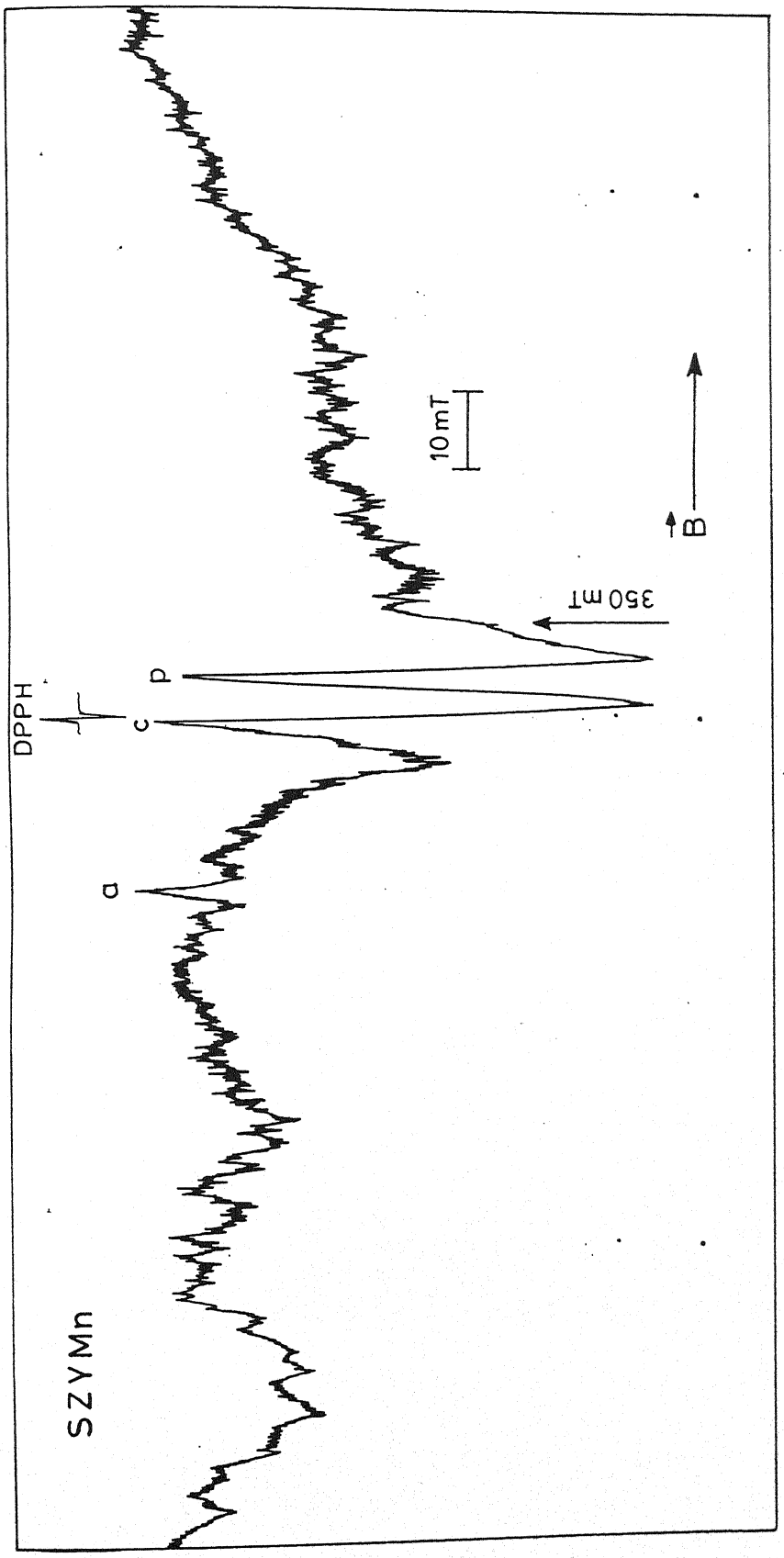

Fig. 4.5: EPR spectrum of sample SZYMn.

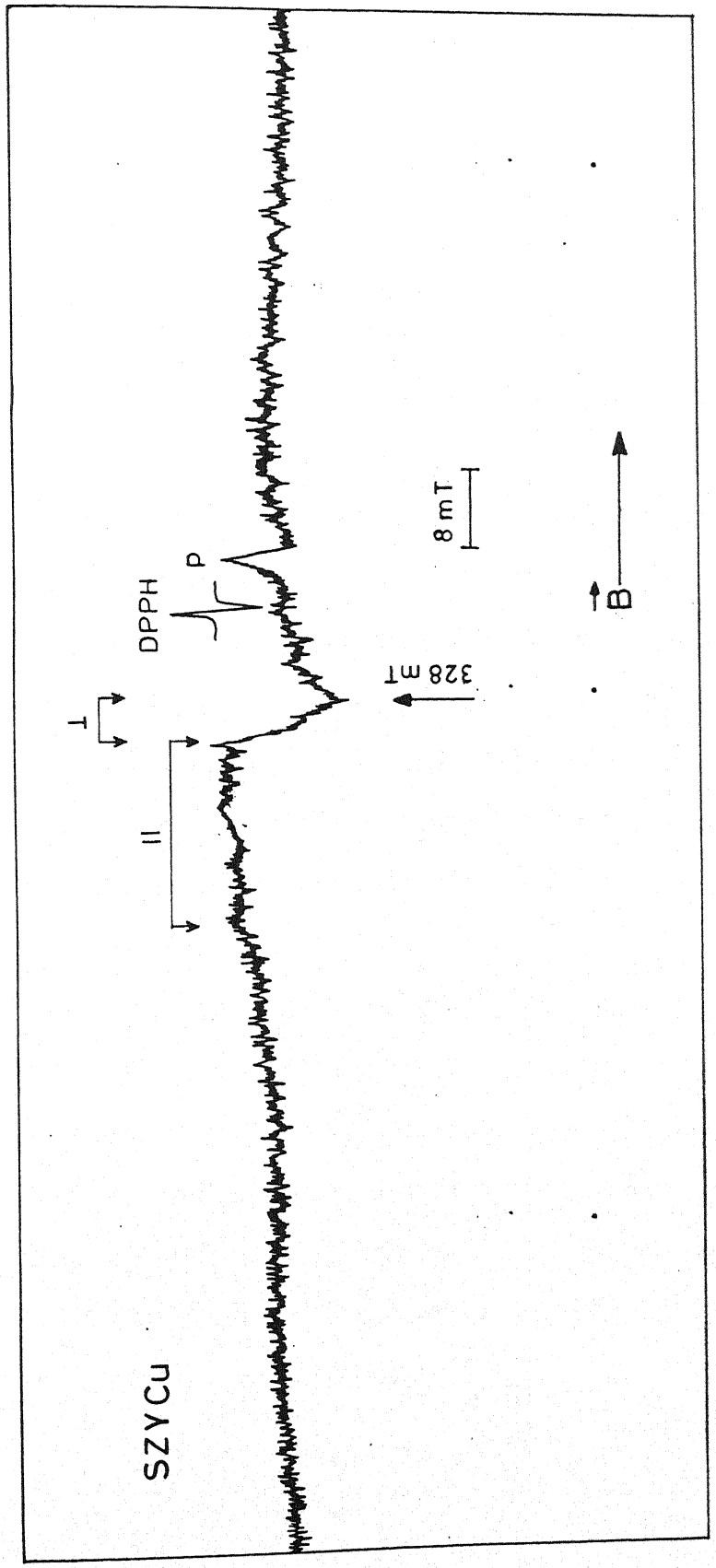

Fig. 4.6: EPR spectrum of sample SZYCu.

REFERNCES

1. R. Stevens " Zirconia Engineering Ceramics", Hand Book of Ceramics, Supplement to interceram. **34,** 1 (1985)
2. A.R.Burkin, H. Saricimen and B.C. Steel, Trans. J. Brit. Ceram. Soc., **79**, 105 (1980).
3. N.M. Ghoneim and S.B. Hanna, J. Mater. Sci., **25**, 5192 (1990)
4. N.R.Shankar, H.Herman, S.P. Singhal and C.C.Berndt, Thin Solid Films, **119**, 159, (1984).
5. N.Iwamoto, N. Umeski and S. Endo, Thin Solid Films, **127**, 129 (1985).
6. E. A. Zhilinskaya, V.N. Lazukin and I. V. Chepeleva, Magnetic Resonance and Related Phenomena, **325**, (1979).
7. R.A. Miller, J. L. Smaialek and R. J. Garlic, Adv. Ceramaic, **3**, 241 (1981).
8. B. D. Cullity, Elements of X-ray differaction, Addison-Wesley Publishing Company, Inc. , California 919780.
9. J.E. Wertz and J. R. Bolton, Elevtron Spin Resonance: Elementary Theory and Practical Applications, McGraw Hill, Chap. 11 (1972).
10. C. J. Ballhausan, Introduction to Ligand Field Theory, McGraw Hill, Chap. 10 (1962).
11. J. W. Orton, Electron Parramagnetic Resonance, Iliffe Book Ltd., London, Chap. 11 (1968).

12. A. Carrington and A. C. McLachlan, Introduction to Magnetic Resonance, Chapman and Hall Ltd., Chap. 10 (1979).

13. A .S. Marfunin, Spectroscopy, Luminescence and Radiation Centers in Minerals, Springer Verlag, Chap. 3, (1979).

14. Bleaney Plil. Mag., **42**, 441 (1951).

15. A. Abragam and B. Bleaney, Electron Parramagnetic Resonance of Transition ions, Clarendon Press (1970).

16. P. Chand, V.K. Jain and G.C.Upreti, Mgn. Resonan. Rev.,**14**,49 (1988) .

17. K.K. Tiwari,S.D.Pandey, and P.Chand, Solid State Commun., **69**,1109 (1989).

18. M. Stempi, H.Szymczak and A.A. Andreev., Acta Physica Pol., **63**, A.627 (1982).

19. T.H.Yeon, S.H. Choh, J.Phys.; Condensed Matter (UK), Vol.4,No.2, 587 (1992).

20. N.L. Shukla, S.V. Sharma, P. Chand and B. N. Mishra, Acta Physica Polonica A, 4, Vol.83, 441-449, (1993).

21. B. N. Mishra, S.V. Sharma, P. Chand and N.L. Shukla, Phys. Stat. Sol.(a)**139**, 295 (1993).

22. Scanning Probe Microscopy and Magnetic Resonance, Adv. Mater. (Germany), Vol.6, No.5, p.401 -404,1994.

23. K.G. Ressler, Mater. Res. Soc., p.605-610 (1996).

24. Tae Ho Yeom, Soo Hyung Lee, J. Korea Phys. Soc., Vol.32, p.5705-07 (1998).

CHAPTER – 5

ELECTRON PARAMAGNETIC RESONANCE OF Mn^{2+} IN DIAMMONIUM OXALATE MONOHYDRATE SINGLE CRYSTAL

5.1 INTRODUCTION

The electron paramagnetic resonance of Mn^{2+} ion doped in a single crystal of diammonium oxalate monohydrate [$(NH_4)_2\ C_2O_4.\ H_2O$] has been studied at room temperature. No EPR study seems to have been made on this crystal doped with impurity ions. However, EPR study of γ-irradiated crystal has been reported [1] and it shows the formation of $C_2O_4^{2-}$ radical derived from $C_2O_4^{2-}$ ion and OH^- radical derived from the water molecule in the crystal lattice.

5.2 EXPERIMENTAL PROCEDURE

Single crystals of diammonium oxalate monohydrate doped with Mn^{2+} ion were grown from an aqueous solution of the salt containing about 1 percent of $MnCl_2$ by weight and evaporating the solution in a desiccator containing concentrated sulphuric acid at room temperature. The crystals were transparent and prismatic in shape with the growth axis along the c-axis of the crystal. This axis was confirmed by x-ray rotation picture taken with a Weisenburg camera. The crystal used for the EPR study had dimensions 0.5 x 0.1 x 0.1 cm^3.

The EPR spectra were recorded with an X-band Varian E-109 EPR spectrometer. The magnetic field was produced by a Varian 12 inch electromagnet and modulated at 100 kHz. The cylindrical as well as rectangular resonant cavities were used. The spectra were recorded with a dual channel strip chart recorder. The frequency of the Klystron was measured with Hewlett Packard frequency meter. DPPH was used as a field marker.

5.3 CRYSTAL STRUCTURE

The crystal structure of diammonium oxalate monohydrate has been studied in detail by X-ray[2] and neutron diffraction[3] techniques. The crystal belongs to an orthrombic system and its space group is D_2^3 $(P2_12_12)$. In the *ab* plane of the crystal lattice, there are four screw diads, one set of two being parallel to the crystal a-axis and the other two to b-axis. There are four ammonium ions in the unit cell.

The X-ray analysis places all atoms except the oxygen of water molecules in the general positions of the D_2^3 $(P2_12_12)$ space group:

xyz; $\bar{x}\,\bar{y}z$; x+ 1/2, 1/2 -y, $\bar{z}$; 1/2 - x, y+1/2, $\bar{z}$ with the following parameters [4].

C	: x = 0.092,	y = 0.027,	z=0.066
0 (1)	: x = 0.200,	y = -0.056,	z = 0.140
0 (2)	: x = 0.118,	y = 0.142,	z = 0.001
NH_4	: x = 0.386,	y = 0.228,	z = 0.424

The water molecules are situated at 0, 1/2, u; 0, $\bar{u}$ with u = 0.192. The above parameters are referred to the unit cell dimensions.

$$a = 8.04\ A^{0},\ b = 10.27\ A^{0},\ c = 3.82\ A^{0}$$

The structure of diammonium oxalate monohydrate projected on the basal plane is shown in Fig. 5.1

5.4 RESULTS AND DISCUSSION

The electronic configuration of Mn^{2+} is $3d^5$ and consequently the ground state of the free ion is $^6S_{5/2}$. This state is orbitally non-degenerate but has six-fold spin degeneracy. Under the action of the crystalline field of orthorhombic symmetry or lower symmetry, this degenerated state splits into three Kramers' doublets which further split into six levels under a static magnetic field. The EPR spectrum of Mn^{2+} ion in such an environment is expected to show five fine structure transitions and each of these will consist of six hyperfine components due to nuclear spin I= 5/2. Figures 5.2, 5.3 and 5.4 show the z, x, and y-axis spectra respectively of Mn^{2+} ion

in $(NH_4)_2C_2O_4.H_2O$ single crystals of room temperature. The Z-axis spectrum, corresponding to the maximum spread has been obtained by rotating the crystal in different planes using two-plane goniometer. Z-axis has been found to lie in the crystallographic *ab* plane. X and Y axes are located by studying the angular variation in the *ab* plane and in a plane obtained by making the c-axis horizontal with the help of two plane goniometer [5] and looking for the extreme separated by 90^0. The angular variation further revealed the existence of two identical Z-axis spectra at an angular separation of 60^0 in *ab* plane. On further rotation of the crystal in this plane no such spectrum was obtained till 180^0 part of the first Z-axis spectrum appeared. The angular variation of the spectrum for one complex in ZX plane is shown in Fig. 5.5. This clearly indicates the existence of two physically identical complexes which are magnetically inquivalent for a random direction, with their Z-axis separated by an angle of 60^0 in the *ab* plane. The most probable site which Mn^{2+} ion will occupy is a substitutional position at NH_4^+ site. In Fig. 5.6 the positions of four ammonium ions in the unit cell are marked by I, II, III and IV. The ammonium ions marked by I and II in Fig. 5.6 are related by C_2 symmetry about the c-axis, and so also those marked by III and IV. These two sets are not quite independent and are related by screw diads. If Mn^{2+} occupies an NH^{4+} site and is not associated with any

charge compensating defects the spectrum essentially should reflect the symmetry of the crystal with c-axis (C_2) as the Z-axis[12,13] However, this has not been the case. The observation of a complex having two possible orientations such that the corresponding Z-axes are separated by about 60^0 in the *ab* plane is consistent with the following model. Mn^{2+} occupies the NH_4^+ ion sites I (or II) and is associated with a first neighbour cation vacancy at II_1. A symmetry related configuration of such a Mn^{2+} vacancy complex will be Mn^{2+} at III associated with a vacancy at IV_2. This is illustrated in Fig. 5.7. This results in two magnetically in-equivalent complexes having Z-axes separated by 60^0 in the *ab* plane. A similar model with second neighbour cation vacancies either in *ab* plane or out of *ab* plane does not result in the observed behaviour and hence it has not been considered.

The Z, Y and X-axes spectrum of Mn^{2+} ion (S= 5/2, I = 5/2) corresponding to transitions $\Delta M_S = \pm 1$, $\Delta m_I = 0$ were analysed using the spin Hamiltonian [6].

$$\mathcal{H} = \beta g_z H_z S_z + \beta g_x H_x S_x + \beta g_y H_y S_y$$

$$+ D\left[S_z^2 - (1/3)S(S+1)\right] + E\left(S_x^2 - S_y^2\right)$$

$$+ A_z S_z I_z + A_x S_x I_x + A_y S_y I_y$$

The suffixes x, y and z represent corresponding components along principal axes. In case of D and E << Zeeman term and

E << D, the terms upto third order as given by Chambers et al [5] were found sufficient for this system. The resonance magnetic fields for different transitions for the magnetic field along Z-direction of the crystalline field are given [6] below:

(i) Fine Structure Transitions:

$$H(M_S \pm 5/2 \leftrightarrow \pm 3/2) = H_0 \mp 4D + 4\frac{E^2}{H_0} \pm \frac{6DE^2}{H_0^2} + \frac{36D^2E^2}{H_0^3} + \frac{28E^4}{H_0^3}$$

$$H(M_S = \pm 3/2 \leftrightarrow \pm 1/2) = H_0 \mp 2D - \frac{5E^2}{H_0} \pm \frac{33DE^2}{H_0^2} + \frac{45D^2E^2}{H_0^3} - \frac{5}{4}\frac{E^4}{H_0^3} \quad (5.3.1)$$

and $$H(M_S = +1/2 \leftrightarrow -1/2) = H_0 - \frac{8E^2}{H_0} + \frac{72D^2E^2}{H_0^3} + \frac{56E^4}{H_0^3}$$

(ii) Hyperfine Transitions:

$$H(M_s, m_I \leftrightarrow M_s \pm 1, m_I) = -Am_I - \frac{B^2}{2H_0} \times \left[\frac{35}{4} - m_I^2 + m_I(2m_S - 1)\right] \quad (5.3.2)$$

where A = A_Z and B = $\frac{(A_X + A_y)}{2}$

When the magnetic field is along the X or the Y-axis, the above equations are modified [7-8] by replacing D by 1/2 (3E - D), and E by (1/2) (D+E) for H along X-axis; and D by -1/2 (D+3E) and E by 1/2 (D-E) for H along Y-axis.

In evaluating the spin-Hamilton parameters [9-11] from the Z-axis spectra four fine structure positions have been used. The

position of the central (+1/2 ↔ - 1/2) transition could not be accurately determined due to overlap of other lines from the second site. The values of H_0 were approximately calculated from the expressions for extreme fine structure positions H_1 and H_5[14,15], & also the next H_2 and H_4, neglecting higher order terms in these expressions. A rough estimate of D was made by averaging its value obtained from the differences of H_1 and H_5 and H_2 and H_4, neglecting higher order terms in these expressions.

The value of D obtained from the Z-axis spectrum was further more accurately calculated taking into account the contribution from higher order terms using average value of E of X and Y-axis spectra. The value of E could not be estimated from the Z-axis spectrum since there is no linear term in E and contribution from the $\frac{E^2}{H_0}$ term is very small. The values of (D + 3E) from the Y-axis spectrum was first estimated roughly by taking the difference of H_4 and H_2, H_5 and H_1 and (D-E) from the H_3. The equation (5.3.1) were used to estimate D and E. Further refinement was made by taking into account the contribution from higher order terms in the transformed expression for Y-axis spectrum. A similar procedure was adopted to get the refined values of D and E. From the X-axis spectrum the values of H_0 were obtained by adding H_5 and H_1, H_4 and H_2, taking into account the contributions from higher order terms involving D and E. The

spin Hamiltonian parameters calculated from the X, Y and Z axis spectra are given in Table 5.I. The consistency of the parameters obtaining is satisfactory.

Table 5.1

The spin Hamiltonian parameters for Mn^{2+} doped in $(NH_4)_2C_2O_4.H_2O$

	Z	Y	X
D (cm^{-1})	513×10^{-4}	511×10^{-4}	511×10^{-4}
E (cm^{-1})	*	37×10^{-4}	32×10^{-4}
g	2.0069	2.0099	2.007
A (cm^{-1})	82×10^{-4}	84×10^{-4}	87×10^{-4}

* The value of E from Z-axis spectrum could not be calculated due to small value of $\frac{E^2}{H_0}$ term. E does not appear in linear form in the expressions for Z-axis fine structure transitions, $\Delta M_S = \pm 1$.

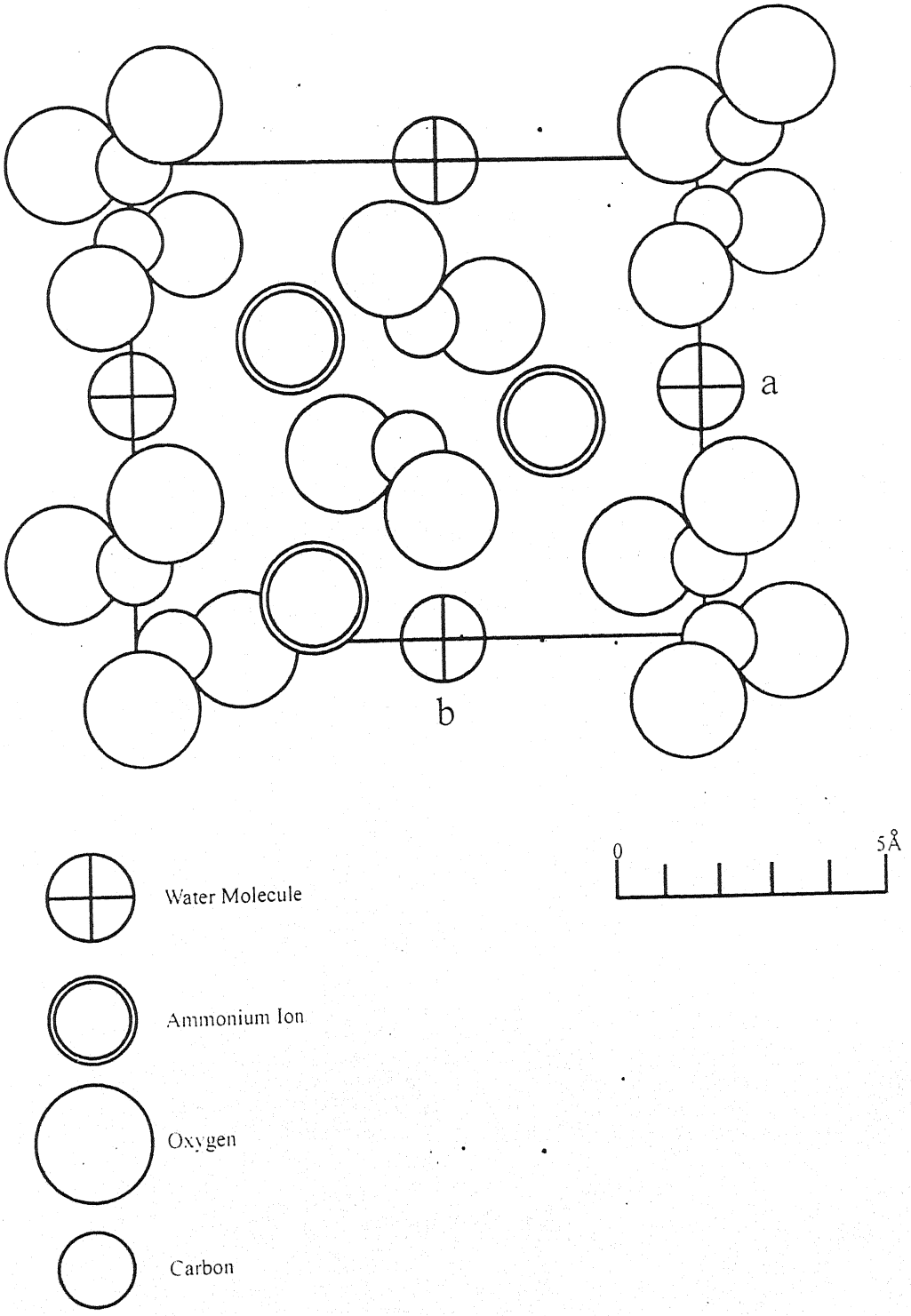

Fig. 5.1 The structure of $(NH_4)_2C_2O_4 . H_2O$ Projected on the basal plane[4] ab.

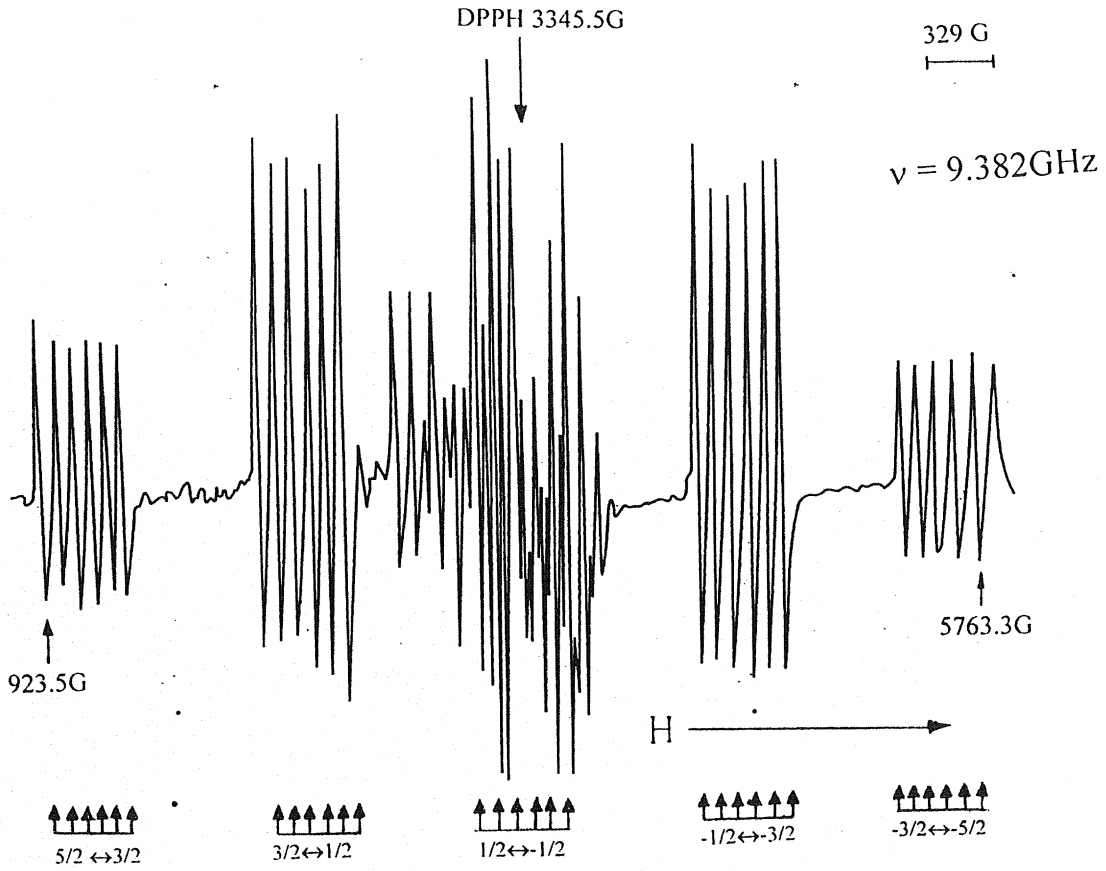

Fig. 5.2: The EPR Spectrum of Mn^{2+} ions doped in $(NH_4)_2\ C_2O_4.H_2O$ single crystal with H along Z axis of one of the sites at room temperature. The coalasced spectrum (corresponding to $\theta = 60^0$) of the second site is seen in the center of the spectrum.

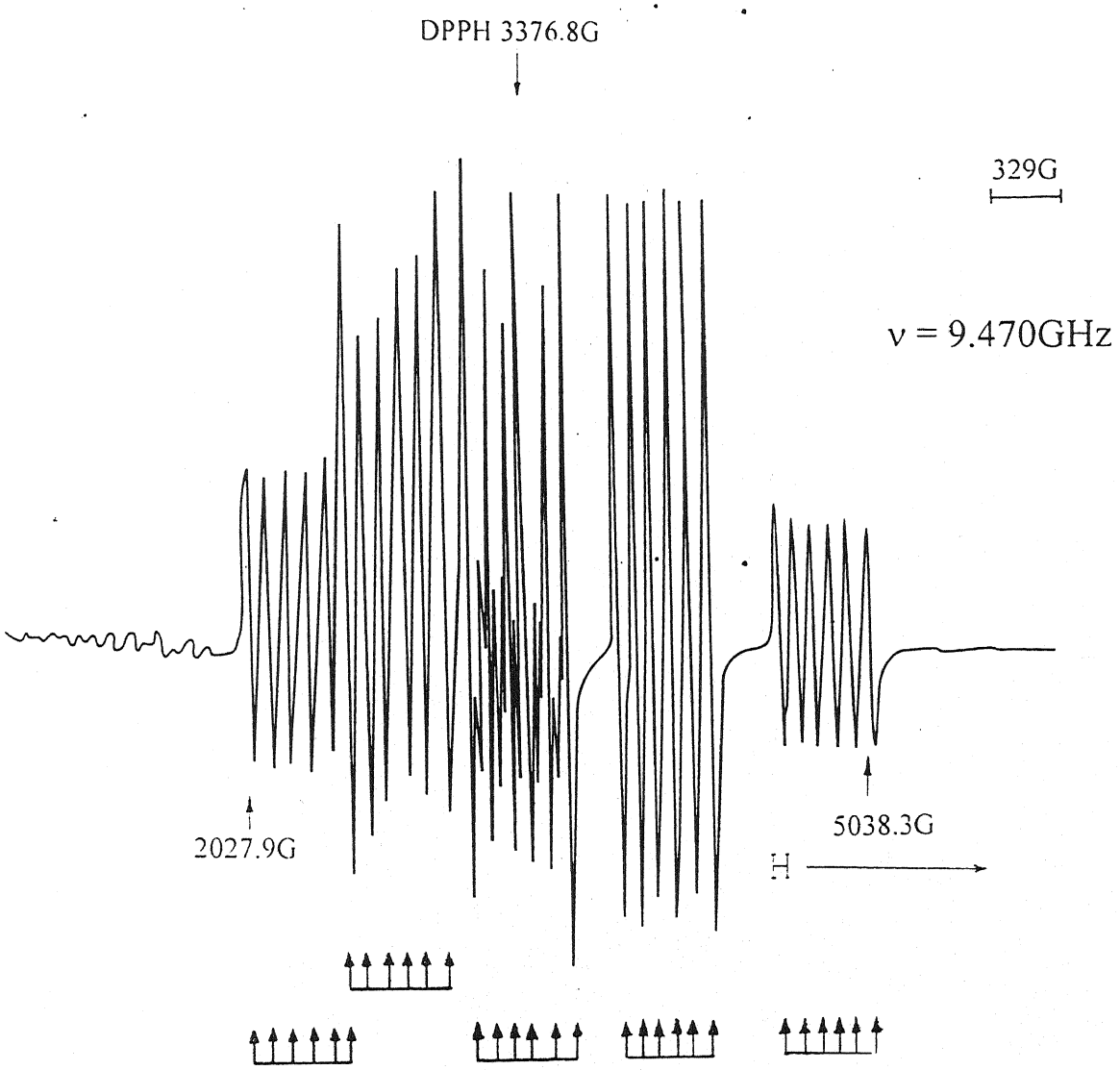

Fig. 5.3: The EPR spectrum of Mn^{2+} ion doped in $(NH_4)_2\ C_2O_4.H_2O$ single crystal with magnetic field along x axis at room temperature. The extra lines seen in the central part of the spectrum are due to the second site.

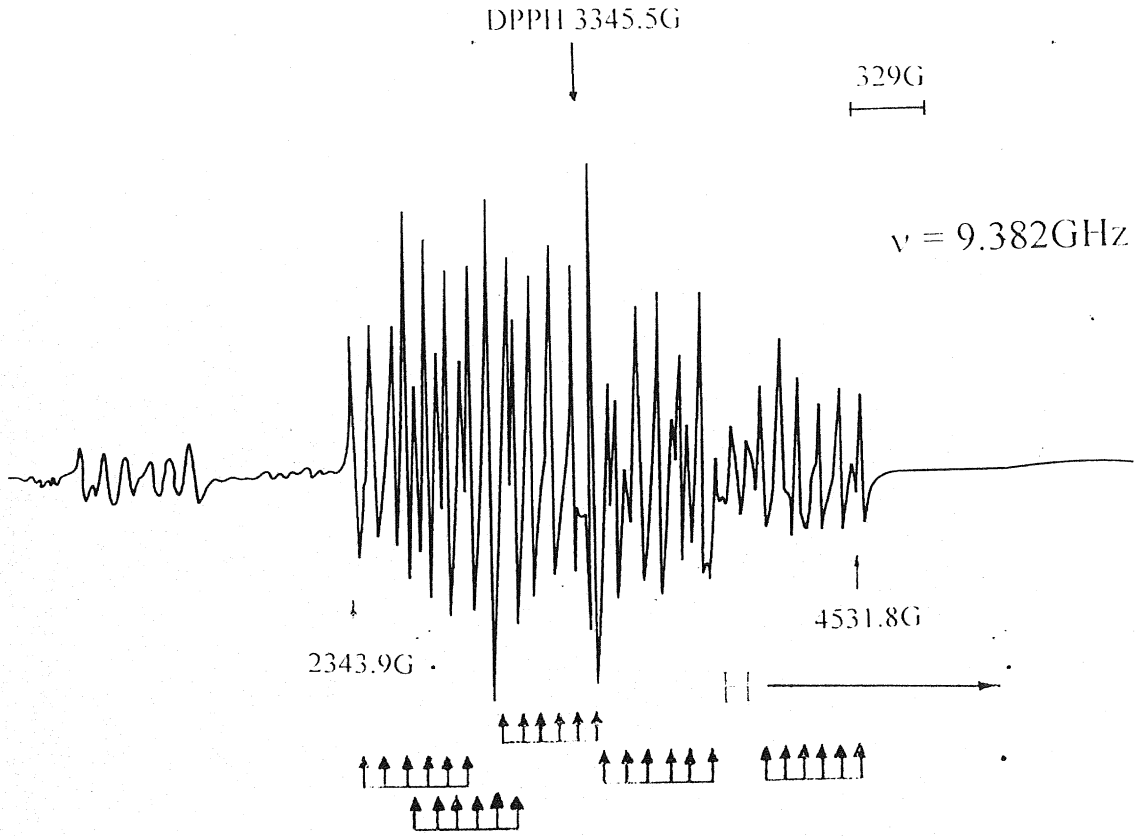

Fig. 5.4 : The EPR spectrum of Mn^{2+} ion doped in $(NH_4)_2\ C_2O_4.H_2O$ single crystals with magnetic field along y axis of one of the sites at room temperature . The hyperfine set seen at the low field side shows uneven hyperfine spacing which decreases with increase in H. This is in contrast to the other hyperfine sets shown in this figure. The low field transition is probably due to an electronic forbidden transition.

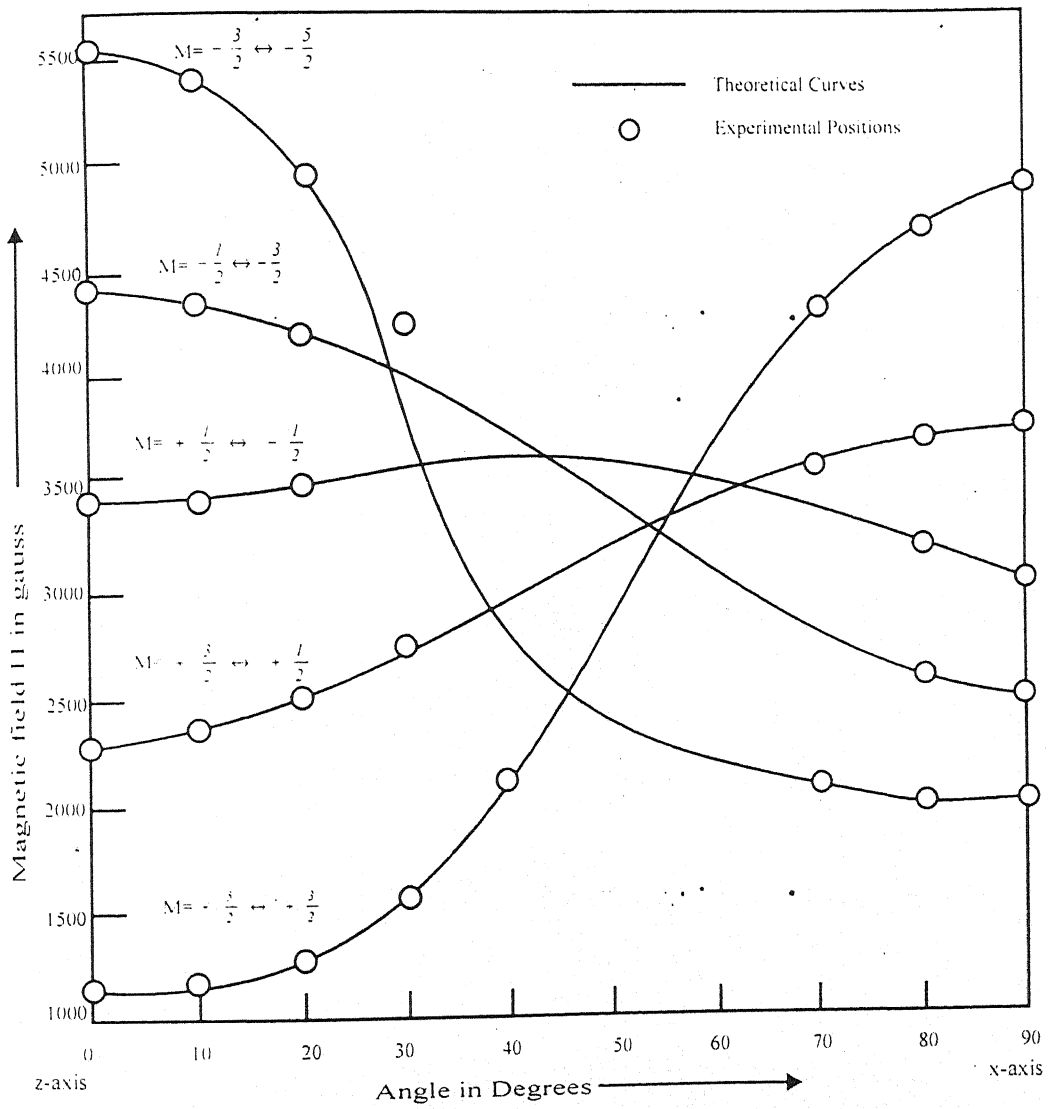

Fig: 5.5

Angular variation of the allowed fine structure transitions in the ZX plane of the one of the magnetic complexes of Mn_2^+ in $(NH_4)_2C_2O_4.H_2O$ single crystals.

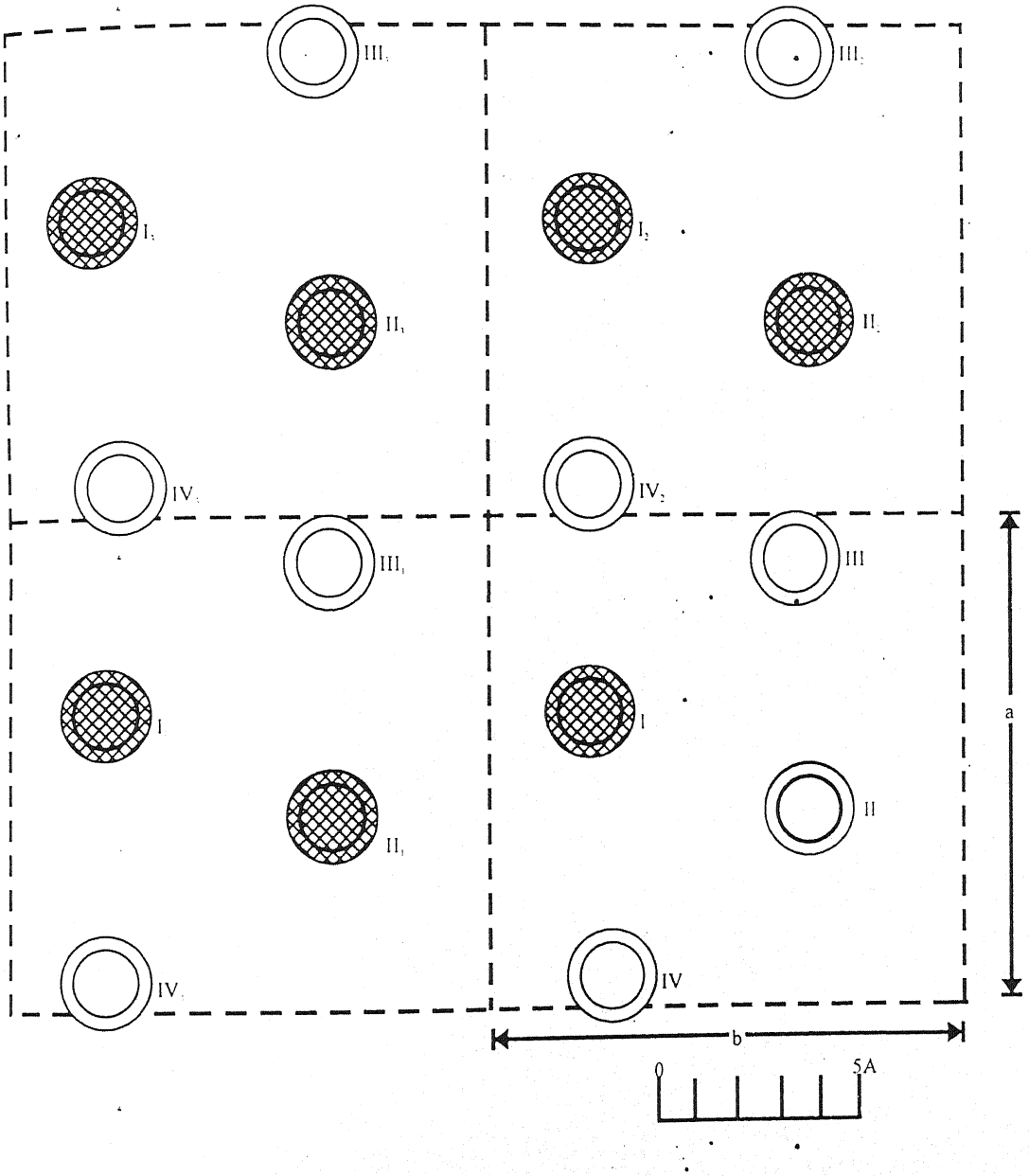

Fig 5.6

Projection of ammonium ions in the *ab* plane showing four adjoining unit cells of diammonium oxalate monohydrate. Shaded rings represen NH_4^+ ions above the plane of the paper and unshaded ones represent th below the plane of the paper.

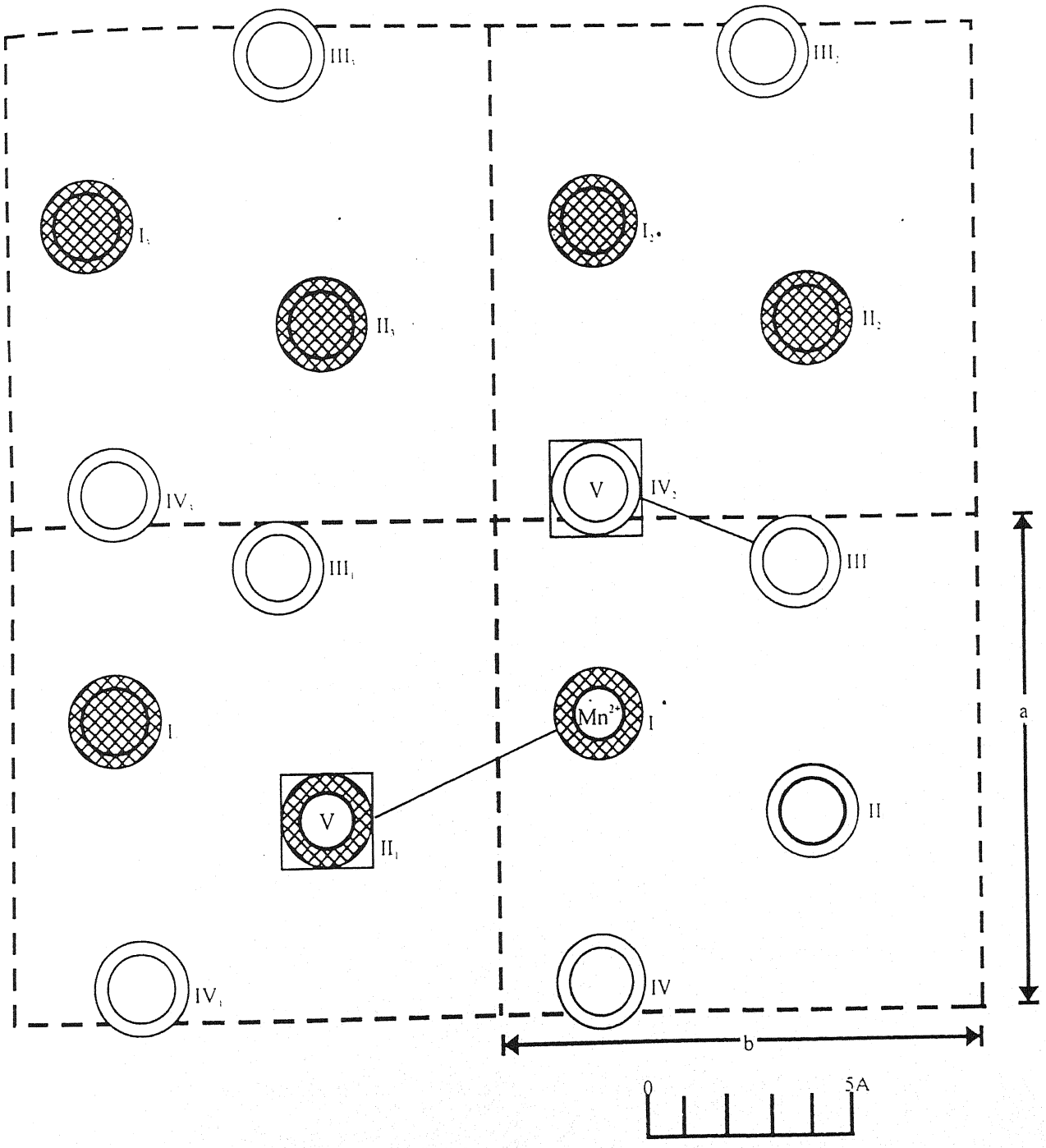

Fig 5.7

Projection of ammonium ions in the *ab* plane showing four adjoining unit cells of diammonium oxalate monohydrate. Shaded rings represent NH_4^+ ions above the plane of the paper and unshaded ones represent. Those below the plane of the paper. A two possible Mn^{2+} vacancy pairs in two adjoining unit cells are shown. Mn^{2+} is in the substitutional position.
V Stands for vacancy of NH_4^+ ion

REFERENCES

1. M.V. Krishnamurty, Mol. Phys., **24**, 1353 (1972).
2. J.H. Robertson, Acta Crystallogr, **18**, 410 (1965).
3. V.M. Padmanabham, S. Sribanta and S. Medhi Ali, Acta Crystallogr., **18**, 576 (1965).
4. Ralph W.G. Wyckoff, **Crystal Structure**, Vol, 5 (Inter Science Publishers, 2nd Edition p: 412).
5. R. Janakiraman, 'Electron Paramagnetic Resonance Studies of Mn^{2+} in some Dia and Paramagnetic single Crystals'. Ph. D. Thesis, Indian Institute of Technology, Kanpur, India (1970).
6. J.G. Chambers, W.R. Datars and C. Calvo, J. Chem. Phys., **41**, 806 (1964).
7. A.V. Jagannadham, 'Electron Paramagnetic Resonance of Mn^{2+} and VO^{2+} ion in single crystals'. Ph.D. Thesis, Indian Institute of Technology, Kanpur, India (1969).
8. J.S. Phor, Radiat. Eff. Defects Solids (UK) **116**, No. **1-2**, 149 (1991).
9. V.K. Jain, G. Lehmann, Phys. Status Solidi B (East Germany), **159**, No. 2, 495 (1990)

10. J.L. Rao, G.L. Narendra, B. Sreedhar, Phys. Status Solidi B (East Germany), **153**, No. 1, 257 (1989).

11. B.J. Reddy, S. Vedanand, G. Srinivaslu, Solid State Communication (USA), 78, No.8, 751 (1991).

12. Z. Nate . Forsch. A, Phys. Chem. Kosmophys. (Germany)., Vol.54A, No.6-7, p. 370-374 (1999).

13. O. Dezel et al, Indian J. Pure and Applied Phys., Vol.37, No.2, p.123-126 (1999).

14. M. Ikram and R.J. Singh, Mod. Phys. Lett. B (Condensed Matter Physics; Statistical Physics and Applied Physics), Vol. 17 , No.19, p.1067-1071 (2003).

15. Sushil K. Mishra, Sergui I. Andronenkoa, Gino Rinaldia, Prem Chand, Keith A. Earlec and Jack H. Freed, J. Mag. Res.,Vol.160, Issue 2, p.131-138 (2003).

Chapter – 6

ELECTRON PARAMAGNETIC RESONANCE OF Cu^{2+} ION IN CIS-CATENA - μ - SULPHATO AQUOTRIS IMIDOZOLE CADMIUM SINGLE CRYSTALS

6.1 INTRODUCTION

Cu^{2+} is one of the first row transition metal ions which has been extensively studied by EPR. Cu^{2+} ion forms stable complexes easily with a wide variety of ligands resulting in mostly elongated octahedron stereochemistries. In such an environment of the ligand field the ground state of Cu^{2+} is t_{2g}^{6} e_g^{3} with three electrons occupying doubly degenerate *eg* orbital. The EPR spectrum is usually observed at room temperature as the orbital angular momentum is quenched by way of lifting the degeneracy of the ground state. The degeneracy is removed either by a component of the ligand field of lower symmetry than trigonal or because of J.T. distortions. The energy level diagram is shown in Fig. 6.1 (a). Under these conditions a single electron occupies either d_{x}^{2}-$_{y}^{2}$ or d_{3z}^{2}-$_{r}^{2}$ of the *eg* states. The observed EPR spectrum is characteristic of an orbitally singlet ground state and is sensitive to the immediate environment of the ligands around Cu^{2+} ion. In favourable cases the ligand-metal ion interaction is also observed and is manifested in the form of the ligand hyperfine structure or super hyperfine structure (s.h.s). From an analysis of s.h.s. and the spin Hamiltonian parameters, obtained from a single crystal, it is possible to estimate the bonding parameters[1]. It is also possible

---

1.

to infer the extent of s-p- hybridization [2] of the ligands. Bonding parameters are of interest as these reflect a trend regarding the degree of tetragonality[3] and molecular stability [4] and also the mixing of various excited states to the ground state [5]. In this chapter we report the analysis of the EPR spectra of Cu^{2+} doped $CdIm_3SO_4.H_2O$ single crystals.

6.2 CRYSTAL STRUCTURE

The crystal structure of Cis-Catena-μ-Sulphato Aquotris Imidozole Cadmium (II) (Henceforth referred as CdImS) has been carefully investigated by Mino Caira et al [6] using single crystal X-ray diffraction technique. These crystallize in the monoclinic system with space group $P2_1 / n$. The unit cell has four molecules with cell dimensions as a = 11.85 $\mathring{A}$, b = 9.0 $\mathring{A}$, c = 14.32 $\mathring{A}$ and β= 95.2 $\mathring{A}$. The central ion has a distorted octahedran environment where it is bonded to tertiary pyridine nitrogen atom (>N) N (11), N (1) and N (6) of the 3 imidazole rings, a hydrate oxygen 0 (16) and an oxygen atom 0(1) of the sulphate group. The distorted octahedron is completed by an oxygen atom 0 (2') of a screw axis related sulphate group. The Table 6.I gives bond lengths and direction cosines of various bonds w.r.t. orthonormalised sets of

crystallographic axis. The relation of the g tensor to these axes would be discussed in section 6.7. The Table 6.I also gives the angles subtended by various bonds w.r.t. these axes. It may also be noted that [6] 0 (1) - Cd - O (16) has an angle of 175.7^0 and is almost perpendicular to the plane formed by N (6), N (11), 0 (2) and N (1).

6.3 PREPARATION OF THE SINGLE CRYSTALS

Single crystals of CdImS were grown following the procedure reported [6]. The crystals were obtained by mixing 1M aqueous solution of Cadmium Sulphate and imidazole in the molecular ratio of 1:2. The pH of the solution was adjusted to 7.5 with 6M H_2SO_4. A small amount of copper sulphate was added to this solution. Beaker containing this solution was covered with a filter paper and kept in a desiccator, desiccant used was $CaCl_2$. After two days usually small polycrystals appeared with very little copper ion concentration. These were redissolved. A small amount of Cadmium-Sulphate was added since it was noted from experience, that a slight excess of Cadmium Sulphate helped in slowing down the crystallization.

This however did not affect the pH of the solution. After two or three recrystallisatios, good quality single crystals with

sufficient copper concentration could be obtained. These are slightly bluish in colour and are needle shaped with well developed faces. The morphology is shown in Fig. 6.1 (b). The b axis was found to be perpendicular to the needle axis. The crystals were found to cleave in a plane containing b axis. These conclusions were confirmed from the observed fringes in a polarizing microscope [7].

6.4 POWDER SPECTRUM

The powder spectrum of Cu^{2+} doped CdImS was recorded both at 300^0K and 77^0K. The spectra were found to be similar at these two temperatures except for a better resolution at 77^0K. These spectra are shown in Fig. 6.2. The powder spectrum at 300^0K is seen to consist of a broad intense line with additional structure at high field followed by four groups of less intense lines at low field side. The additional structure is more pronounced at 77^0K. This low field spectrum is labeled as parallel spectrum because four lines appearing at low field can be readily identified as the hyperfine lines of the Cu^{2+} ion. The high field spectrum is labeled as the perpendicular spectrum. Both $g_{\parallel}$ and $A_{\parallel}$ are estimated from the parallel spectrum and only $g_{\perp}$ could be estimated from the perpendicular spectrum. The additional

structure appearing is attributed to the ligand hyperfine structure arising from Cu-N interaction.

These parameters, though approximate, are very useful as these provide a cross-check for the single crystal analysis. An examination of the above parameters suggest that Cu^{2+} ion occupies tetragonally elongated Octahedron site. The spectrum of an aqueous solution of this complex at 300^0K and also of the frozen state (at 77^0K) were recorded. The isotropic and anisotropic spin Hamiltonian parameters were estimated. The values together with the powder values are given in Table 6.II. It was concluded that the complex in the solution form is not the same as in the powder form. Probably in the solution $CuIm_4SO_4$ is established. Consequently $CuIm_4SO_4$ was also prepared following the procedure reported[8]. The EPR spectrum of this complex was recorded both in the solution and in the frozen state. The estimated parameters confirmed the above conclusions. Electronic spectrum (unpolarised) of the single crystal of Cu^{2+}:$CdIm_3SO_4.H_2O$ was recorded which showed three bands at 29,000 cm^{-1}, 15,150 cm^{-1} and at 14,150 cm^{-1}. The electronic spectrum of pure imidazole showed three peaks at 42,400 cm^{-1}, 36,200 cm^{-1} and 33,000 cm^{-1}. The electronic spectra of $CuIm_4SO_4$ in the solution form was also recorded which showed two bands at 34,000 cm^{-1} and 16,000 cm^{-1}. All these spectra are shown in Fig. 6.3. They were recorded on

DW-2a UV-Vis spectrophotometer of American Instrument Company in the double beam mode.

6.5 SINGLE CRYSTAL EPR STUDY

Single crystal EPR spectra were examined both at 300^0K and 77^0K. In a general orientation two non-equivalent sites of Cu^{2+} could be observed with partially resolved ligand hyperfine structure[35]In order to determine the principal axes of g and A tensor, the anisotropic behaviour was initially examined in the ac plane. In this plane spectra due to non-equivalent sites of Cu^{2+} coincide but exhibit observable anisotrophy. From the anisotropic behaviour of the spectra, in this plane, the direction containing cleavage plane in the crystal (Fig. 6.1) was found to have minimum hyperfine coupling and was labeled as ac min. direction. Subsequently this direction was chosen as the axis of rotation. In this plane the two in equivalent sites could be clearly seen with maximum anisotrophy. When the magnetic field was oriented along or perpendicular to the b axis, spectra due to both the sites coincide showing only main copper hyperfine lines with super hyperfine structure (Fig. 6.4). As the magnetic field was rotated away from the b axis in either direction, the lines associated with one of the sites moved towards the low field and attained a

maximum at 63^0 from b axis. This direction was identified as one of the principal axis of the sites and was labeled as z axis. Spectrum along this direction is shown in Fig. 6.4. The directions of the principal components of g and A tensors were found to coincide along this direction. An identical behaviour is observed when the magnetic field is rotated away from the b axis in the opposite direction as expected for a monoclinic system g_z and A_z values are directly calculated from this direction. $A_{\perp}^{N}$ coupling was also estimated from this spectrum. These are presented in Table 6.II. These values are consistent with powder values. Along z axis it can be seen (Fig. 6.4) that all the copper hyperfine lines show well resolved super hyperfine structure. The lowest field line corresponding to m_I = -3/2 exhibits eight ligand hyperfine lines whereas the line corresponding to m_i= -1/2 displays only 7 lignad hyperfine lines. The crystal was remounted with z axis as axis of rotation to examine the rhombic character of g and A tensor and also to determine the other principal components. In this plane the spectra appeared generally to be complicated. This complexity arises because of small g (approx. 50 Gauss) and A (approx. 30 Gauss) anistropy together with the inequivalent N interaction and the overlap of the two non equivalent sites of Cu^{2+}. Hence complete anisotropic behaviour of the lines could not be followed in this plane. However maximum and minimum direction of g

tensor could be identified which are labeled as x and y directions respectively. Spectra along those directions are shown in Fig. 6.5. Y axis spectrum consists of a single broad line with poorly resolved hyperfine lines. This spectrum is flanked by the other site spectrum[31]The g (g_y) value was calculated corresponding to the center of this line. X axis spectrum has a larger spread than Y axis spectrum. It appears on the high field side and could be separated from the spectrum of the other site which appears at lower field. X axis spectrum consists of approximately equally spaced 17 lines with coupling constant of about 14 Gauss. From the total spread of this spectrum, g and A values were approximately estimated. Anisotropic behaviour in ZX and ZY planes was also examined to obtain more accurate values along principal X and Y axis. This will be discussed in Section 6.7.

6.6 SPIN HAMILTONIAN

A variety of systems doped in different host lattices have been analysed in terms of spin Hamiltonian formalism and have been reported in literature [9]. The spin Hamiltonian for Cu^{2+} in rhombic symmetry can be written as:

$$\mathcal{H} = \beta \left[g_x H_x S_x + g_y h_y S_y + g_z H_z S_z \right]$$

$$+ A_x S_x I_x + A_y S_y I_y + A_z S_z I_z - \gamma \bar{H}.\bar{I}. \qquad (6.6.1)$$

The equation for the transition fields for $\Delta m = O$, $\Delta M = \pm 1$ where m is the nuclear spin and M is the electron spin given as follows:[10]

$$H_m = H_0 - \frac{Km}{g\beta} - \frac{2}{g^2\beta^2 H}\left[|K_1|^2 m^2 + \left\{ |K_2|^2 + |K_3|^2 \right\} \left\{ I(I+1) - m^2 \right\} \right]$$

(6.6.2)

$$with\ g^2 = g_x^2 l^2 + g_y^2 m^2 + g_z^2 n^2 \qquad (6.6.3.)$$

$$g^2 K^2 = g_x^2 A_x^2 l^2 + g_y^2 A_y^2 m^2 + g_z^2 A_z^2 n^2 \qquad (6.6.4.)$$

$$|K_1|^2 = \left(4g^2K^2\right)^{-1} \left\{ A_x^4 g_x^2 l^2 + A_y^4 g_y^2 m^2 + A_z^4 g_z^2 n^2 - g^4 K^4 \right\} \qquad (6.6.5.)$$

$$|K_2|^2 + |K_3|^2 = \left(8g^2k^2\right)^{-1} \left\{ \begin{matrix} A_y^2 A_z^2 \left(g_y^2 m^2 + g_z^2 n^2\right) + A_z^2 A_x^2 \left(g_z^2 n^2 + g_x^2 l^2\right) \\ + \left(A_x^2 A_y^2\right)\left(g_x^2 l^2 + g_y^2 m^2\right) \end{matrix} \right\}$$

(6.6.6.)

where (l, m, n) are the direction cosines of the magnetic field with respect to the (X,Y,Z) principal axes. These equations were used to calculate the anisotropy in the different planes so as to obtain more accurate values of the tensor as discussed below.

6.7 ANALYSIS OF THE SPECTRA

The experimental results showed that the Z axis makes an angle of 63^0 with b axis. An examination of the crystallographic data (Table 6.I) suggests that the Z axis is almost along Cd-O (1) bond direction. It is further noted that this is perpendicular to the plane containing 3 nitrogens (Fig. 6.1). Hence along Z axis one expects a leg and hyperfine pattern arising from 3 equivalent nitrogens, with A_1^N coupling. Thus when magnetic field is along Z axis each hyperfine line of Cu^{2+} splits into 7 lines with the intensity ratio 1:3:6:7:6:3:1. having equal coupling constant. Referring to Fig. 6.4 it is seen that m = $\pm \frac{1}{2}$ lines show this expected behaviour but the lowest field line assigned as m = -3/2 has 8 lines of ligand hyperfine structure with intensity ratio approx. 1:3:6:7:6:3:2:1. This could be readily understood due to the presence of two isotopes of Cu^{2+} viz. ^{63}Cu and ^{65}Cu. The ^{65}Cu isotope will have a hyperfine coupling constant of 136 G as compared to 126 G of ^{63}Cu isotopes. The nitrogen coupling constant is measured to be 11Gauss along this direction and the pattern is consistent with the expectations. The hyperfine line corresponding to m= -1/2 has only 7 components of ligand hyperfine structure with approximately expected intensity ratio. Here the effect of ^{65}Cu is likely to alter the line widths only. The

isotope effect was taken into account in locating the centers of the hyperfine lines in the Z axis spectrum and g_z and A_z values were calculated directly from the spectrum These values were corrected after making allowances for the IInd order corrections using eq. (6.6.2.). To calculate more accurate values of g and A tensors along the X axis, the line positions of the center of the groups were measured from the experimental derivative tracings upto 50^0 at 5^0 intervals starting from Z axis in the ZX plane. The IInd order corrections were applied to the approximate values of the g and A tensors obtained for each of these angles. These parameters thus obtained were matched with the parameters obtained following equation (6.6.3) and equation (6.6.4.). The values of g_x and A_y were taken from the X axis spectrum and were used in equation (6.6.2.) and (6.6.4.) These parameters were adjusted till a best fit to the observed anisotrophy in the XZ plane was obtained. Similar procedure was followed for the YZ plane. The anisotropic curves are shown in Fig. 6.6. However, a similar procedure could not be followed in the XY plane, because of small anisotrophy.

The direction cosines of various bonds w.r.t. the principal g and A tensor axes were calculated. These are given in Table 6. III. It was noted that X axis lies along Cd-N (1) bond direction. Y axis is along Cd- O(2'). It follows from this, that along X axis, N (1) and N (11) will be equivalent and the 3rd Nitrogen N (6) will have

a $\perp_r$ coupling whereas along Y axis, Nitrogen (6) will have a parallel coupling and the other two nitrogens will have a $\perp_r$ coupling. With these final values of spin Hamiltonian parameters and understanding of the Cu-N interaction, X axis spectrum was simulated using a computer programme. This programme simulates the relative intensities taking into account not only the differences in the natural abundance of ^{63}Cu but also the expected equivalence of the nitrogen couplings. A typical comparison is shown for the X axis spectrum in Fig. 6.7 which shows a satisfactory agreement. The spin Hamiltonian parameters are given in Table 6.II.

6.8 (i) BONDING PARAMETERS

In this system the Cu^{2+} hyperfine and ligand hyperfine structures are well resolved which enables to estimate more accurately the bonding parameters. These estimations are based on semi-emperical methods following the approach developed by McGarvey [1] and subsequently modified by Gresmann et al[11] and Ammeter et al [12] for different symmetries. Even though this approach makes a number of approximations, it continues to provide reasonable qualitative estimates of the covalency effects[13]. More detailed methods have been developed [14] and

applied [3,15] which involve the estimations of overlap integrals, information of charge transfer bands etc.

In our present system the copper ion is surrounded by 3N atom and one oxygen atom in a plane. We assume that each atom has available 2s and 2p orbitals for the formation of the molecular orbitals with the d orbitals of the Cu^{2+} ion.

Assuming the ground state to be $d_{x^2-y^2}$, following molecular orbitals are involved.

$$B_{1g} = \alpha d_{x^2-y^2} - \alpha' \left(\sigma_x^{(1)} + \sigma_y^{(2)} - \sigma_x^{(3)} - \sigma_y^{(4)}\right) / 2 \qquad (6.8.1.)$$

$$B_{2g} = \beta_1 d_{xy} - \beta' \left(p_y^{(1)} + p_x^{(2)} - p_y^{(3)} - p_x^{(4)}\right) / 2 \qquad (6.8.2.)$$

$$A_{1g} = \gamma d_{z^2} - \gamma' \left(\sigma_x^{(1)} + \sigma_y^{(2)} - \sigma_x^{(3)} - \sigma_y^{(4)}\right) / 2 \qquad (6.8.3.)$$

$$E_{1g} = \delta_1 d_{yz} - \frac{1}{2} \delta'_1 \left(p_z^{(1)} + p_y^{(2)} - p_z^{(3)} - p_y^{(4)}\right) \qquad (6.8.4.)$$

$$E_{2g} = \delta_2 d_{xz} - \frac{1}{2} \delta_2' \left(p_x^{(1)} + p_z^{(2)} - p_x^{(3)} - p_z^{(4)}\right) \qquad (6.8.5.)$$

where

$$\sigma^{(1)} = np^{(1)} \mp (1 - n^2)^{1/2} S' \qquad (6.8.6.)$$

with $0 \leq n \leq 1$.

The overlap between copper and ligand (Nitrogen atom) orbitals has been considered. The effect of oxygen atom has been ignored in our formulation. The normalization of the B_{1g} orbital gives

ignored in our formulation. The normalization of the B_{1g} orbital gives

$$\alpha^2 + \alpha'^2 - 2\alpha\alpha' S = 1 \qquad (6.8.7.)$$

where S is the overlap integral

$$S = \langle d_{x^2-y^2} \mid -\sigma_x^{(1)} + \sigma_y^{(2)} + \sigma_x^{(3)} - \sigma_y^{(4)} \rangle / 2 = 2 \langle d_{x^2-y^2} \mid -\sigma_x^{(1)} \rangle \qquad (6.8.8.)$$

Similar relations are also defined for the other coefficients but have been neglected since these are small[16]. Using these molecular orbitals, following spin Hamiltonian parameters are obtained for the symmetry lower than D_{4h}[17].

$$g_z = g_e - \frac{8\lambda}{\Delta E_{xy}} \alpha^2 \beta_1^2 (\cos\phi) \left\{ \begin{array}{l} \cos\phi - \frac{\alpha_1}{\alpha} S - \frac{1}{2}\left(\frac{\alpha'}{\alpha}\right) \\ \left[\left(1 - \beta_1^2\right)^{1/2} / \beta_1 \right] T(n) \end{array} \right\} \qquad \textbf{(6.8.9.)}$$

$$g_y = g_e - \frac{2\lambda}{\Delta E_{xz}} \alpha^2 \delta_2^2 (\cos\phi - \sqrt{3}\sin\phi) \left\{ \begin{array}{l} \cos\phi - \sqrt{3}\sin\phi - (\alpha'/\alpha) S - \frac{1}{\sqrt{2}} (\alpha/\alpha' \\ [(1-\delta_2^2)^{1/2} / \delta_2^2] T(n) \end{array} \right. \qquad \textbf{(6.8.10)}$$

$$g_x = g_e - \frac{2\lambda}{\Delta E_{xz}} \alpha^2 \delta_1^2 (\cos\phi + \sqrt{3}\sin\phi) \left[\begin{array}{l} \cos\phi + \sqrt{3}\sin\phi - \frac{\alpha'}{\alpha} S - \frac{1}{\sqrt{2}} \alpha/\alpha' \\ (1-\delta_1^2)^{1/2} / \delta_1 T(n) \end{array} \right] \qquad \textbf{(6.8.11)}$$

where ϕ represents the extent of mixing of $3z^2$-r^2 level with x^2-y^2 because of rhombic distortion. Here λ is the spin orbit coupling constant of copper. α, β_1, δ_1, δ_2 are the LCAO

coefficients of the copper 3d part and α' β', δ'_1 δ'_2 are the LCAO coefficient of the lignad part. T (n) is a function of the 2p/2s ratio in the ligand hybrid orbitals.

The expressions for the hyperfine tensors are complicated. The expression for only A_z is given below:

$$A_Z = P\left[\begin{array}{l} -\frac{4}{7}\alpha^2 - K + (g_z - g_e)\,\alpha\cos\phi \begin{pmatrix} \alpha\cos\phi - \alpha' s - \\ -\frac{1}{\sqrt{2}}(\alpha'/\beta_1)(1-\beta_1)^{1/2}T(n) \\ +\frac{3}{14}(g_x - g_e)\,\alpha\,(\cos\phi \\ -\sqrt{3}\sin\phi)(\cos\phi - \sqrt{3}\sin\phi) \end{pmatrix}^{-1} \\ \alpha - \frac{\alpha'}{S} - \frac{1}{\sqrt{2}}(\alpha'/\delta_2)(1-\delta_2^2)^{1/2}T(n) \end{array}\right]$$

$$+\frac{3}{14}(g_x - g_e)\,\alpha\,(\cos\phi - \sqrt{3}\sin\phi)(\cos\phi - \sqrt{3}\sin\phi)\,\alpha$$

$$-(\alpha' S) - \frac{1}{\sqrt{2}}(\alpha'/\delta_1) \qquad (1-\delta_1^2)^{1/2}T(n)\}^{-1}$$

[6.8.12]

Similar expressions for A_x and A_y are available but are not given here as they will not be used. Here K is the fermi contact term. P is the free ion dipole term proportional to $1/r^3$ and has a value of 0.036 cm^{-1}.

(ii) Calculation of the parameters:

The value of α' and hence of α was calculated directly using the expression.[1]

$$A_{ii}^{N} = \left(\frac{\alpha'^2}{4}\right)(2\gamma\beta_0\beta_N)\left[-\frac{8\pi}{9}\delta(r) + \frac{8}{15}\langle r^3\rangle_p\right]$$

$$A_{\perp}^{N} = \left(\frac{\alpha'^{2}}{4}\right)(2\gamma\beta_{0}\beta_{N})\left[-\frac{8\pi}{9}\delta(r) - \frac{1}{15} < r^{-3} >_{p}\right]$$

(6.8.13)

Where $A_{//}^{N}$ and $A_{\perp}^{N}$ are coupling constants in the direction of Cu-N bond and perpendicular to it respectively. These have been obtained from X and Y axis spectra directly δ (r) is the 2s electron density at the nucleus of N atom. $<r^{-3}>_p$ is evaluated for the 2p orbital of nitrogen. γ is the magneto gyric ratio of the N^{14} nucleus which has value of 0.4036[16]. δ (r) and $<r^{3}>_p$ values have been calculated from the self consistent field wave functions of the N atom[1]. The values used are 33.4×10^{-24} cm^{-3} and 21.1×10^{24} cm^{-3} respectively . Using these parameters α' was calculated to be 0.5. and from the normalising condition (6.8.7) the value of α^2 was calculated to be 0.84. The value of S the overlap integral was taken to be 0.094[16]. From the expression (6.8.9), the β_1^2 was calculated to be 0.92. T (n) value was taken to be 0.33[16] and ΔE_{xy} = 14,500 cm^{-1}. The value of ϕ was calculated from the expression[17].

$$\frac{g_y - g_e}{g_x - g_e} = \frac{(\cos\phi + \sqrt{3}\sin\phi)^2}{(\cos\phi - \sqrt{3}\sin\phi)^2} \qquad \textbf{(6.8.13)}$$

It was found to be 6^0 only. Similarly δ_1^2 *and* δ_2^2 were also calculated to be 0.5 and 1.0, where $\Delta E_{xy} = \Delta E_{xz}$ = 15,150 cm^{-1} was taken. The value of K was calculated from the equation (6.8.12).

from the solution spectrum at room temperatures. Hence to estimate A, following expressions were used[17]..

$$\frac{A_{iso}}{P} = -K + \left(Z_x g_x + Z_y g_y + Z_z g_z\right) \qquad \textbf{(6.8.14)}$$

Where

$$Z_x = \alpha\left[\alpha - \alpha' S - \frac{1}{\sqrt{2}}\frac{\alpha'}{\delta_1}\left(1 - \delta_1^2\right)T(n)\right]$$

$$Z_y = \alpha\left[\alpha - \alpha' S - \frac{1}{\sqrt{2}}\frac{\alpha'}{\delta_2}\left(1 - \delta_2^2\right)T(n)\right]$$

$$Z_z = \alpha\left[\alpha - \alpha' S - \frac{1}{2}\frac{\alpha'}{\beta}\left(1 - \beta^2\right)T(n)\right]$$

These parameters were calculated to be 0.69, 0.80 and 0.80 respectively

Using these expressions A_{iso} was calculated to be $|4.6 \times 10^{-3}|$ cm^{-1}. This would mean that relative sign of A_z and A_x should be negative and A_y should be positive. The negative sign indicates that the hyperfine field is found to be anti-parallel to the net spin on the ion[18,36] The estimated values of covalency parameters are presented in Table 6.II.

6.9 DISCUSSION

The choice of the ground state is very important in formulating the molecular orbitals and in subsequent calculations of LCAO coefficients. Hence in deciding the ground state, one should not only know the effective point group of the molecule but also the orientation of the g tensor with respect to the bonds. Complexes belonging to point groups such as D_{2h} or C_{2v} have the principal g_i directions along the axes defined by the symmetry elements of the point group. The ligand field is considered to be a low symmetric perturbation to a strong D_{4h} field. In such cases x and y axes can lie either along the lobes or along the nodes of orbitals. In the latter type of systems the ground state is |xy> and no excited d states are mixed. g anisotropy is therefore expected to be small $(g_x - g_y \cong 0.003)$ being due to the difference in energy and orbital coefficients of |xz> and |yz>. Typical example of these is b-acetyl acetonato Cu (II)[11]. In case where x and y are along the lobes, the ground state is $|x^2-y^2>$ and by the ligand field $|3z^2-r^2>$ can be mixed with the ground state. This mixing usually increases the in-plane anisotropy in g and A. It is interesting to note that, according to Hitchman[19], this mixing is caused only by the perturbation of the ground state lobes. It implies that in complexes of such kind, there should be a strong tendency for g axes to lie

along metal ligand bond directions. Our choice of the ground state as $d_{x^2-y^2}$ is consistent with the above, also from crystallographic data g_x lies along Cu-N (6) g_y lies along Cu-N(6). The assignment of the electronic spectra is also important in calculating the bonding parameters. As mentioned in section 6.4, three bands are observed at 29,000 cm^{-1}, 15,150 cm^{-1} and 14,500 cm^{-1}. Incidentally all the bands have same extinction coefficients hence the assignment is some what a problem because in many Cu complexes $E_{xy,yz}$ is of this order[20]. It is because of this reason pure Imidazole (powder) spectrum was examined. On the basis of the comparison with the Cd compound, the band at 29,000 cm^{-1} was assumed to be n-π^* transition[21].

Bonding Parameters:

The in plane σ bonding, the extent of which is determined by α^2, plays an important role in the stabilization of the most typical tetragonally elongated Octahedral structures. Because of this in almost all copper complexes the main contribution to bonding comes from σ type of bonding. The value of α^2 ranges from 0.5 to 1 i.e. from most convalent to most ionic systems. In the present case α^2 = 0.82, which represents a moderately covalent system. However, σ bonding alone is not sufficient for the molecular stability and some further binding capacity is needed, which is

provided by π bonding. In present case in plane π, bonding represented by β^2, is 0.92, which represents an ionic character. It suggests that the $2p_x$ and $2p_y$ orbitals necessary for in plane π bonding are not fully available and perhaps are utilized in Imidazole ring itself. The parameter obtained for out of plane π bonding points towards interesting features. δ_1^2 is calculated to be = 0.5 and δ^2_2 is one. These results are indicative of the fact that the bonding is largely convalent in XZ whereas it is completely ionic in YZ.

The fermi contact term K has also been calculated[34]The estimated value is 0.25 which is considered to be rather low[21]. This underlines the importance of considering the effect of mixing 4s level. However such estimates need more detailed qualitative analysis employing more sophisticated methods. The possible reason for such a low value are qualitatively discussed below. The fermi contact term consists of two terms [22] a negative contribution because of exchange polarization of the electron spin in the filled shell. This contribution is not expected to change much. The second contribution results from the unpaired S electron density in the 4s copper orbitals. This gives a positive contribution to the fermi contact term. It is possible this contribution is responsible for the anomalous behaviour of the fermi contact term.

The mixing of 4s into the ground state could be caused through the vibronic coupling of the high lying orbitals. In such cases the admixture of 4s character is allowed from the symmetry consideration[23]. But possibly this mechanism does not seem to be operative because of the low molecular symmetry. The other mixing is a direct mixing of 3d-4s levels via the static distortion of D_{4h} symmetry[24]. In this case invariably $d_{x^2-y^2}$, $d_{3z^2-r^2}$ mixing will also be involved. The reason is that both $3z^2$-r^2 and 4s transfer under the totally symmetric a_{1g} representation of the D_{4h} but $3z^2$-r^2 is closer to the ground state in comparison to 4s. Indeed this is the case here also. The mixing is calculated to be about 6%. The rhombicity of the Spin Hamiltonian parameters have been attributed to this mixing.[32,33] It is very difficult to comment about the extent of the reduction of K by such mixing. To other possible way is the spin polarization of the partially occupied 4s orbitals[25-30].

This could be via:

1. The meta 3d spin polarises the metal 4s electrons.
2. The spin delocalised onto the ligand through σ bonding polarises those electrons which occupy σ bonding orbtials between the ligand and metal 4s orbital. Again it is difficult to assess these contribution to the fermi contact

term. Considering all these mechanisms it seems that direct mixing of 4s into the ground s state could be responsible for such a low value of K.

Table 6.I:

Direction cosines of various bonds with respect to orthonormalised sets of axes

S. No.		Bond lengths (A^0)	Direction cosines (angles^0)			Remarks
			l	m	n	
1.	Cd-0 (16)	2.43	-0.0094 (90.5)	0.5221 (58.53)	0.852 (31.50)	-Z Direction
2.	Cd-0 (1)	2.321	0.00699 (89.6)	-0.460 (62.6)	0.88 (27.4)	
3.	Cd-N (1)	2.521	-0.505 (60)	0.786 (38.17)	0.356 (9.15)	
4.	Cd-N (11)	2.256	0.609 (52.5)	-0.66 (131.7)	-0.432 (64.4)	
5.	Cd-N (6)	2.28	-0.83 (146.5)	-0.48 (119.8)	-0.269 (105.6)	

Table 6-II

Spin Hamiltonian Parameters

Sr. No.	Param--eters	Cu^{2+}: $CdIm_6$ (powder)	CdIms single crystals	Soluti-ons	Solution $CuIm_4SO_4$	$CuIm_4SO_4$ (frozen state)
1.	g_z	2.320	2.326			2.26
2.	g_x	2.07	2.046			2.06
3.	g_y		2.094			
4.	A_z	120	126			160
5.	A_x	25	44			40
6.	A_y		20			
7.	g_{iso}	2.14	2.155	2.128	2.128	
8.	A_{iso}	-	46	80	80	
9.	α^2		0.82			0.78
10.	β_1^2		0.92			0.86
11.	δ_1^2		0.5			$\beta'^2=0.85$
12.	δ_2^2		1.0			
13.	K		0.25			0.34

Hyperfine coupling constants are given in terms of Gauss

Table 6.III:
Direction cosines of g tensors with respect to crystallographic axes

Sr. No.	Bond	Direction cosines (angles^0)			Remarks
		L	m	n	
1.	Cd-0 (16)	-0.009 (90.54)	0.07 (85.95)	-0.99 (175.9)	Close to Z-axes
2.	Cd-0 (1)	0.006 (89.6)	-0.00018 (90.0)	0.99 (0)	Z- axis
3.	Cd-N (1)	-0.505 (120)	0.86 (30.5)	-0.046 (92.65)	X- axis
4.	Cd-N (6)	-0.83 (146.5)	-0.551 (123.5)	-0.0173 (91)	Y- axis

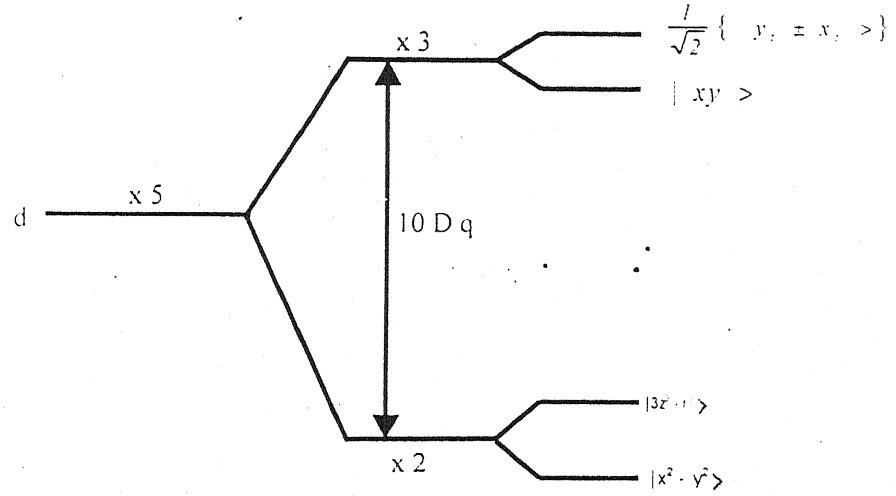

(a)

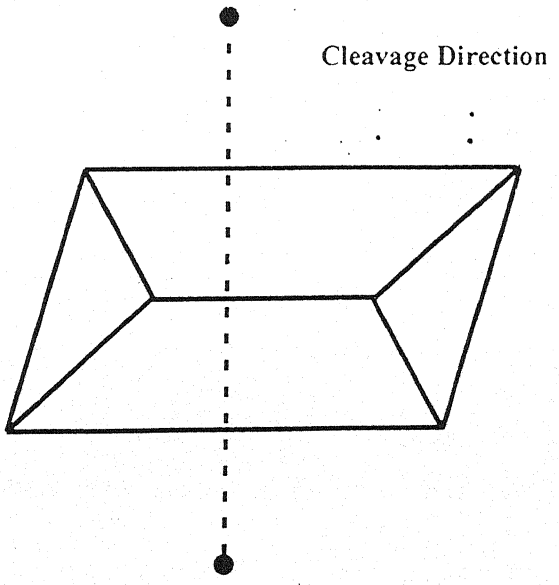

(b)

Fig. 6.1 (a) Energy level diagram
(b) Morphology of the Crystal

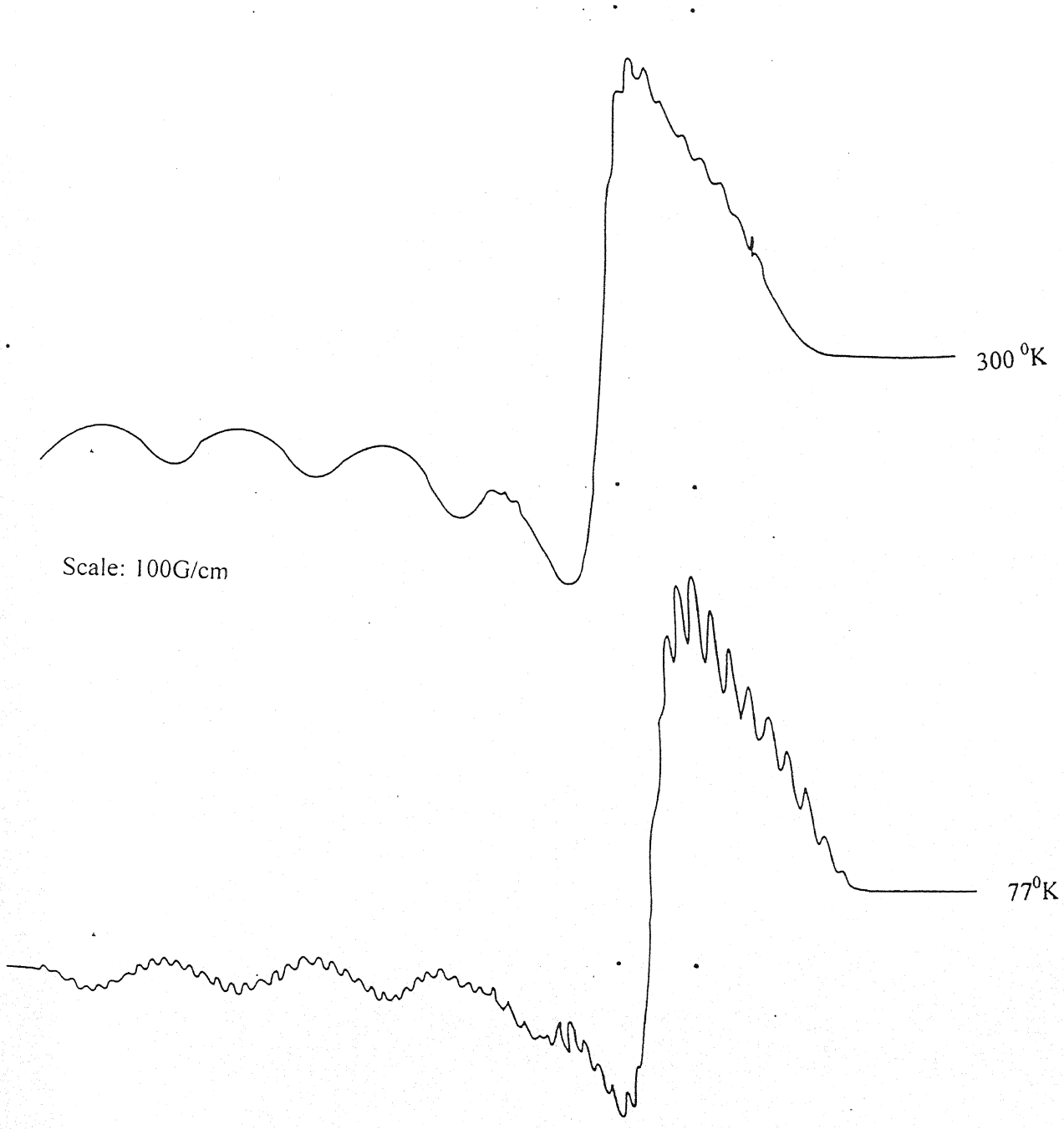

Fig. 6.2: Powder spectra of Cu^{2+}: $CdIm_3SO_4.H_2O$

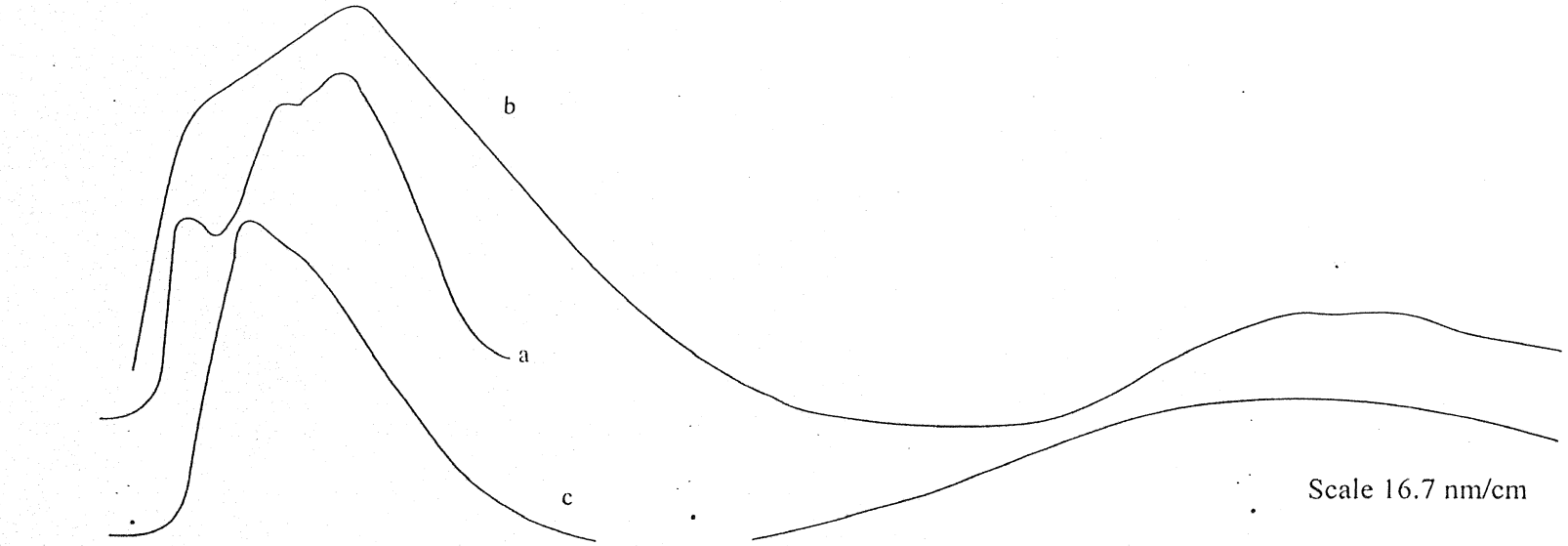

Fig.6.3: Electronic Spectra of
(a) Pure imidazole (Solution)
(b) Cu^{2+}: CdImS (Single crystal)
(c) $CuIm_4SO_4$ (Solution)

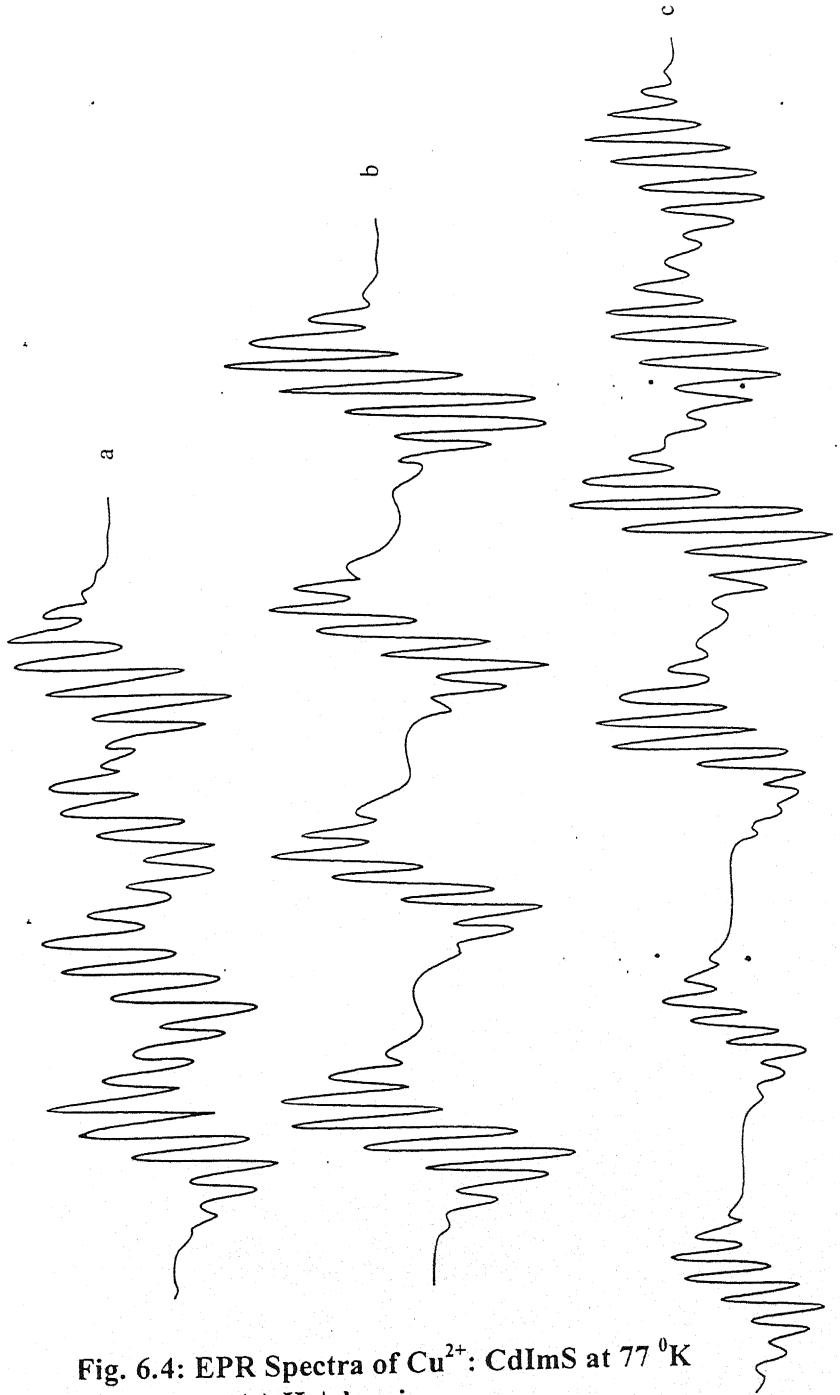

Fig. 6.4: EPR Spectra of Cu^{2+}: CdImS at 77 ^{0}K

(a) H ⊥ b axis

(b) H || b axis Scale: 25G/cm

(c) H || z axis

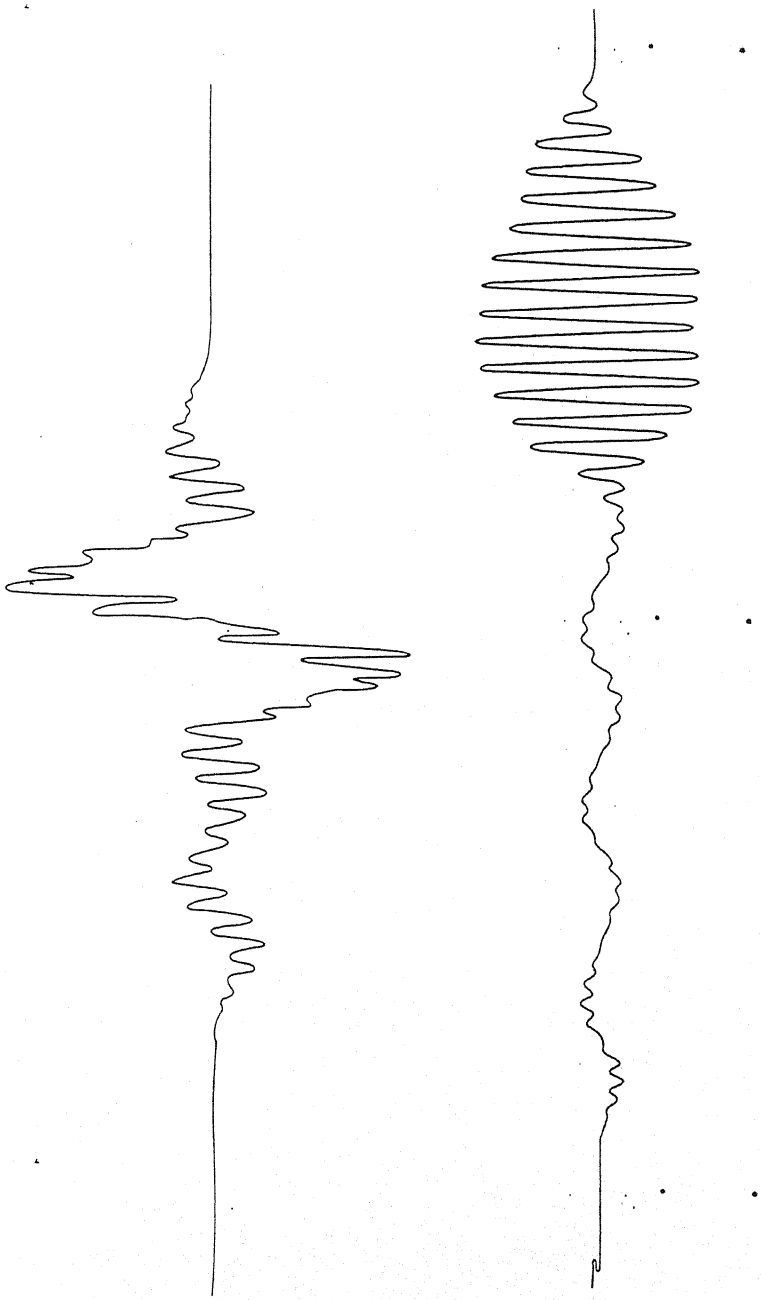

Fig. 6.5: EPR Spectra at 77 ^{0}K:
(a) H || Y axis
(d) H ⊥ X axis.

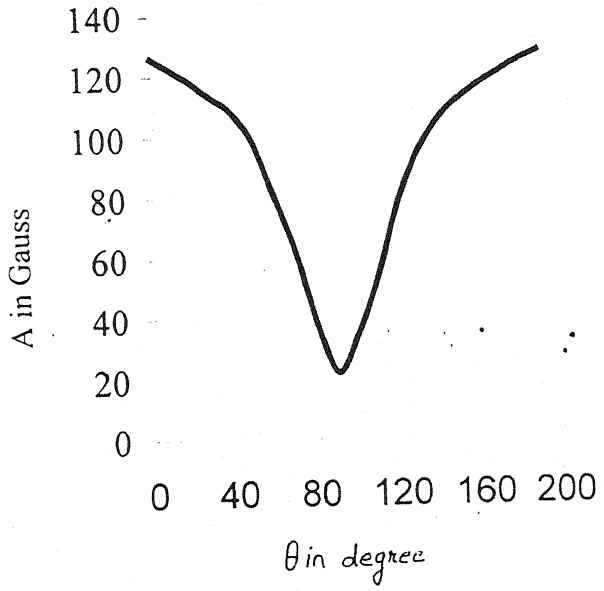

Fig. 6.6(a) : ZY Plane A anisotropy

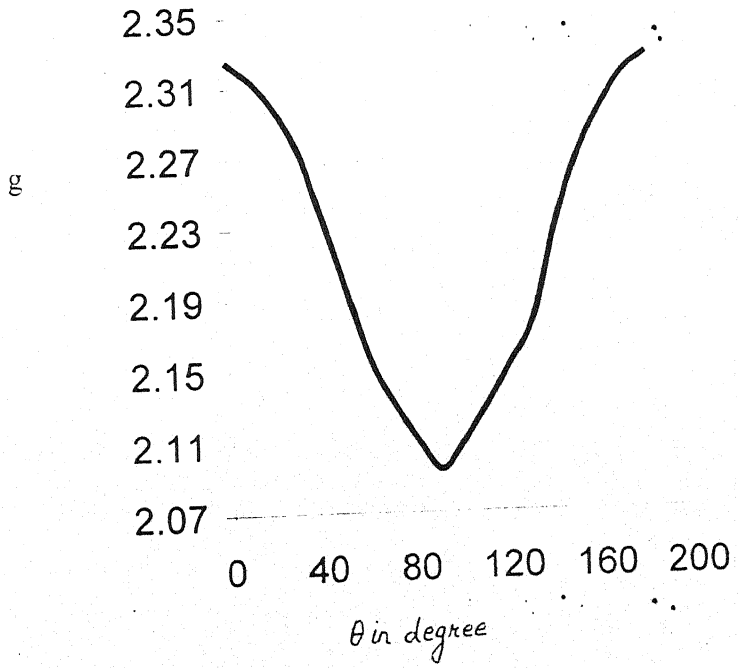

Fig. 6.6(b) : Cu^{2+}: $CdIm_3SO_4H_2O$ ZY Plane g anisotropy

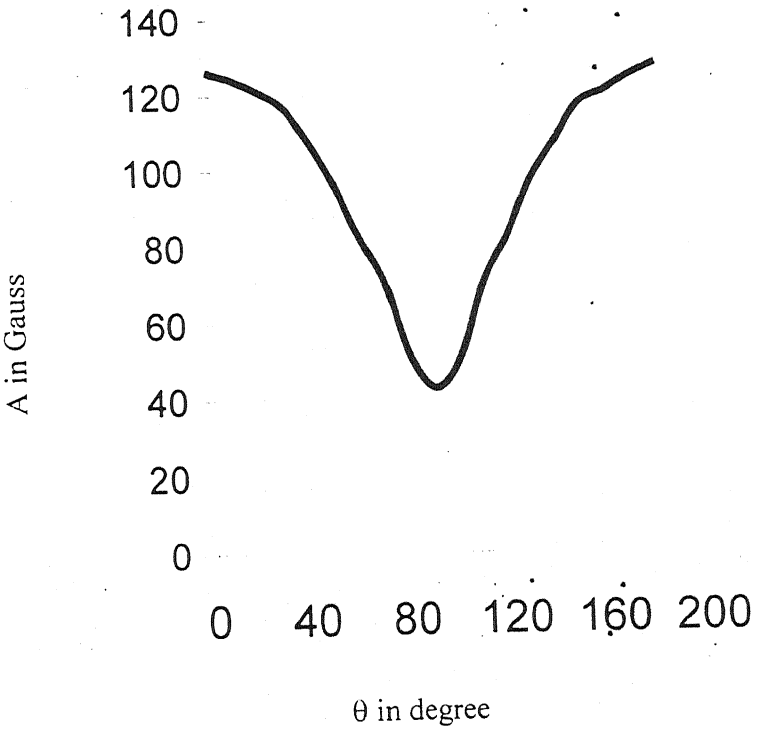

Fig. 6.6 (c): ZX Plane A anisotropy

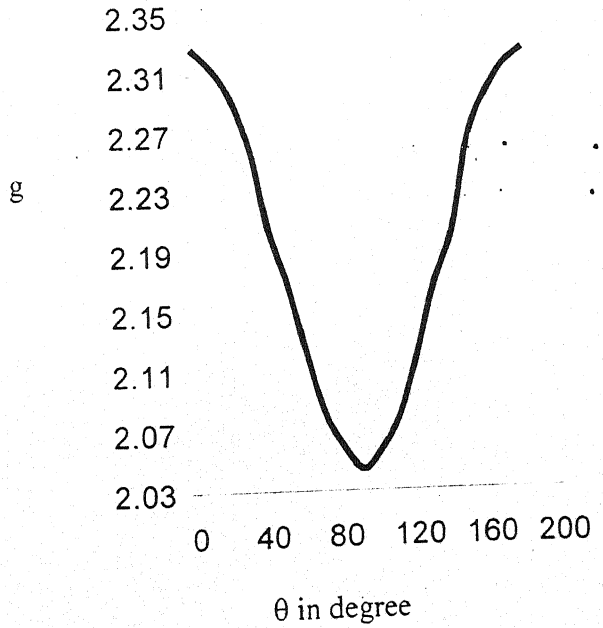

Fig. 6.6(d) : Cu^{2+}: $CdIm_3SO_4H_2O$ ZX Plane g anisotropy

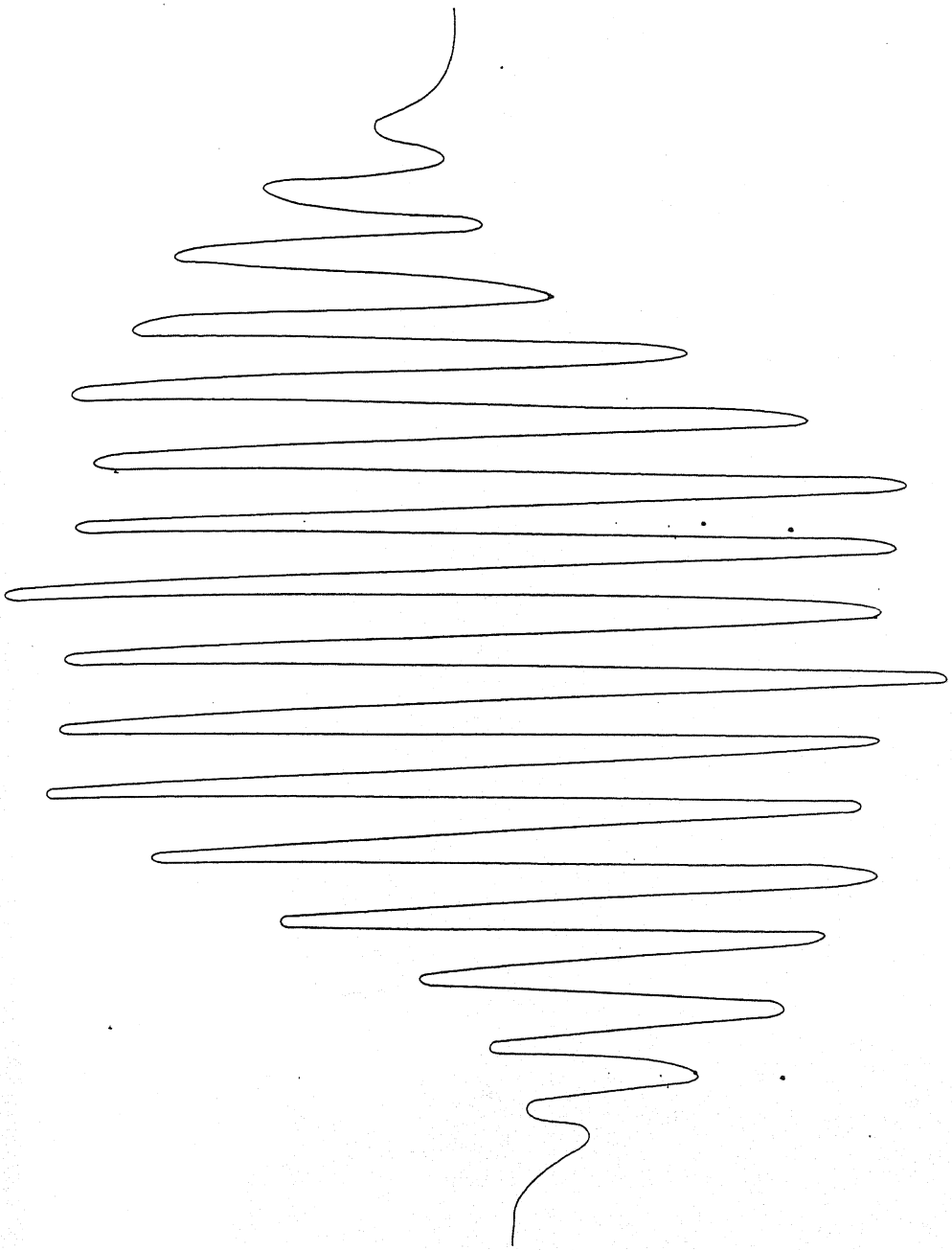

Fig. 6.7: X axis (Computer) simulated spectrum

REFERENCES

1. A.H. Maki, B.R. McGarvey, J. Chem. Phys., **29** (1958).
2. C.M. Guzy, J.B. Raynor and M.C.R. Symons, J. Chem. Soc(A)., 2299 (1969).
3. Chee Chow, Kunchang and R.D. Wilet, J. Chem. Phys., **59**, 2629 (1973)
4. R Barbucii, J. M. Campbell, Inorganic Chamica Acta., **16**, 113 (1976).
5. B. Roos, Acta Chemica Scan., **21**, 1855 (1967).
6. M.R. Caira, L.R. Nassimbani, G. Orpen, Acta Cryst., **B32** 140 (1976).
7. John-Sinkankas- Micrology, Dram-Nostram Comp. Inc, Canada (1960).
8. G. Fransson, K.S. Lundberg, Acta Chemica Scand., **26**, 3969 (1972).
9. B.J.Hatheway, Coordination Chemistry Rev., **35**, 221 (1981).
10. G.E. Pake and T.L. Estle, The Physical Principles of Electron Paramagnetic Resonance, W.A. Benjamin, 2nd edn: (1973).

11. H.R. Gresmann, J.D. Swalen, J. Chem. Phys., **36**, 3221 (1962).

12. J.H. Ammeter, H.B. Burgi, Comp. E., V. Meyer-Sandrin. and W.P. Jensen, Inorganic Chem., **18,** 733 (1979).

13. B.A. Satstry, S. Md. Asadullah, G. Ponticelli and M. Massacessi, J. Chem. Phys., **70**, 2834 (1979).

14. D.W. Smith, J. Chem. Soc., (A) 3108 (1970).

15. K.E. Falk, E. Rusus Bjorn Ivanova and T. Vanngard, Inorg. Chem, **9**, 556 (1970).

16. D. Kivelson , R. Neimann, J. Chem. Phys., **35,** 149 (1961).

17. H.A. Kuska, M.T. Rogers, J. Chem. Phys., **43**, 1744 (1965).

18. R.E. Watson, A.J. Freeman, Hyperfine Interaction (A.J. Freeman and R.B. Frankel Eds), Acad. Press (1967).

19. M.A. Hitchman, C.D. Olson and R.L. Belford, J. Chem. Phys., **50** 1195 (1969).

20. C.N.R. Rao, Ultraviolet and Visible Spectroscopy-Chemical Applications, 2nd edition, London-Butterworth (1967).

21. D. Dyressen, E. Ivanova and K.E. Folk, Acta Chemica. Scand., **26**, 3865 (1972).

22. A.J. Rockembauer, Mag. Reso., **35,** 429 (1979).

23. T. Chiang, J. Chem. Phys., **48**, 1814 (1960).

24. B.R. McGarvey , J. Chem. Phys., **71**, 51 (1967).

25. A. Abragam, G. Bleaney, Electron Paramagnetic Resonance of Transition Ions; PP. 680, Claredon Press, Oxford (1970).

26. S.K. Mishra, Chumzhang Wang, Mag. Reso. Review (UK). Vol 14. No. 3-4, 157 (1990).

27. P. Shiv Prasasd. K. Ramesh, Y. P. Reddy, J. Phys Condens. Matter (UK). Vol. 2. No.25, 5595 (1990).

28. J. Lakshman, B. Sreedhar, M. Ramchandra Reddy and S.V.J. Lakshman. J. Non. Cryst. Solids (Netherlands), 111, No.2-3, 228 (1980).

29. R. M. Krishan, J.L. Rao, Phys. Stat. Solid B (East Germany), 151, No.2, 615 (1989).

30. S. N. Rao, Y. P. Reddy, Solid State Comm. (USA), 78, No.12, 1025 (1991).

31. EPR of Gamma Irradiated Imidazole Complex Cd(Im)3SO4.H2O., Indian J. Phys. A(India), Vol.68A, No.3, p.297-300 (1994).

32. F.Aoksal, I.Kartal, Solid State Comm. (USA) Vol.98, No.12, p.1887-1890 (1996).

33. Hua Giang Zeng et al., Crystal. Res. Technol. (Germany), Vol.32, No.3, p.467-473 (1997).

34. B.N. Mishra, Ram Kripal and A. Narayan, Indian J. Pure Appl. Phys. (India), Vol.36, No.7, p.412-414 (1998).

35. K.V. Narasimhulu, C.S. Sunandana and J. Lakshmana Rao, Physica Status Solidi (b) Vol.217, Issue 2, p.991-997 (2000).

36. V.M. Vinokurov, A.R. Al-Sufi and A.E. Usachev, Magnetic Resonance in Solids, Electronic Journal. Vol.6, No.2 (2002 4)

GENERAL REFERENCES

(i) D.J.E. Ingram, "Spectroscopy at radio and microwave frequencies; Butter-worths, London (1955).

(ii) W. Gordy, "Theory and Application of Electron Spin Resonance" (John Wiley & Sons, Inc, 1972).

(iii) C.P. Poole Jr. and H.A. Farah, "The Theory of magnetic resonance" (John Wiley & Sons Inc. 1972).

(iv) W.Low "Paramagnetic resonance in solids" (Academic press, New York and London 1960).

(v) A. Abragam, B. Bleaney, "Electron Paramagnetic Resonance of Transition Ions (Clarendon press, Oxford 1970).

(vi) C.J. Ballhausen, Introduction to legand field theory (McGraw Hill Book Co. Inc. New Delhi 1962).

(vii) M.W. Porter and R.C. Spiller, Barker Index of crystals, Haffer Cambridge (1956).

(viii) R.W.G. Wyckoff, Crystal Structure, (Vol. 3, Interscience Publ. 1965).

(ix) K.A. Muller and H. Thomas, "Structural Phase Transitions I' (Springer Verlag Berlin, Heidelberg, New York 1981).

(x) F.J. Owens, C.P. Poole Jr. and H.A. Farah, Magnetic Resonance of Phase Transitions, Academic Press (1979).

(xi) A.Carrington and A.D. Mclachlen, Introduction to Magnetic Resonance (Chapman and Hall, 1979).

(xii) J.E. Wertz and J.R. Bolton, Electron Spin Resonance; Elementary theory and Practical Applications, McGraw Hill (1972).

(xiii) J.W. Orton, Electron Paramagnetic Resonance, Iliffe Books Ltd. London (1968).

(xiv) B.D. Cullity, Elements of X-ray diffraction, Addison-Wisley Pub. Company, Inc. California (1978).

(xv) Kaiser and L. Kavad, Electron Spin Resonance of first row transition Metal Complex ions, John Wiley (1968).

(xvi) R.K. Watts : Points Defects in crystals. John-Wiley & Sons (1977).